STUDY OF ADDITIVE EFFECTS ON THE STRUCTURAL, MAGNETIC PROPERTIES AND MÖSSBAUER SPECTROSCOPIC ANALYSIS OF COBALT CADMIUM FERRITES

By

Md. Torikul Islam
Roll No: 1055552
Session: July-2010

A THESIS SUBMITED TO THE DEPARTMENT OF PHYSICS, KHULNA UNIVERSITY OF ENGINEERING & TECHNOLOGY, KHULNA- 9203 IN PARTIAL FULFILMENT OF THE REQUIRMENT FOR THE DEGREE OF MASTER OF PHILOSOPHY

DEPARTMENT OF PHYSICS
KHULNA UNIVERSITY OF ENGINEERING & TECHNOLOGY
KHULNA - 9203, BANGLADESH
FEBRUARY- 2014

KHULNA UNIVERSITY OF ENGINEERING & TECHNOLOGY
DEPARTMENT OF PHYSICS

Approval

This is to certify that the thesis work submitted by *Md. Torikul Islam* entitled *"Study of Additive Effects on the Structural, Magnetic Properties and Mössbauer Spectroscopic Analysis of Cobalt Cadmium Ferrites"* has been accepted by the board of examiners for the partial fulfillment of the requirements for the degree of *Master of Philosophy* in the Department of *Physics*, Khulna University of Engineering & Technology, Khulna, Bangladesh in 27 February 2014.

Board of Examiners
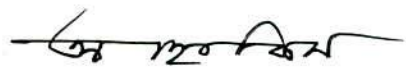
Sl. No.   Name, Designation & Address

1. Prof. Dr. Shibendra Shekher Sikder
   Department of Physics
   Khulna University of Engineering & Technology
   Khulna-9203, Bangladesh

   Chairman & Supervisor

2. Head
   Department of Physics
   Khulna University of Engineering & Technology
   Khulna-9203, Bangladesh

   Member

3. Dr. A. K. M. Abdul Hakim
   Chief Engineer (Retd.)
   Atomic Energy Centre, Ramna
   Dhaka -1000, Bangladesh

   Co- Supervisor & Member

4. Prof. Dr. Md. Abdullah Elias Akhter
   Department of Physics
   Khulna University of Engineering & Technology
   Khulna-9203, Bangladesh

   Member

5. Prof. Dr. Md. Mostak Hossain
   Department of Physics
   Bangladesh University of Engineering and Technology
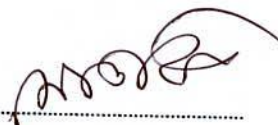   Dhaka-1000, Bangladesh

   Member (External)

DECLARATION

This is to certify that the thesis work entitled as **"Study of additive effects on the structural, magnetic properties and Mössbauer spectroscopic analysis of Cobalt Cadmium Ferrites"** has been carried out in partial fulfillment of the requirement for M. Phil. degree in the Department of Physics, Khulna University of Engineering & Technology, Khulna-9203, Bangladesh. The above research work or any part of this work has not been submitted to anywhere for the award of any degree or diploma. No other person's work has been used without due acknowledgement.
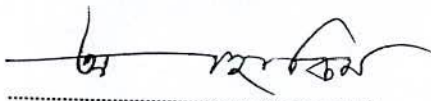
1. **Supervisor**

Prof. Dr. Shibendra Shekher Sikder

Candidate

Md.Torikul Islam

2. **Co-supervisor**

Dr. A. K. M. Abdul Hakim

To

My PARENTS

Acknowledgements

ABSTRACT

The present work is focused on the structural, magnetic properties and Mössbauer spectroscopic analysis of Co-Cd ferrites. The ferrite samples of the compositions $Co_{1-x}Cd_xFe_2O_4$ (where x=0.0, 0.1, 0.3, 0.4 and 0.5) were prepared by using the solid state reaction technique. The phase identification was carried out by using the X-ray diffraction (XRD). The XRD analysis revealed that all the samples were found to crystallize in single phase cubic spinel structure. The lattice constant of $Co_{1-x}Cd_xFe_2O_4$ ferrites increases linearly with the increase Cd-content, followed Vegard's law. Bulk density and X-ray density significantly increase with the increase of Cd- content. Curie temperature (T_c) decreases almost linearly with increasing Cd-content. Initial permeability was found to increase with Cd-content at constant sintering temperature which may be attributed to enhanced density and reduced anisotropy energy as well as increase in grain size of the studied samples. The permeability spectrum with frequency follows the Snoek's limit. Saturation magnetization (Ms) increases with Cd-content with high value of 49 emu/g for x =0.5 emu/g.

All Co-Cd ferrites have been investigated using Mössbauer spectroscopy. The Mössbauer measurements were performed with a conventional constant acceleration spectrometer at room temperature in transmission geometry, using ^{57}Co in a rhodium matrix. The velocity scale of a thin ^{57}Fe sample and the isomer shifts are given relative to the centroid of the spectrum. The isomer shifts of Fe atoms in all Co-Cd ferrites sample behave trivalent ions. The spectrum for the $Co_{1-x}Cd_xFe_2O_4$ ferrites consists of six lines which are broad as compared with Mössbauer spectrum of a pure ^{57}Fe samples in the form of a thin foil up to x = 0.5. After x ≥ 0.6, Co-Cd ferrites consists a paramagnetic doublet, reflecting a severe chemical disorder. One of the magnetic signals is a sextet typical of those associated with a good magnetic order at room temperature.

List of the Symbols Used

Absolute value of admittance	$|Y|$
Absolute value of impedance	$|Z|$
Angular frequency	ω
Antiferromagnetic	AFM
Arrot-Belov-Kouvel	ABK
Anisotropy constant	K_1
Bohr magneton	μ_B
Bragg's angle	θ
Bulk density	ρ_B
Charge of electron	e
Coercivity	H_c
Cross-sectional area of toroid	S
Curie temperature	T_c
DC resistivity	ρ_{dc}
Dielectric constant	ε'
Exchange integral	J
Exchange-coupling constant	J_{ij}
Face centered cubic	f c c
Field cooled	FC
Ferromagnetism	FM
Frequency	f
Grain size	D
Imaginary part of initial permeability	μ''
Impedance	Z
Inductance	L
Initial permeability	μ_i
Inter planner spacing	d
Lattice parameter	a
Local spin canting	LSC
Loss factor	$\tan\delta$
Magnetization	M

Magnetic field	H
Magnetic induction	B
Neel temperature	T_N
Nelson-Riley function	$F(\theta)$
Permeability in free space	μ_0
Porosity	P
Real part of initial permeability	μ'
Rear-earth	RE
Re-entrant spin-glass	RSG
Retentivity	Br
Resistance	R
Saturation magnetization	M_s
Saturation induction	B_s
Spin freezing temperature	T_f
Sintering temperature	T_s
Superconducting Quantum Interface Device	SQUID
Susceptibility	χ
X-ray density	ρ_x
X-ray diffraction	XRD
Yafet-Kittel	Y-K
Zero-field-cooled	ZFC
Wavelength	λ

List of Tables

List of Figures

CHAPTER- II

CHAPTER- III

CHAPTER- IV

Contents

CHAPTER- I: Introduction

CHAPTER- II: Theoretical Background

CHAPTER- III Experimental Procedure

CHAPTER- IV: Results and Discussion

CHAPTER- V Conclusions

CHAPTER - I

Introduction

Chapter-I Introduction

1.1 Introduction

Ferrites are magnetic ceramics containing iron oxide as a major constituent in it. It is now some 75 years since ferrites debuted as an important new category of magnetic materials. There are very well established group of metallic oxides materials are called ferrites. Ferrites are a class of ferromagnetic oxide materials with spinel structure having structural, magnetic electric and dielectric properties. Ferrites have proved them commercially important magnetic materials ranging from the very ordinary radio sets to the complicated and exhaustive hardware involved in computers. Ferrites are extensively used in many kinds of magnetic devices such as transformers, inductors, magnetic heed in resonance circuits for high frequency (ranging from 10^3 to 10^{11} Hz) because of their high electrical resistivity low eddy current losses, high initial permeability, high saturation induction, low hysteresis loss and reduced physical size. The term ferrites mean certain double oxide of iron and another metal, which have two unequal sub lattices and are ordered antiparallel to each other. Magnetic spinels ferrites have the general formula $MOFe_2O_3$ where M is a divalent metal ion such as Mg, Mn, Zn, Ni, Co, Fe, Cd and Cu, etc [1.1].

Spinel ferrites commanded the attention first when S. Hilpert [1.2] focused on the usefulness of ferrites at high frequency applications. The ferrites were developed into commercially important materials, chiefly during the years 1933 - 1945, by Snioek [1.3] and his associates at the Philips Research Laboratories in Holland[1.4].The normal spinel ferrites MFe_2O_4 the divalent ions are all in 'A' sites and the Fe^{+3} ions occupy 'B' sites. In spinel structure the magnetic ions are distributed among two different lattices, tetrahedral (A) and octahedral (B) sites and and are ordered anti parallel to each other.

In ferrites, the cations occupy the tetrahedral (A) and octahedral (B) sites of the cubic spinel lattice and experience competing nearest neighbor (J_{AB}) and the next nearest neighbor (J_{AA} and J_{BB}) interactions with $|J_{AB}| \gg |J_{BB}| > |J_{AA}|$. The magnetic properties of ferrites are dependent on the type of magnetic ions residing on the A and B sites and the relative strengths of the inter (J_{AB}) and intrasublattice (J_{BB}, J_{AA}) interactions. When the J_{AB}

is much stronger than J_{BB} and J_{AA} interactions, the magnetic spins have a collinear structure in which the magnetic moments on the A sublattice are antiparallel to the moments on the B sub lattice. But when J_{BB} or J_{AA} becomes comparable with J_{AB}, it may lead to non-collinear spin structure [1.5]. When magnetic dilution of the sublattices is introduced by substituting nonmagnetic ions in the lattice, frustration and/ or disorder occurs leading to collapse of the collinearity of the ferromagnetic phase by local spin canting exhibiting a wide spectrum of magnetic ordering e.g. antiferromagnetic, ferrimagnetic, re-entrant spinglass, spinglass, cluster spinglass properties [1.6, 1.7]. Small amount of site disorder i.e. cations redistribution between A and B site is sufficient to change the super-exchange interactions which are strongly dependent on thermal history i.e. on sintering temperature, time and atmosphere as well as heating/cooling rates during materials preparation.

Now a day, modern technology has generated growing demand of soft magnetic materials in manufacturing electronic device. Among the soft magnetic materials, polycrystalline ferrites have received special attention due to their good magnetic properties and high electrical resistivity over a wide range of frequencies; starting from a few hundred Hz to several GHz. The low coercivity means the material's magnetization can easily reverse direction without dissipation much energy while the material's with high resistivity prevents eddy current in the core, another source of energy loss. Eddy current induced in conductors that oppose the change in flux that generated them.

The number of magnetically ordered Fe ions increases within few minutes of ball milling. This trend can be explained by an induced chemical disordee which resulte in Fe ions occupying both sub lattices of the spinel, and thus the formation of localized magnetic clusters. The size and shape of these magnetic clusters are influenced by the strong J_{AB} interaction between Fe ions on A-sites and Fe-ions on the B-sites. A random arrangement of Fe ions on both sides will yield many clusters with different volumes and magnetic order [1.8]. Since the relaxation time is sensitive to volume [1.9], the Mossbauer spectrum is the sum of spectra with different- relaxation times. One of the magnetic signals is a sextet typical of those associated with a magnetic order, even though thermal effects at room temperature are apparent from the considerable broadening of the special lines. In principle, in Mossbauer measurements super paramagnetic effects prevail at room temperatures where the fluctuation relaxation time becomes less than the lamer precession

2

time of the nuclear magnetic moments with the effect being strongly dependent on the volume of single domain magnetic clusters. The line broadening of the β pattern with increasing temperatures originates from different temperatures dependencies of magnetic hyperfine fields at various Fe-sites using the molecular field theory [1.10-1.11]. In our earlier work [1.12], spin canting decrease as a result of rare eart substitution was assured to explain this increase in saturation magnetization. However, information about spin canting can be obtained from Mossbauer measurements in high magnetic field [1.13]

Co-ferrite is considered as a potential magnetic material due to its high electrical resistivity, high Curie temperature, and low cost, high mechanical hardness. $CoFe_2O_4$ is generally an almost inverse ferrite in which Co^{2+} ions mainly occupies B-sites and Fe^{3+} ions are distributed almost equally between A and B sites. It has been demonstrated that the inversion is not complete in $CoFe_2O_4$ and the degree of inversion sensitively depends on the thermal treatment and method of preparation condition [1.14], Co-ferrite is known to have a large cubic magnetocrystalline anisotropy ($K_1 = +2 \times 10^6$ erg/cm^3) [1.15] due to the presence of Co^{2+} ions on B-sites. It is well-known that Co-ferrite is a hard magnetic material due to its high coercivity (5.40 kOe) and moderate saturation magnetization (80 emu/g) as well as its remarkable chemical stability and mechanical hardness [1.16].

It is therefore a good candidate for use in isotropic permanent magnets, magnetic recording media and magnetic fluids. Co-ferrite crystallizes in partially inverse spinel structure are represented as $(Co_x^{2+}Fe_{1-x}^{3+})_A[Co_{1-x}^{2+}Fe_{1+x}^{3+}]_BO_4$, where x depends on thermal history and preparation conditions [1.17, 1.18]. It is ferromagnetic with Curie temperature (T_c) around 520^{0}C [1.19] which suggests that the magnetic interaction in these ferrites is very strong and show a relative large magnetic hysteresis which distinguishes it from the rest of spinel ferrites. $CdFe_2O_4$ is assumed to be normal spinel with all Fe^{3+} ions on B-sites and all Cd^{2+} ions on A sites [1.5, 1.6]. The magnetic properties of ferrites such as permeability, magnetization, coercive field, Curie temperature are affected by composition as well as by the type of substitution, cation distribution and method of preparation [1.7]. It was concluded that the variation of magnetic properties results from the ion concentration as well as difference in ionic radius.

Moreover, these low cost materials are easy to synthesize and offer the advantages of greater shape formability than their metal and amorphous magnetic counterparts.

3

Almost every item of electronic equipment produced today contains some ferrimagnetic spinel ferrite materials. Loudspeakers, motors, deflection yokes, electromagnetic interference, radar absorbers, antenna rods, proximity sensors, humidity sensors, memory devices, recording heads, broadband transformers, filters, inductors etc. are frequently based on ferrites. Ferromagnetic materials are defined as one which below a transition temperature exhibits a spontaneous magnetization that arises from non parallel arrangement of the strongly coupled magnetic moments.

Ferrites are ferrimagnetic cubic spinels which possess the combined properties of magnetic materials and insulators. They have been extensively investigated and become the subject of great interest because of their importance of in many technological applications from both the fundamental and the applied research point of view. The important structural, electrical and magnetic properties of these spinels are responsible for their applications in various fields. The spinel ferrite belongs to an important class of magnetic materials because of their remarkable magnetic properties, particularly in radio frequency region, physical flexibility, high electrical resistivity, mechanical hardness and chemical stability [1.20 - 1.22].

The partial replacement of nonmagnetic Cd ions in cobalt ferrite is expected to weaken the magnetic coupling resulting in decrease of Curie temperature. A little works were found on mixed Co-Cd ferrites [1.23, 1.24]. Co ferrites are quite important in the field of microwave industry which is a mixture of $CoFe_2O_4$ with long range ferromagnetic ordering with $T_c \approx 520^0C$.. Thus, with increasing x, the Fe_A-O-Fe_B interaction becomes weak and T_c is expected to decrease. A selective magnetic dilution is very important in ferrites. The nonmagnetic ions such as Cd^{2+} ions that can be used in such dilution should have ionic radius comparable with that of the magnetic ions. This is because the spinel ferrites intra-sublattice interactions are weaker than the inter-sublattice interaction; as a result there are unsatisfied bonds in the ferromagnetic phase. Due to these unsatisfied bonds, increasing the magnetic dilution accentuates the competition between the various exchange interactions resulting in a variety of magnetic structures [1.25-1.27]. A phase diagram has been proposed by J. L. Dormann *et. al.* [1.28] to classify the different substituted ferrite compounds. . Some works have been performed on Co-Cd [1.29, 1.31] ferrites. The effects of substitution Cd^{2+} ions in place of Co^{2+} ions covering a wide range of concentration on the structural, magnetic and electrical properties of Co-Cd ferrites.

Mossbaure Spectroscopy, because of the influence of the local environment on the iron moment, is directly reflected in the hyperfine field distribution studied by Rodmarcq et.al.[1.32] Chappert et.al.[1.33] and Chein et.al.[1.34]. The moment variation can be directly derived from the hyperfine field distribution, because the proportionality between hyperfine field and magnetic moment was established from crystalline by Gubbem et.al [1.35]. Our studies involve the finding of how the iron moment is directly reflected in the hyperfine field distribution measurements by Mossbauer spectroscopy, because of the influence of the local environment.

In the present work efforts have been taken to synthesize Co-Cd ferrites and substituted Cd by using a solid state reaction technique and to study their structural, magnetic and Mossbauer spectroscopic analysis by constant sintering conditions. Study the effect of Cd substituted on the composition $Co_{1-x}Cd_xFe_2O_4$ ferrites. However, attempts have been made to present a systematic review of various experimental and theoretical observed facts related on this study. To carried out for a complete understanding on these two scientifically interesting systems.

1.2   The Aims and Objectives of the Present Work

$CoFe_2O_4$ is an important technical material because of its specific hard magnetic properties which other spinel ferrites do not have. Again $CoFe_2O_4$ is a good magnetostrictive material suitable for use in transducer which has been observed recently. Also it is a good inductor material for ultra high frequency application when suitably additives/dopants are incorporated.

The objective of the present work is to study the effect of nonmagnetic additives such as Cd to the basic $CoFe_2O_4$ ferrites.

The main objectives of the present research works are:

- To synthesize a series of $Co_{1-x}Cd_xFe_2O_4$ (where x=0.0, 0.1, 0.3, 0.4 and 0.5) ferrites by conventional ceramic method and to investigate the co-relation between the structural parameters and various non-magnetic substituted ions in Co-ferrites.

- To investigate in detail the effects of substitution of Cd^{2+} ions in place of Co^{2+} ions covering a wide range of concentration on the structural magnetic and

5

transport properties of Co-Cd ferrites.

- To study the site occupancy of various ion on tetrahedral and octahedral sites.
- The prepared samples have been characterized in terms of their crystal structures, unit cell parameters and phases present in the prepared samples with the help of X-ray diffraction (XRD). The porosity of the prepared sample has been calculated from the theoretical density and bulk density.
- The magnetization of the samples has been measured as a function of field and temperature using Vibrating Sample Magnetometer (VSM).
- To investigate the magnetic behavior of the prepared sample by measuring Cure temperature, effective magnetic moment, paramagnetic Cure temperature and domain exchange interaction.
- Permeability, Magnetic loss factor and relative quality factor as a function of frequency and temperature have been determined using an Impedance Analyzer.
- To study hyperfine structure of Co-Cd ferrites with Mössbauer Spectroscopy.
- To study hyperfine field distribution measurement of Co-Cd ferrites by Mossbauer spectroscopy. We have measured the Isomer shift(IS), Quadrapole splitting(E_Q), Hyperfine field (H_{hf}), Full Width Half Maximum(FWHM) and Absorption percentage.
- To develop and standardize the indigenous technology for the manufacture of low cost permanent magnets.

1.3 Reason for Choosing this Research Work

- Co-Cd ferrites have not been investigated in different sintering time. The sintering time dependence of the imaginary part of complex permeability curves are very interesting to note that resonance frequency decreases with increasing Cd content and is maximum of $CoFe_2O_4$ Sintered.
- Detail permeability study as a function of frequency and sintering time on $Co_{1-x}Cd_xFe_2O_4$ (where x=0.0, 0.1, 0.3, 0.4 and 0.5) ferrites has not been carried out before. The quality factor, i.e, measure of performance and utility range of frequency increases with increasing Cd .
- Our plan is to study most exhaustively the permeability and magnetization of the series as a function of frequency and sintering time. An enhancement of

6

permeability with Cd contents is observed which means Co-ferittes which well known for its hard magnetic nature that has been converted to softer magnetic materials due to its increasing permeability with increasing Cd contents.

- Our studies involve the finding of how the iron movement is directly reflected in the hyperfine field distribution measurements by Mössbauer spectroscopy because of the influence of the local environment. Mössbauer spectra for Co-Cd were not investigated before.

1.4   Review Works

Ferrites play a useful role in many magnetic applications. They have been extensively investigated and are the subject of great interest from both the fundamental and the applied research point of view. The important structural, electrical and magnetic properties of these spinels are responsible for their applications in various fields specially in electronics and electrical circuits. The use of ferrites for certain application depends on their structural, magnetic and transport properties, which in turn are sensitive to the preparation condition (sintering time& sintering temperature) as well as the type and amount of substitution. A large number of scientists and technologists are engaged in this area of research to bring about improvement on the properties of ferrites.

A.M. Abdeen et.al [1.36] has studied the compositions of $Co_{1-x}Cd_xFe_2O_4$ ferrites. The main results are that the lattice parameter, the radius of tetrahedral sites and the density of samples increase with increasing Cd content, where as the prosity decreases. The DC conductivity increases as cd content increase up to x=0.7; it reaches a maximum where the activation energy for for conduction decreases and reaches a maximum. The electrical conductivity of Fe_3O_4, Fe_2O_4 and $Co_xZn_{1-x}Fe_2O_4$ $(0 \leq x \leq 1)$ ferrites was studied in [1.37]. The electrical conductivity of ferrites with composition Fe_3O_4, $CdFe_2O_4$ and $Co_xZn_{1-x}Fe_2O_4$ $(0 \leq x \leq 1)$ was studied in a nitrogen atmosphere as a function temperature, Fe_3O_4, $ZnFe_2O_4$ and $CdFe_2O_4$ showed n-type conduction, whereas $CoFe_2O_4$ showed p-type conduction.

Co^{+2} is used to improve electromagnetic properties in ferrites. Groenon et.al.[1.38] prepared Co-substituted $(Ni_{0.78} Zn_{0.22}) Fe_2O_4$ ferrite. The results showed that Co^{2+} was the anisotropic ion responsible for the magnetic response time. The Co^{3+} ions and presumable

7

cation vacancies in association with Co^{3+} provide the means whereby Co^{2+} was transported through the lattice. Byun et. al.[1.39] investigated the electromagnetic properties of $(Ni_{0.2} Cu_{0.2} Zn_{0.6})_{1.02-x}Co_x Fe_{1.98}O_4$ ferrites. The results showed that the grain size and sintered density changed a little. It also showed the concentration of cation and the increase in induced anisotropy results in the decrease of initial permeability. The magnetostriction of Co-ferrite is many times higher than that of Ni-Zn ferrites.

Electrical properties of Co-Zn ferrites have been studied by M. A. Ahmed [1.40]. It was found that the lattice parameter increases linearly with the increase of zinc content. The X-ray densities for all compositions of Co-Zn ferrites increase with the increase of zinc content. The X-ray densities are higher than the bulk values. The addition of Zn, reduce the porosity thus increasing the density of the sample. The conductivity increases due to the increase in mobility of charge carriers. P. B. Panday et.al [1.41] has synthesized Co-Zn ferrite by the co-precipitation method and studied the structural and bulk magnetic properties. All the samples are single phase spinel showed the X-ray diffraction pattern. The lattice constant gradually decreases on increasing Zn content, shows a minimum at x ~ 0.5 and then increases on further dilution. The magneton number, i.e., saturation magnetization per formula unit in Bohr magneton (n_B) at 298K initially increases and then decreases as x is increased up to $x \le 0.3$. The decrease in magnetization of these materials after x = 0.3 is primarily associated with canting of the magnetic moments. Curie temperature decreases with small addition of Zn.

R.V. Upadhyay et. al. [1.42] studies th magnetic properties of a Zn substituted $Co_{1.2-x}Zn_xTi_{0.2} Fe_{1.6}O_4$ Ferrite system using AC susceptibility, magnetization and Mossbauer technique. The results suggest that the present system exhibits paraferri-cluster spin glass type magnetic ordering for $x \le 0.5$ while for $x>0.5$ it exhibits only cluster spin glass type ordering. The AC susceptibility and Mossbauer results supports this concept. The magnetic and magnetoresistive properties spinel type $Zn_{1-x}Co_xFe_2O_4$[x=0.02 & 0.4] ferrites are extensively investigated in studied Akther Hossain et. al.[1.43]. They observed the origin of the MR may due to the suppression of the scattering of carriers from the paramagnetic spins or the canted spin (yk angle) or magnetic polaron. The MR is almost linear with applied magnetic field, making it suitable for magnetic sensor fabrication.

Suman Kumar Nath *et.al.* [1.44] have been investigated on the magnetization behavior of $Ni_{1-x}Cd_xFe_2O_4$ ferrites for $x \geq 0.00$ & ≤ 0.8 prepared by conventional ceramic method. They observed Neel's two sublattice collinear model is applied for the initial rise of the magnetization up to $x \leq 0.5$ and beyond that three sublattices non-collinear model proposed by yafet-kittel are predominant and indicates the appearance of spin canting structure in these ferrites with higher Cd-content.

A.R shitre *et.al* [1.45] have been investigated the $Co_{1-x}Cd_xFe_{2-x}Cr_x$ system with a view to determine the effect of Co-substitution of Cd-Cr on dielectric properties of the system. It is observed that dielectric constant decrease with increasing frequency. The dielectric loss decrease with increasing frequency at a faster rate that the dielectric constant.

B.H. Liu et.al [1.46] studies the milling induced micro structural evolution and in the magnetic properties of the milled $CoFe_2O_4$ materials. The results indicated that the milling –induced high coercivity was associated with the highly-strained and defective microstructure. The enhancement in magnetic anisotropy was observed in large-grained $CoFe_2O_4$ after milling, which might be mainly attributed to the stress anisotropy.

Z.H.Khan *et.al* [1.47] and K.O.low *et.al* [1.48] reported that Ni-Cu-Zn ferrites are well established soft magnetic material for MLCI applications because of their relatively low sintering temperature, high permeability in the RF frequency region and high electrical resistivity. Z.H. khan *et.al* [1.49] studied complex permeability spectra of Ni-Cu-Zn ferrites. The particle size increase when the sintering temperature is raised. For the chemical composition and different sintering temperature it was found that the real permeability in the low frequency region decreases CuO.

Saroaut Noor *et.al* [1.50] reported the effect of Cd-substitution on the variation of saturation magnetization, curie temperature and magnetic moment of $Co_{1-x}Cd_xFe_2O_4$ ferrites have been investigated using SQUID magnetometer and impedance analyzer Curie temperature decreases almost linearly with increasing x content up to x=0.7. Samples having $x \geq 0.8$ display complex behavior with competing antiferromagnetic and ferromagnetic unteraction with the manifestation of large hysteresis a low temperature and no sign of saturation.

9

A. M. M. Farea *et.al* [1.51] has studied dielectric properties, loss tangent, ac conductivity as a function of frequency, temperature and composition of $Co_{0.5}Cd_xFe_{2.5-x}O_4$. The dielectric constant, loss tangent and ac conductivity decreases as the frequency of applied ac electric field increase but these parameters increase as the temperature increases due to the increase in thermal activation of hopping frequency and drift mobility of charge carriers. These are explained on the basis of space charge polarization according to Maxwell and Wagner's two layer models and the hoping between adjacent Fe^{2+} and Fe^{3+} as well as the hole hopping between Co^{3+} and Co^{2+} ions on B-sites.

A .A Ghani *et.al* [1.52] reported the composition dependence of magnetization in $Co_{1-x}Cd_xFe_2O_4$ ferrites. The saturation magnetization is maximum at x = 0.35 at high magnetic field up to 150 kOe and in the temperature range 4.2 to 300K. The non-collnear spin structure (canted) was found from the behavior of magnetization in the high field region 75 - 150 kOe.

S.NOOR *et.al* [1.53-1.54] investigated composition dependence of $Co_{1-x}Cd_xFe_2O_4$ sintered at $1050^0C/3hrs$.They h found Variation of lattice parameter with Cd content obey's Vegards's law and the linear variation of X-ray densities with Cd content. Bulk density is found to increase while porosity decreases with increasing Cd content. Curie temperature decreases linearly with the addition of Cd ions. The initial permeability increases with Cd content and sintering temperature has little effect on permeability. Saturation magnetization increases with increasing Cd content at $x \geq 0.4$ and then it decreases. The hysteresis behavior and initial permeability reveals the softer ferromagnetic nature of the studied sample. DC electrical resistivity is found to increase with the increase of Cd content.

Chul Sung kim et,al [1.55] studied Mossbauer spectra of $N_{0.065}Zn_{0.25}Cu_x Fe_{2-x}O_4$ that was taken at various temperatures ranging from room temperature to 725k. Mossbauer spectra was observed and interpreted as originating from different temperature dependence of the magnetic hyperfine field at various iron sites. The isomer shifts indicated that the iron ions were ferrite at the tetrahedral (A) and the octahedral sites (B).The quadrapole shifts showed that the orientation of the magnetic hyperfine field with respect to the principle axes of the electric field gradient was random. The spectra to a model based on a random distribution of Fe and Zn ions on the A sites [1.56].

Magnetic properties of the mixed spinel $CoFe_{2-x}Cr_xO_4$ have been investigated. by H. Mohan et.al [1.57]. The measured variation of magnetic moment per formula unit at 80k with Cr-content obtained from magnetization and Mossbauer data for x=0-0.6display a discrepancy between them, thus exhibiting a significant canting on B-sites. M.A Hakim et.al.[1.58] studied Hyperfine field of Co-Fe-based amorphous ribbon by Mossbauer Technique. The Mossbauer Spectra for all samples clearly show Lorentzian shaped lines in sextet with broad distribution of magnetic hyperfine field as compared to pure ^{57}Fe foil. A five to six fold increase of the broadening of the spectral line width at FWHM for the Co-based alloys compared to pure Fe.

1.5 Outline of the Thesis

The thesis has been divided into five chapters: **Chapter I** presents a brief introduction of Co-Cd ferrite and organization of thesis. This chapter incorporates background information to assist in understanding the aims and objectives of this investigation, and also reviews recent reports by other investigators with which these results can be compared. **Chapter II** briefly describes the theories necessary to understand the present work. **Chapter III** enunciates with the detail experimental process related to this research work. **Chapter IV** describes the results and discussion about the structural and magnetic properties of $Co_{1-x}Cd_xFe_2O_4$ ferrites. **Chapter V** contains the concluding remarks.

Chapter - II
Theoretical Background

Chapter-II Theoretical Background

2.1 Origin of Magnetism

With the concept of electron spin introduce by Goudsmit in 1925 and Ublenbeck in 1926, the origin of magnetism was explained. Spin corresponds to movement of electric charge in the electron hence an electric current which produces a magnetic moment in the atom. Fig 2.1illustrated the magnetism in solids arise due to orbital and spin motions of electrons as well as spins of the nuclei of an atom. The motion of electrons is equivalent to an electric current which produces the magnetic effects. The major contribution comes from the spin of unpaired valence electrons which produces permanent electronic magnetic moments. A number of such magnetic moments may align themselves in different directions to generate a net non-zero magnetic moment. Thus the nature of magnetization produced depends on the number of unpaired valence electrons present in the atoms of the solid and on the relative orientations of the neighboring magnetic moments. The net magnetic moment is the vector sum of the individual spin and orbital moments of the electrons in the outer shells [2.1].
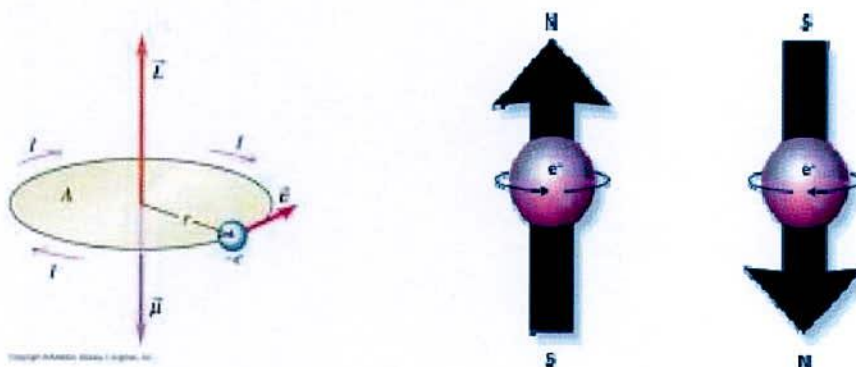
Fig.2.1 (a) Electron orbit around the nucleus (b) Electron spin.

Fig2.1 (b) illustrate these two phenomena the electron spin can be represented in two modes pointed up or down.

i.   In an atom, with opposed paired spins paired spins cancel and do not result in manetic moment, while

ii. The unpaired spins will give rise to a net magnetic moment.

The magnetism in solids can be classified in to the following five major groups.

- Diamagnetism
- Paramagnetism
- Ferromagnetism
- Antiferromagnetism
- Ferrimagnetisms

2.1.1 Diamagnetism

Diamagnetism is a fundamental property of all matter, although it is usually very weak. It is due to the the non-cooperative behavior of orbital electrons when exposed to an applied magnetic field. Diamagnetic substance is composed of atoms which have no net magnetic moment. The orbital motion of electrons creates tiny atomic current loops, which produce magnetic fields .When an external field is applied to a material, these current loops will tend to align in such a way as to oppose the applied field. This may be viewed as an atomic version of Lenz's law: induced magnetic fields tend to oppose the change which created them. Materials in which this effect is the only magnetic response are called diamagnetic. The other characteristic behavior of diamagnetic materials is that the susceptibility is temperature independent. The typical values of susceptibility are in the order of 10^{-5} to 10^{-6}. Any conductor will show a strong diamagnetic effect in the presence of changing magnetic fields because circulating currents will be generated in the conductor to oppose the magnetic field changes [2.2]. A superconductor will be a perfect diamagnet since there is no resistance to the forming of the current loops. Most of the materials are diamagnetic, including Cu, B, S, Ag, Si, N_2 and most organic compounds.

13

2.1.2 Paramagnetism

Paramagnetic material posse's permanent dipole moments due to incomplete cancellation of electron spin and/or orbital magnetic moments (unpaired electron). In the absence of an applied magnetic field in dipole moments are randomly oriented; therefore the materials have no net macroscopic magnetization. In an applied magnetic field these moments start to align parallel to the field. Materials that are paramagnetic become magnetized in the same direction as that of an applied magnetic field and the amount of magnetization is proportional to that of the applied magnetic field [2.3-2.7].

Paramagnetic materials are attracted to magnetic fields; hence have a relative magnetic permeability greater than one or equivalently, a positive magnetic susceptibility and the values of susceptibility are very small with the order of 10^{-5} to 10^{-3}. Paramagnets do not retain any magnetization in the absence of an externally applied magnetic field. Superparamagnetism is a phenomenon by which magnetic materials may exhibit a behavior similar to paramagnetism even when at temperatures below the Curie temperature. This is a small length scale phenomenon, where the energy required to change the direction of the magnetic moment of a particle is comparable to the thermal energy at room temperature. At this point, the rate at which the particles will randomly reverse direction becomes significant. O_2, NO, Mn and Cr are just a few examples of the paramagnetic materials. The susceptibility of a paramagnetic material is inversely dependent on temperature, which is known as Curie law

$$X = \frac{C}{T}$$
(2.1)

where C is the Curie constant.

2.1.3 Ferromagnetism

Ferromagnetic material differs from diamagnetic and paramagnetic materials in many different ways.In a ferromagnetic material, the exchange coupling between neighbouring

14

moments leads the moments to align parallel with each other. In a ferromagnetic materials, this permanent magnetic moment is the result of the cooperative interaction of large numbers of atomic spins what are called domains regions where all spins are aligned in the same direction.. Every ferromagnetic substance has its own individual temperature, called the Curie temperature, above which it loses its ferromagnetic properties [2.5]. This is because the thermal tendency to disorder overwhelms the energy lowering due to ferromagnetic order. The susceptibility of a ferromagnetic material does not follow the Curie law, but displayed a modified behavior defined by Curie-Weiss law Fig. 2.3 (b).

$$X = \frac{C}{T - \theta} \qquad (2.2)$$

where C is a constant and θ is called Weiss constant. For ferromagnetic materials, the Weiss constant is almost identical to the Curie temperature (T_c). At below T_c, the magnetic moments are ordered whereas above T_c material losses magnetic ordering and show paramagnetic character. The elements Fe, Ni and Co and many of their alloys are typical ferromagnetic materials.
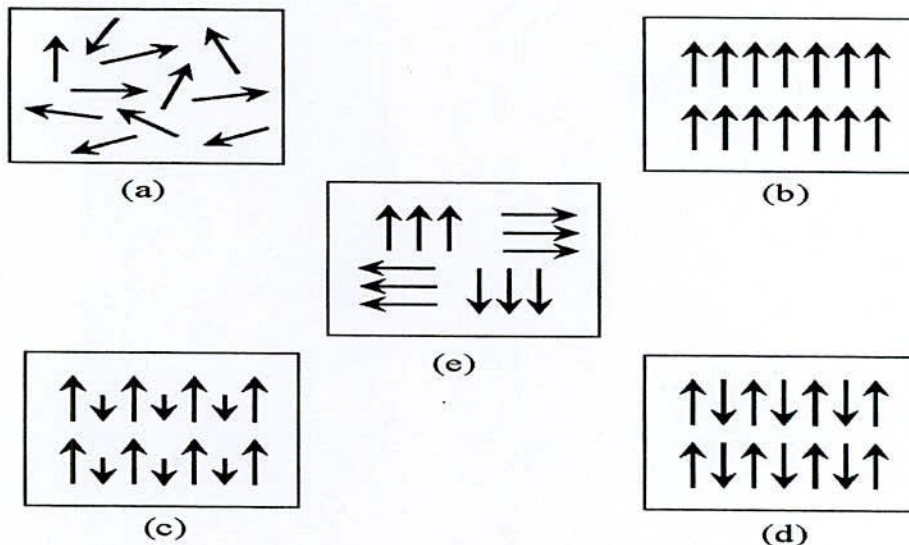
Fig. 2.2 Varieties of magnetic orderings (a) Paramagnetic, (b) Ferromagnetic, (c) Ferrimagnetic, (d) Antiferromagnetic and (e) Superparamagnetic.

15

Two distinct characteristics of ferromagnetic materials are:

  i.   Spontaneous magnetization and

  ii.   The existence of magnetic ordering temperature (Curie temperature)
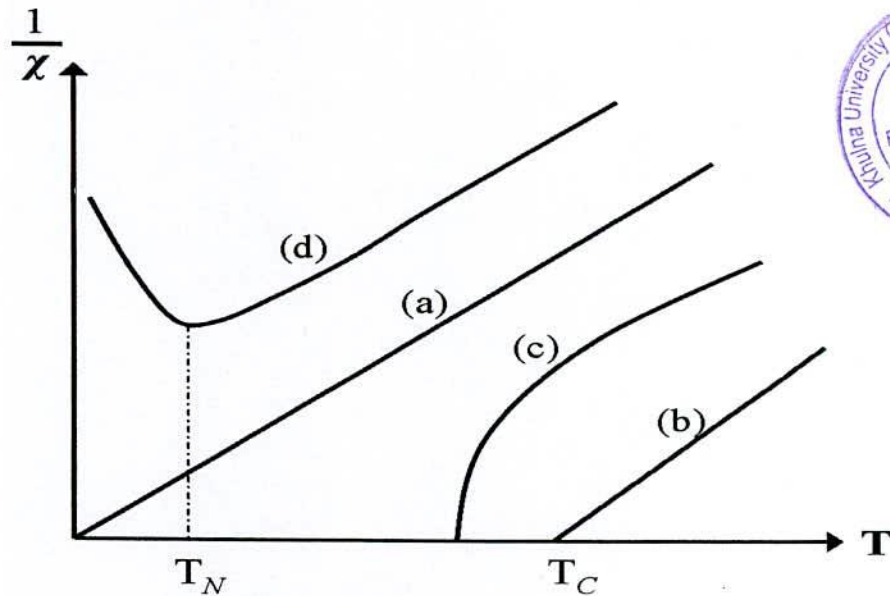
Fig. 2.3. The inverse susceptibility varies with temperature T for (a) Paramagnetic, (b) Ferromagnetic, (c) Ferrimagnetic, (d) Antiferromagnetic materials. T_N and T_c are Neel temperature and Curie temperature, respectively.

The spontaneous magnetization is the net magnetization that exists inside a uniformly magnetized microscopic volume in the absence of a field. The magnitude of this magnetization, at 0K is dependent on the spin magnetic moments of electrons. Spontaneous magnetization is the term used to describe the appearance of an ordered spin state (magnetization) at zero applied magnetic field in a ferromagnetic or ferrimagnetic material below a critical point called the Curie temperature or T_c. This fact led Weiss to make the bold brilliant assumption that a molecular field acted in a ferromagnetic substance below its Curie temperature as well as above and that this field was so strong that it could magnetize the substance to saturation even in the absence of an applied field. The substance is then self-saturating or spontaneously magnetized. Saturation magnetization is an intrinsic property

16

independent of particle size but dependent on temperature. Even through electronic exchange forces in ferromagnets are very large thermal energy eventually overcomes the exchange energy and produces a randomizing effect. This occurs at a particular temperature called the Curie temperature (T_c). Below the Curie temperature the ferromagnetic is ordered and above it, disordered. The saturation magnetization goes to zero at the Curie temperature. The Curie temperature is also an intrinsic property.

2.1.4 Antiferromagnetism

Antiferromagnetic material aligns the magnetic moments in a way that all moments are anti-parallel to each other, the net moment is zero. The antiferromagnetic susceptibility is followed by the Curie-Weiss law with a negative θ as in equation (2.2). The inverse susceptibility as a function of temperature is shown in Fig. 2.3 (d).The natural state makes it different for the material to become magnetized in the direction of the applied field but still demonstrates a relative permeability slightly greater than above a critical temperature known as the Neel temperature the material becomes paramagnetic [2.7]. Common examples of materials with antiferromagnetic ordering include MnO, FeO, CoO and NiO.

2.1.5 Ferrimagnitism

Ferrimagnetic material has the same anti parallel alignment of magnetic moments as an antiferromagnetic material does. However, the magnitude of magnetic in one direction differs from that of the opposite direction. This type material contains two different types of ions. Moments of the ions remain antiparallel but moments are not of the same size Fig. 2.2(c). An overall magnetization is produced but not all the magnetic moment may give a positive contribution to the overall magnetization. As a result a net magnetic moment remains in the absence of external magnetic field the behavior of susceptibility of a ferrimagnrtic material also obeys Curie-Weiss law and has a negative θ as well as in Fig. 2.3(c. Ferrimagnetism is therefore similar to ferromagnetism. It exhibits all the hallmarks to ferromagnetic behavior like spontaneous magnetization, Curie temperature hysteresis, and remanence. However ferro and ferrimagnets have very different magnetic ordering.). while these materials may also

17

demonstrate a relative permeability greater than1, their temperature dependence are not as consistent as with ferromagnetic materials and can result is some very unusual results In ionic compounds, such as oxides, more complex forms of magnetic ordering can occur as a result of the crystal structure. The magnetic structure is composed of two magnetic sublattices (called A and B) separated by oxygens. The exchange interactions are mediated by the oxygen anions. When this happens, the interactions are called indirect or superexchange interactions.

2.2 Classification of Ferrites and its Relevance

Ferrites are essentially ceramic materials, compound of iron, boron, barium strontium, lead, zinc, magnesium or manganese. The ingredients are mixed, prefired, milled / crushed, dried, shaped and finally pressed and fired into their final hand an brittle state. Ferrites are a class of chemical compounds with the formula AB_2O_4, where A and B represent various metal cations usually including iron. These ceramic materials are used in applications ranging from magnetic components in micro electronics.

At high frequencies ferrites are considered superior to other magnetic materials because they have low eddy current losses and high DC electrical resistibility. The DC electrical resistivity of ferrites at room temperature can vary depending upon the chemical composition between about 10^{-2} Ω-cm and higher than 10^{11} Ω-cm [2.8].

Ferrites are classified into two categories based on their coercive field strength. They are:
   (i) Soft ferrite with coercive field strength < 10 Oe
   (ii) Hard ferrite with coercive field strength > 125Oe

2.2.1 Soft Magnetic Materials

Materials with low coercivity are said to be magnetically soft. They are ursed in transformer and inductor cores, recording heads, microwave devices and magnetic shielding. The wide variety of magnetic materials can be divided into two groups, the magnetically soft and the magnetically hard. Soft magnetic materials are those materials that are easily magnetized and demagnetized. They are easily magnetized and demagnetized. They are low

18

mmagnetocrystalline anisotropy resulting in reduced coercivity and high permeability. They typically have intrinsic coercivity less than 1000 Am^{-1}. They are used primarily to enhance and/or channel the flux produced by an electric current. The important parameter, often used as figure of merit for soft magnetic materials, is the high relative permeability. The other main parameters of interest are the coercivity, the saturation magnetization and the electrical conductivity.

The types of applications for soft magnetic materials fall into two main categories: AC and DC. In DC applications the material is magnetized in order to perform an operation and then demagnetized at the conclusion of the operation, e.g. an electromagnet on a crane at a scrap yard will be switched on to attract the scrap steel and then switched off to drop the steel.

The main consideration for material selection is most likely to be the permeability. For example, in shielding applications the flux must be channeled through the material. Where the material is used to generate a magnetic field or to create a force then the saturation magnetization may also be significant.

In AC applications the material will be continuously cycled from being magnetized in one direction to the other throughout the period of operation e.g. a power supply transformer. A high permeability will be desirable for each type of application but the significance of the other varies. The important consideration is how much energy is lost in the system as the material is cycled around its hysteresis loop. The energy loss can originate from three different sources:

i.   Hysteresis loss; which is related to the area contained within the hysteresis loop

ii. Eddy current loss, which is related to the generation of electric current in the magnetic material and the associated resistivelosses and

iii. Anomalous loss, which is related to movement of domain walls within the material.

2.2.2 Soft Ferrites

Soft ferrites are those that can be easily magnetized or demagnetized. These are characterized by low coercive forces and high magnetic permeabilities. The low coercivity means the materials magnetization can easily reverse direction without dissipating much energy(hysteresis losses), while the materials high resitivity prevents eddy currents in the core, another source of energy loss, the generally exhibit small hysteresis losses. At high frequency metallic soft magnetic materials simply cannot be used due to the eddy current losses. Therefore soft ferrite, which is ceramic insulators, becomes the most desirable material. These materials are ferromagnetic with a cubic crystal structure and the general composition $MO.Fe_2O_3$ where M is a transition metal such as nickel, manganese, magnesium, zinc, cobalt or cadmium. The magnetically soft ferrites first came into commercial production in 1948. Additionally, part of the family of soft ferrite are the microwave ferrites e.g.Ytrium iron garnet .These ferrite are used in the frequency range from 100 MHz to 500GHz. For waveguides for electromagnetic radiation and in microwave device such as phase shifters. Application of soft ferrite include: cores for electro-magnets, electric motors, transformers, generators, and other electrical equipment.

2.2.3 Hard Ferrites

Hard ferrites are difficult to magnetized or demagnetized. Hard magnets are characterized by high remanent inductions and high coercivities. They generally exhibit large hysteresis losses. Hard ferrite referred to as permanent magnets retain their magnetism after being magnetized. Hard ferrite likes Ba-ferrite, Sr-ferrite, Pb-ferrite are used in communication device operating with high frequency currents because of their high resistivity, negligible eddy currents and lower loss of energy due to Joule heating and hysteresis. These are found useful in many applications including fractional horse-power motors, automobiles, audio- and video-recorders, earphones, computer peripherals, and clocks. According to the crystallographic structures ferrite fall into three categories.

(i) Cubic ferrites of spinel type

(ii) Cubic ferrites of garnet type and

(iii) Hexagonal Ferrites.

2.2.4 Cubic Ferrite with Spinel Structure

Cubic ferrites are said to have the spinel structure and are sometimes called ferrospinels, because their crystal structure is closely related to that of the natural mineral spinel. The cubic ferrite has the general formula $MO.Fe_2O_3$, where M is one of the divalent cations of the transition elements such as Mn, Ni, Mg, Zn, Cd, Co etc. A combination of these ions is also possible and it can named as solid solution of two ferrites or mixed spinel ferrites. Generally, M represent a combination of ions which has an average valency of two. The trivalent Iron ion in $MO.Fe_2O_3$ can partially be replaced by another trivalent in such as Al^{+3} or Cr^{+3}, giving rise to mixed crystals. The structure of ferrite is derived from the mineral $MgAl_2O_4$ determined by Bragg [2.9].

$$AB_2O_4$$

⊗ A   ⊙ B   ◯ o
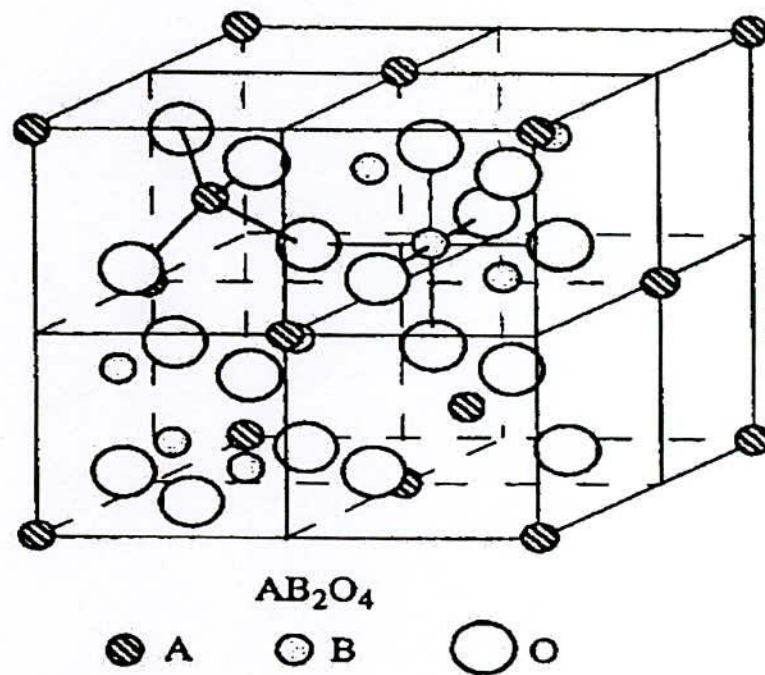
Fig. 2.4 Schematic of two sub cells of a unit cell of the spinel structure, showing octahedral and tetrahedral sites.

21

The crystal structure of ferrite is based on a face-centered cubic lattice of the oxygen ions. Each unit cell contains eight formula units. Therefore there are $32O^-$ anions $16Fe^{3+}$ cations and $8 Me^{2+}$ cations in the cell and the lattice constant is rather large of the order of 8.50 in each unit cell there are 64 tetrahedral or A- sites and 32 octahedral or B- site .These site are so named because they are surrounded by four and six oxygen ions at equal distances respectively.

The lattice characteristics of a spinel include a face centre cubic (FCC) site for the oxygen atoms and two cationic sites occupying A and B-sites [2.10, 2.12]. In a spinel, there are 64 A-sites, 32 B-sites, and 32 oxygen sites in a unit cell. Due to their exchange coupling, spinel ferrites are ferrimagnetically aligned where all of the moments of A-sites 34 are aligned parallel with respect to one another while moments of A and B-sites are antiparallel to each other. The charge neutrality requires the presence of the cations within the structure to counter balance the charge of these oxygen anions. These cations rest on two types of interstitial sites to preserve the charge neutrality namely A and B-sites. The magnetic properties of spinel ferrites are generally influenced by composition and cation distribution. Variation of cation distribution between the cationic sites leads to different electrical and magnetic properties even if the composition of the spinel is the same. The distribution of cations over A and B-sites is determined by their ionic radius, electronic configuration and electrostatic energy in the spinel lattice [2.8]. The octahedral sites are larger than the tetrahedral sites, thus, the divalent ions are localized in the octahedral sites whereas trivalent ions are in the tetrahedral sites [2.13]. Each type of lattice site will accept other metal ions with a suitable, 0.65 - 0.80Å at B-sites and 0.40 - 0.64Å at A-sites.

2.2.5 Cation Distribution in spinels

The cation distribution in the spinel $Me^{2+}Me^{3+}O_4$ can be as follows [2.13, 2.14]

2.2.5.1 Normal Spinel Structure

The divalent cation (Me^{2+}) are in tetrahedral A-sites and two trivalent (Fe^{3+}) cations are in octahedral B- site which is represented as $(Me^{2+})_A[Fe^{3+}Fe^{3+}]_BO_4$. Both zinc and cadmium ferrite have this structure and they are both magnetic i.e. paramagnetic

22

2.2.5.2 Inverse Spinel Structure

In this case divalent (Me^{2+}) cations are in octahedral B-sites and the trivalent (Fe^{3+}) cations are equally divided between A and B sites (The divalent and trivalent ions normally occupy the B sites in a random fashion i.e. they are disordered) arrangement is as $(Fe^{3+})_A[Me^{2+}Fe^{3+}]_BO_4$. Iron cobalt and Nickel ferrites have the inverse structure, and they are all ferromagnetic.

2.2.5.3 Intermediate Structure

X-ray and neutron diffraction experiments and magnetization measurements show that there is a whole range of cation distribution between the normal and inverse structures. The arrangement of the from $(Fe^{3+}_{1-x}Me^{3+}_x)_A[Fe^{3+}_{1+x}Me^{2+}_{1-x}]_BO^{2-}_4$ is often referred as mixed spinel where cations in the parentheses are at (A) sites and those in the brackets are at (B) sites and x is called the inversion parameter. The extreme case x=1 corresponds to the normal spinel structure, and x=0 corresponds to the inverse structure 0<x<1 for intermediate used commercially are mixed ferrite [2.15].

The factor affecting the cation distribution over A and B sites are as follows [2.14, 2.16]

- The size of the cations
- The electronic configuration of cations
- The electronic energy
- The saturation magnetization of the lattice

Smaller cations (trivalent ions) prefer to occupy the A-sites. The cations have special preference for A and B sites and the preference depends on the following factors:

- Ionic radius
- Size of interstices
- Temperature
- Orbital preference for the specific coordination.

23

The preference of cations is according to Verway- Heilmar scheme [2.16, 2.17]

- ions with strong preference for A-sites Zn^{2+}, Cd^{2+}, Ga^{2+}, In^{3+}, Ge^{4+}.
- Ions with strong preference for B-sites Ni^{2+}, Cr^{3+}, Ti^{4+}, Sn^{4+}.
- Indifferent ions are Mg^{2+}, Al^{3+}, Fe^{2+}, Co^{2+}, Mn^{2+}, Fe^{3+}, Cu^{2+}.

Moreover the electrostatic energy also affects the cation distribution in the spinel lattice.

The cations of the smallest positive charge reside on the B-sites having six anions in surrounding i.e. the most favorable electrostatic conduction. It has been observed that X-ray powder diffraction, in conjunction with appropriate computational method, has enough sensitivity to determine the degree of inversion δ, and oxygen positional parameter U. A difference of one electron between two different cations can be enough to render them distinguishable.

2.3   Magnetic properties of Ferrites

Ferromagnetic materials are characterized by a high magnetization (magnetic moments per unit volume) which can be achieved even in polycrystalline materials by the application of relatively small magnetic field. In a ferromagnetic material the individual atomic (atom with partially filled 3d or 4f shells) or ionic moment arising from unpaired spins are permanent and interact strongly with one another in a manner which tends to cause parallel alignment of the nearby moments.

The moments of a large number of neighboring ions are thus parallel, even in the absence of an applied field. These regions or domains, of spontaneous magnetization exit in both single and polycrystalline materials, and within a domain the value of the saturation magnetization, M_s is the maximum that can be achived in the material at interaction lies in the so-called quantum mechanical exchange [2.19-2.20], but in a phenomenological description of magnetism, it is possible to regard that the obliging forces are arising from an internal magnetic field called the molecular field [2.21]. Weiss assumed that spontaneous magnetization properties disappear at the Curie point when the thermal energy is equal to the energy of the individual ionic moment in Weiss induction field. then,

24

$$B_W = KT_c + \mu B_m \,, \tag{2.3}$$

where k is Boltzmann constant, T_c is Curie temperature , μ is permeability and B_m is the Weiss molecular field. It is convenient to write $B_m = \mu_0 H$, below the Weiss molecular field H is used. Weiss assumed that the molecular field H_m was proportional to the magnetization M.

$$H_m = \gamma M \tag{2.4}$$

Where M is the magnetization in the material and γ is the constant proportionality called molecular field co-efficient.

A ferrite may be defined as the one which below a certain temperature bears a spontaneous magnetization that aries from non-parrallel arrangement of the strongly coupled atomic dipole, Ferrite is the substance consists of two sublattices with magnetic moments of one sublattice tending to antiparallel to those of other. When the sublattice magnetization are not equal these will be a net magnetic moment. The term ferromagnetism has been used in broad sense in order to include the materials with more than two sublattice and with other spin configuration , such as triangular or spinel configuration. It is usually assumed that a ferromagnetic material has an appreciable net magnetization although no precise definition of the term appreciable has been given. The two sublattics are denoted by A and B-sites are denoted by A and B. If the magnetic moments of the ions at A and B-sites are unequal, this inequality may be due to:

      i. Presence of elements in different ionic states, e.g. Fe^{+3} and Fe^{+2}

      ii. Different elements in the same or different ionic states, e.g. Fe^{+3} and Co^{2+}

      iii. Different crystalline field acting at two sites

The competition between the forces on the B spins may lead to the triangular configuration.

2.3.1 Magnetic Dipole

The Earth's magnetic field which is approximately a magnetic dipole. However, the N - pole and S - pole are labeled here geographically, which is the opposite of the convention for labeling the poles of a magnetic dipole moment.

In physics, there are two kinds of **dipoles**:

(i)   An **electric dipole** is a separation of positive and negative charges. The simplest example of this is a pair of electric charges of equal magnitude but opposite sign, separated by some (usually small) distance. A permanent electric dipole is called an electret.

(ii) A **magnetic dipole** is a closed circulation of electric current. A simple example of this is a single loop of wire with some constant current flowing through it [2.22, 2.23].

2.3.2 Magnetic Field

The **magnetic field (B)** is a vector field. The magnetic field vector at a given point in space is specified by two properties:

(i)   Its direction, which is along the orientation of a compass needle.

(ii)   Its magnitude (also called *strength*), which is proportional to how strongly the compass needle orients along that direction.

The units for magnetic field strength **H** are ampere/meter. A magnetic field strength of 1 ampere/meter is produced at the center of a single circular conductor with a one meter diameter carrying a steady current of 1 ampere.

2.3.3   Magnetic Moment

A magnet's **magnetic moment** (μ) is a vector that characterizes the magnet's overall magnetic properties. For a bar magnet, the direction of the magnetic moment points from the magnet's south pole to its north pole, and the magnitude relates to how strong and how far apart these poles are. In SI units, the magnetic moment is specified in terms of A-m^2. A magnet both produces its own magnetic field and it responds to magnetic fields. The strength of the magnetic field it produces is at any given point proportional to the magnitude of its magnetic moment. In addition, when the magnet is put into an external magnetic field, produced by a different source, it is subject to a torque tending to orient the magnetic moment

26

parallel to the field. The amount of this torque is proportional both to the magnetic moment and the external field. A magnet may also be subject to a force driving it in one direction or another, according to the positions and orientations of the magnet and source. If the field is uniform in space, the magnet is subject to no net force, although it is subject to a torque.

2.3.4 Magnetic Moments of Ferrites

The determination of saturation moments of simple ferrites having the formula $Me^{+2}Fe^{+3}O_4$, Where, Me^{2+} is the divalent cation, such as Cu, Co, Ni, Fe, Mn etc agrees with the Neel's collinear model. The A-B interaction is much larger than the A-A and B-B interactions respectively. The two kinds of magnetic ion from two sublattices each saturated and magnetized in opposite direction at absolute zero.

Table-2.1 Experiment and calculated saturation moments of spinels

Ferittes	$M(\mu_B)$	$2S_{Me}^{+2}$ (cal)
$Mn.Fe_2O_4$	5-4.4	5
$FeFe_2O_4$	4.2-4.08	4
$CoFe_2O_4$	3.3-3.9	3
$NiFe_2O_4$	2.3-2.40	2
$CuFe_2O_4$	1.3-1.37	1
$MgFe_2O_4$	1.1-o.86	1.1
$Li_{0.5}Fe_{2.5}O_4$	2.6	2.5

Saturation magnetic moments of some selected spinels[2.24] are listed in the Table(2.1), the first six ferrites are the inverse type i.e $Fe^{3+}[Me^{2+}Fe^{3+}]O_4$. The magnetic moments of two Fe^{+3} cations compensate each other and the ferrite magnetization becomes equal to $M_{Me}^{+2} = 2S_{Me}^{+2}$.

These values are listed in the Table (2.1) and the experimental and calculated shows good agreement, except Cobalt and copper series. The Li ferrite is also completely inverse and its moment is calculated based on the cation distribution Fe $[Li_{0.5}Fe_{2.25}]$ O_4 is equal to 2.5 (μ_B); per molecule is in good agreement with the measured value. These are two possible reasons

27

for the discrepancies observed between calculated and observed magnetic moments are mentioned in the Table (2.1).

i. The orbital moments of the divalent ions may not be neglected; the crystal field effects therefore become important.

ii. The cation distribution must be taken into account.

2.4 Magnetic Exchange Interaction

In physics, the exchange interaction is a quantum mechanical effect without classical analogue which increases or decreases the expectation value of the energy or distance between two or more identical particles when their wave functions overlap. The exchange interaction is the mechanism responsible for ferromagnetism, among other consequences.

The electron spin of the two atoms S_i and S_j which is proportional to their product .The exchange energy can be written as universally in terms of Heisenberg Hemiltonian [2.25]

$$H = -\sum J_{ij} S_i.S_j = -\sum J_{ij}S_iS_j \cos\varphi, \qquad (2.5)$$

where J_{ij} is the exchange integral represents the strength of the coupling between the spin angular momentum i and j and φ is the angle between the spins. It is well known that the favored situation is the one with the lowest energy and it turns out that there are two ways in which the wave functions can combine there are two possibilities for lowering the energy by H.

These are:

i. If J_{ij} is positive and the parallel spin configuration ($\cos\varphi = 1$) the energy is minimum.

ii. If J_{ij} is negative and the spins are antiparallel ($\cos\varphi = -1$) energy is maximum. This situation leads to antiferromagnetism.

28

2.4.1 Superexchange Interaction

The magnetic interaction in magnetic oxide cannot be explained on the basis of direct interaction because of the following facts:

- The magnetic ions are located too far apart from each other shielded by the non magnetic anion i.e., oxygen. This is because these are not band type semiconductor [2.18] .The non magnetic anion such as oxygen is situated in the line joining magnetic cations

- Superexchange interaction appears, i.e. indirect exchange via anion p-orbital that may be strong enough to order the magnetic moments. The P orbital of an anion (center) internet with the d orbital of the transitional metal cations.

Three major types of superexchange interactions in spinel ferrites are:J_{AB}, J_{BB}, and J_{AA}.

Ferromagnetic oxides are one kind of magnetic system in which there exist at least two in equivalent sublattice for the magnetic ions. The antiparallel alignment between these sub lattices (ferrimagneting ordering) may occur provided the intersublattice (J_{AB}) exchange interaction are antiferromagnetic and some requirements concerning the signs and strength of the intra-sublattice (J_{AA}, J_{BB}) exchange interactions are fulfilled. Since usually in ferromagnetic oxides the magnetic cations are surrounded by bigger oxygen anions (almost excluding the direct overlap between cation orbital) magnetic interactions occur via indirect superexchange interactions depends both on the electronic structure of the cations and their geometrical arrangement [2.24]. In most of ferromagnetic oxides the crystallographic and electronic structure give rise to antiferromagnetic inter and intra-sublattice competing interactions.

The magnitude of negative exchange energies between two magnetic ions M and M' depend upon the distances from these ions to the oxygen ion O^{2-} via which the superexchange take place and on the angle M-O-M' (φ). According to the superexchange theory the angle $\varphi = 180°$ gives rise to the greatest exchange energy, and this energy decrease very rapidly as the distance between the ions increases. The magnetic properties of the spinel ferrites are

governed by the type of magnetic ions residing on the A and B-sites and the relative strengths of the inter-sublattice (J_{AB}) and intra-sublattice (J_{AA}, J_{BB}) exchange interactions.
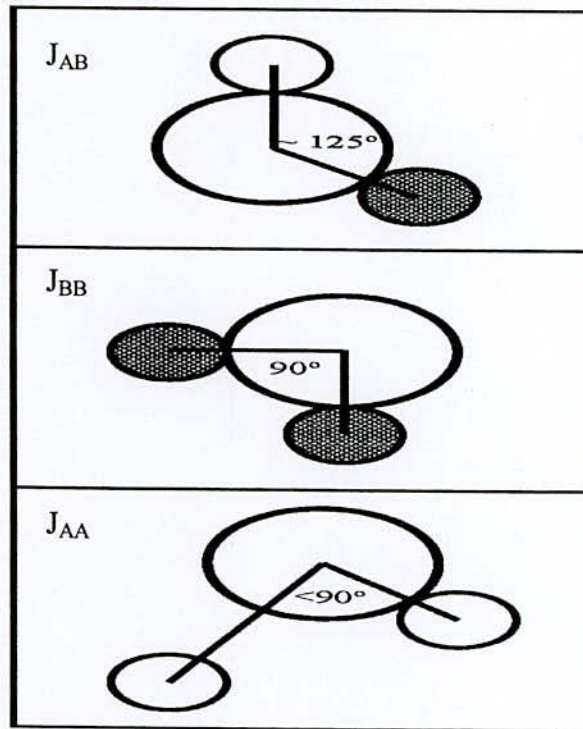
Fig. 2.5 Three major types of superexchange interactions in spinel ferrites are as follows: J_{AB}, J_{BB} and J_{AA}. The small empty circle is A-site, the small solid circle is B-site, and the large empty circle is oxygen anion.

2.4.2 Neel's Collinear Model of Ferrites

Soft ferrites belong to the cubic spinal structure. According to Neel's theory, the magnetic ions are assumed to be distributed among the tetrahedral A and octahedral B-sites of the spinel structure. The magnetic structure of such crystals essentially depends upon the type of magnetic ions residing on the A and B sites and the relative strengths of inter (J_{AB}) and intra-sublattice exchange interactions (J_{AA}, J_{BB}). Negative exchange interactions exist between A–A, A–B and B–B ions. When A–B antiferromagnetic interaction is the dominant one, A and B-sublattices will be magnetized in opposite direction below a transition temperature.

30

When the A–A (or B–B) interaction is dominant, Neel found that the above transition will not take place and he concluded that the substance remains paramagnetic down to the lower temperature. But this conclusion was not correct, as in the presence of strong interactions, some kind of ordering may be expected to occur at low temperature as claimed by Yafet and Kittel [2.26]

2.4.3 Non-Collinear Model of Ferrimagnitism

In general, all the interactions are negative (antiferromagnetic) with $|J_{AB}| >> | J_{BB}| > |J_{AA}|$. In such situation, Collinear or type of ordering is obtained. Yafet and Kittel [2.26] theoretically considered the stability of the ground state of magnetic ordering, taking all the three exchange interactions into account and concluded that beyond a certain value of J_{BB} / J_{AB}, the stable structure was a non-collinear triangular configuration of moment where in the B-site moments are oppositely canted relative to the A-sites moments. Later on Leyons et.al[2.27] extending these theoretical considerations showed that for normal spinel the loest energy correspond to conical spinel structure for the value of $3J_{BB}S_B$ /2 $J_{AB}S_A$ greater than unity. Initially one can understand why the collinear Neel structure gets perturbed when J_{BB}/J_{AB} increases. Since all these three exchange interactions are negative(favoring anti ferromagnetic alignment of moments) the inter- and intra-sublattice exchange interaction complete with each other in aligning the moment direction in the sublattice. This is one of the origins of topological frustration in the spinel lattice. By selective one can effectively decreases the influence of J_{AB} vis-a vis J_{BB} and thus perturb the Neel ordering.

It was found that ferrites which have been substituted sufficiently wtit nonmagnetic atoms showed significant departure from Neel Collinear model. These theoretical models have been uded to explain these departures:

    (i)   a paramagnetic centre model in which a number of magnetic nearest neighbours determine whether a magnetic ion remains paramagnetic or contributes to the magnetization.

    (ii)   a uniform spin canting relative to the average magnetization and

31

(iii)   a localized canting where the canting angle of a magnetic ion spin depands on the local magnetic environment.

The discrepancy in the Neel's theory was resolved by Yafet and Kittel [2.26] and they formulated the non-collinear model of ferrimagnetism. They concluded that the ground state at 0K might have one of the following configurations:

- have an antiparallel arrangement of the spins on two sites
- consists of triangular arrangements of the spins on the sublattices
- an antiferromagnetic in each of the sites separately.

2.5   Initial Permeability of Ferrites

For application is small electronic device, the soft ferrites have somewhat poorer losses and permeabilities than the conventional Fe-Ni alloys, but have better performance than the Fe-Co and Fe-Si alloys in other respects, where the design optimization requires the lower cost of the soft ferrites, their higher induction compared to the Fe-Co, Fe-Si and the Fe-Ni at higher frequencies, the use of the soft ferrites alloys will be favored. The complex magnetic properties of initial permeability (μ_i) may be strongly affected by the presence of an electric current- particularly in ac condition. The measurement of magnetic properties as a function of frequency and its analysis by means of the complex permeability formation has recently led to the resolution of several aspects of the magnetization process [2.28-2.30]. The measurement of complex permeability gives us valuable information about the nature of the domain wall and their movements. In dynamic measurements the eddy current is very important which occur due to irreversible domain wall movements that is frequency dependent.

A large number of possible mechanisms can contribute to the magnetic loss such as local variation of exchange energy, surface detects, compositional in homogeneities, anisotropy and magnetostriction [2.31-3.32], where relative values are determined by grain size, grain orientation and thickness of the sample. The present goal of most of the recent soft ferrites research is to fulfill this requirement. Before going into the complexity of initial

permeability measurement, we discuss in short the theories and mechanism involved in frequency spectrum and initial permeability.

Initial permeability describes the relative permeability of material at low value of B (below 0.1T). The maximum value for μ_i in a material is frequency a factor of between 2 and 5 or more above its initial value. Low flux has the advantage that every ferrite can be measured at the density without risk of saturation. This consistency means that comparison between different ferrites is easy. Also, if you measure the inductance with a normal component bridge then you are doing so with respect to the initial permeability.

For high frequency applications, the desirable properly of a ferrite is the high initial permeability with low loss. The present goal of the recent ferrite researches is to fulfill this requirement: The initial permeability μ_i is defined as the derivative of induction B with respect to the initial field H in the demagnetization state

$$\mu_i = \frac{dB}{dH}\bigg|_{H\to 0, B\to 0}$$

At microwave frequency, and also in low anisotropic amorphous, dB and dH may be in different directions, the permeability thus a tensor character. In the case of amorphous material containing a large number of randomly oriented magnetic atoms the permeability will be scalar, as we have

$$B=\mu_0(H+M) \tag{2.7}$$

And susceptibility

$$\chi = dM\big/dH = \frac{d}{dH}(\frac{B}{\mu_0} - H)$$

$$\chi = \frac{1}{\mu_0}(\mu - 1) \tag{2.8}$$

The magnetic energy density

$$E = \frac{1}{\mu_0} \int H.dB \tag{2.9}$$

For time harmonic field $H=H_0 Sinwt$, the dissipation can be described by a phase difference δ between H and B.

2.5.1 Theories of Permeability

Permeability is namely defines as the proportional constant between the magnetic field induction B and applied intensity H:

$$B = \mu H \tag{2.10}$$

If a magnetic material is subjected to an AC magnetic field as given below:

$$H = H_0 e^{i\omega t} \tag{2.11}$$

Then it is observed that the magnetic flux density B experiences a delay. The delay is caused due to presence of various losses and is thus expressed as

$$B = B_0 e^{i(\omega t - \delta)} \tag{2.12}$$

Where δ is the phase angle and marks the delay of B with respect to H. The permeability is then given by

$$\mu = \frac{B}{H} = \frac{B_0 e^{i(\omega t - \delta)}}{H_0 e^{i\omega t}} \tag{2.13}$$

$$= \frac{B_0 e^{-i\delta}}{H_0} = \mu' - i\mu'' \tag{2.14}$$

$$\text{Where} \qquad \mu' = \frac{B_0}{H_0} \cos \delta \tag{2.15}$$

$$\mu'' = \frac{B_0}{H_0} \sin \delta \tag{2.16}$$

The real Part μ' of complex permeability μ as expressed in Eq^n. (2.10) represent the component of B which is in phase with H, so it corresponds to the normal permeability. If there is no losses , we should have $\mu = \mu'$, The imaging part μ'' corresponds to the part of B which is delayed by phase angle arranging up to 90° from H . The presence of such a component requires a supply of energy to maintain the alternating magnetization regardless of the origin of delay. The ratio of μ'' to μ' gives

$$\frac{\mu'}{\mu''} = \frac{\dfrac{B_0}{H_0} \sin \delta}{\dfrac{B_0}{H_0} \cos \delta} = \tan \delta \qquad (2.17)$$

This $\tan \delta$ is called the loss Factor or loss tangent. The Q-Factor or quality factor is defined as the reciprocal of this loss factor, i.e

$$Q = \frac{1}{\tan \delta} \qquad (2.18)$$

And the relative quality factor $= \mu_i Q$ \qquad (2.19)

The behavior of μ' and μ'' versus frequency is called the permeability spectrum. The intial permeability of a ferromagnetic or ferrimanetic substance is the combined effects of the wall permeability and rotational permeability mechanisms.

2.6   Magnetization Processes

A review of magnetization process, namely the response of ferro-or ferri magnetic material (bulk) to an applied field with a semi-microscopic approach is presented. In ferro- or ferri-magnetic material, the magnetization curves, especially in low magnetic fields differ widely from sample to sample and as a function of the magnetic history of the sample i.e, of the previous fields which have been successively applied.

2.6.1   Magnetization Curve

For un magnetized bulk material, there is a zero net magnetic moment. It can be predicted that there will be an infinite number of degree of magnetization between the unmagnetized and saturation condition, when the material is subjected to an external magnetic field. These extreme situation correspond respectively to random orientation of domains complete alignment is one direction with elimination of domain walls. If we start with the applied magnetic field, the bulk material will be progressively magnetized by the domain dynamics. The magnetization of the sample will follow the course as shown in Fig-2.7(2.33).

35

The slope from the origin to a point on the curve or the ratio M/H is defined as magnetic susceptibility. The curve is called mgnetization curve. This curve is greatly perceived as being made of three major portions.
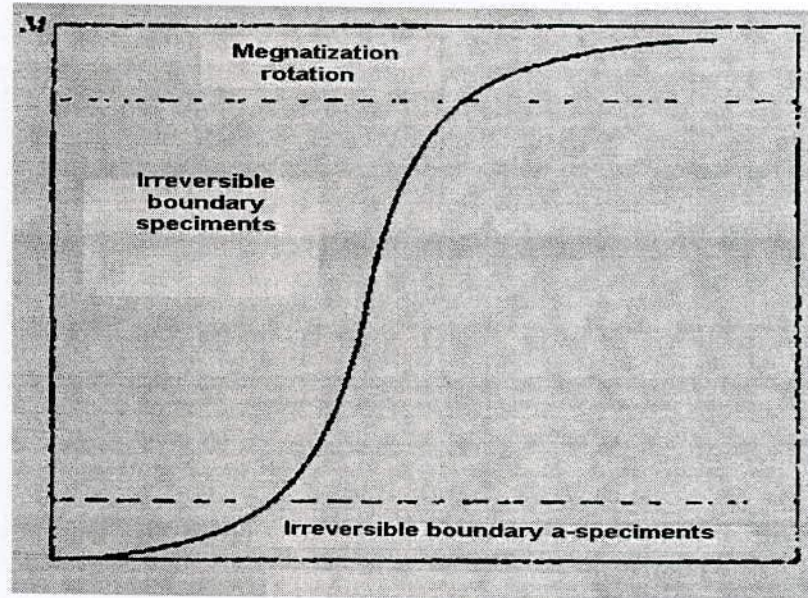
Fig 2.6: Domain dynamics during various parts of the magnetization curve.

The first, the lower section, is in the initial susceptibility region and is characterized by reversible domain wall movements and rotations. By reversible means that after the magnetization slightly with an increase in field the original magnetization conditions can be reversed if the field is reduced to initial value. The combination of the displacement walls to an initial permeability is entirely dependent on the short of material studied.

In the second stage magnetization curve, if the field is increased, the intensity of the magnetization increases more drastically, is called the irreversible magnetization range. This range is obtained mainly by the irreversible domain wall motion from one stable state to another.
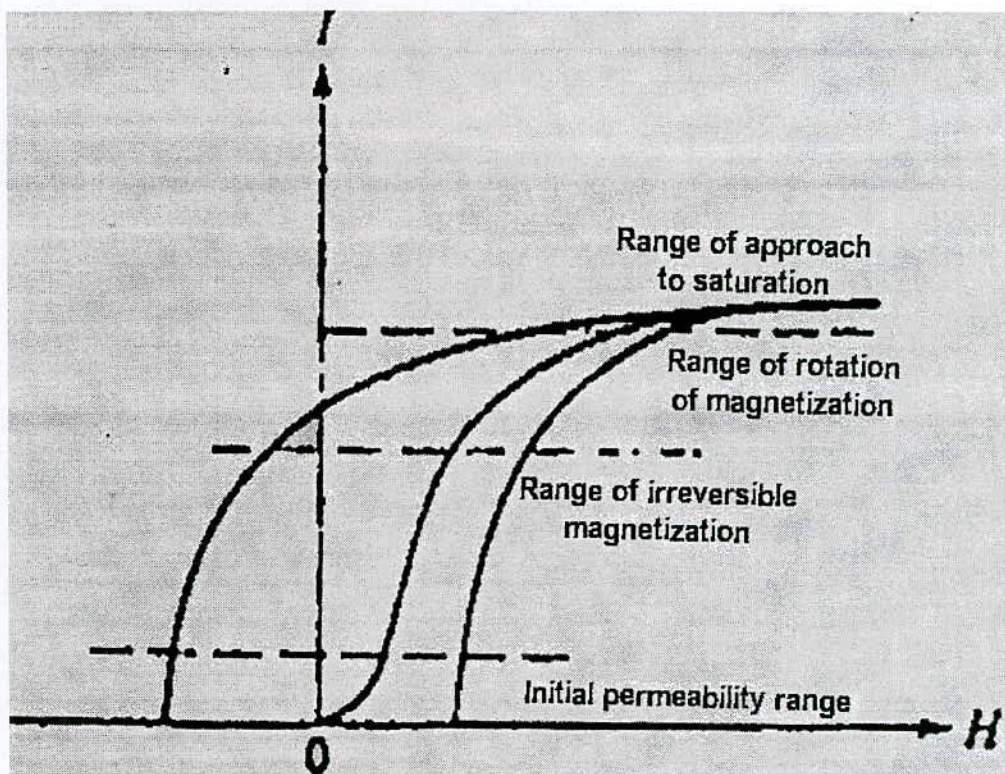
Fig-2.7: Magnetization curve and the classification of magnetization mechanism.

If the field is increased further, the magnetization curve becomes less steep and its process become reversible once more. In the third section of magnetization take place by rotation magnetization. This range is called rotation magnetization range. Beyond this range the magnetization gradually approaches to saturation magnetization shown in Fig-2.8.

2.6.2   Magnetization and Temperature

The influence of temperature on magnetic material can be determinate in the magnetic properties of dose materials. Rising the temperature of a solid, result in the increase of the thermal vibrations of atoms, with this the atomic magnetic moments are free to rotate. This phenomenon the atoms tend to randomize the directions of any moments that may be aligned [2.34]. With increasing temperature, the saturation magnetization diminishes gradually and

37

abruptly drops to zero at what called the Curie temperature (T_c). The Curie point of a ferromagnetic material is the temperature above which it loses its characteristic ferromagnetic ability. At temperatures below the Curie point the magnetic moments are partially aligned within magnetic domains in ferromagnetic materials. As the temperature is increased from below the Curie point, thermal fluctuations increasingly destroy this alignment, until the net magnetization becomes zero at and above the Curie point.
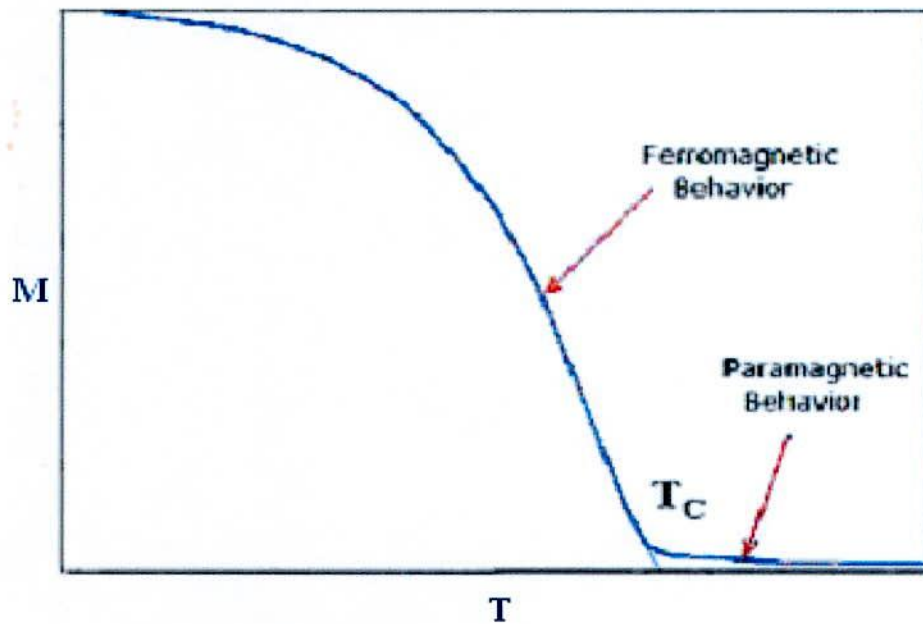
Fig. 2.8 Typical M-T curve for magnetic material.

Above the Curie point, the material is purely paramagnetic. At temperatures below the Curie point, an applied magnetic field has a paramagnetic effect on the magnetization, but the combination of paramagnetism with ferromagnetism leads to the magnetization following a hysteresis curve with the applied field strength.

2.6.3 Hysteresis

Magnetic hysteresis is an important phenomenon and refers to the irreversibility of the magnetization and demagnetization process, when a material shows a degree of irreversibility it is known as hysteretic. When a demagnetized ferromagnetic material is placed in as applied

magnetic field grows at the expanse of the other domain wall. Such growth occurs by motion of the domain walls .Initially domain wall motion is reversible, and if the applied field is removes the magnetization will return to the initial demagnetized state. In this region the magnetization curve is reversible and therefore does not show hysteresis. The crystal will contain imperfections which the domain boundaries encounter during their movement. These imperfections have an associated magnetostatic energy when a domain wall intersects the crystal imperfection this magnetostatic energy can be eliminated as closure domains from this pins the domain wall to the imperfection as it if a local energy minima.

A great deal of information can be learned about the magnetic properties of a material by studying its hysteresis loop. A hysteresis loop shows the relationship between the induced magnetic flux density (**B**) and the magnetizing force (**H**). It is often referred to as the B-H loop. An example hysteresis loop is shown below.
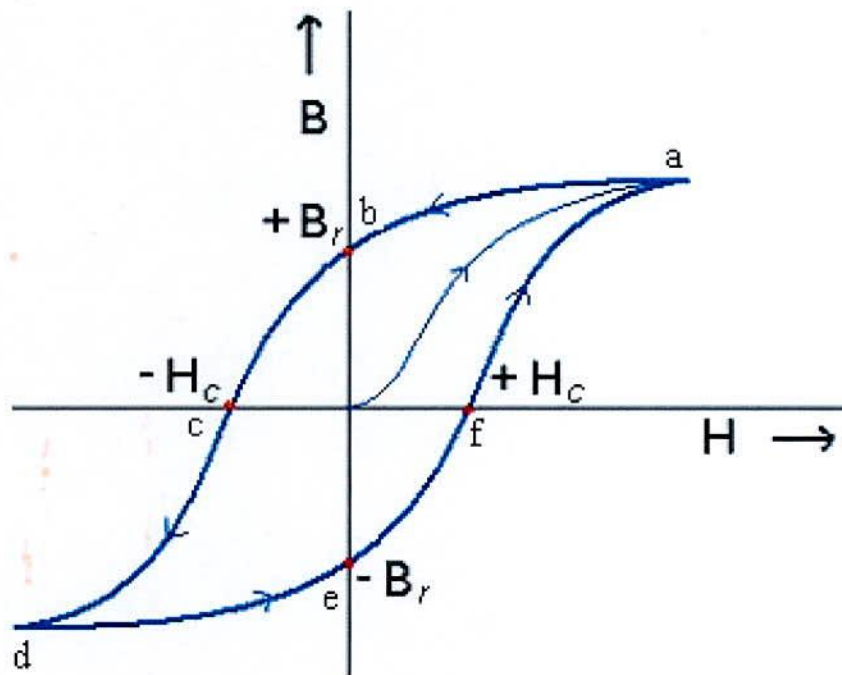
Fig. 2.9 Magnetic hysteresis loop.

The loop is generated by measuring the magnetic flux of a ferromagnetic material while the magnetizing force is changed. A ferromagnetic material that has never been previously magnetized or has been thoroughly demagnetized will follow the dashed line as **H** is increased. As the line demonstrates, the greater the amount of current applied (+**H**), the stronger the magnetic field in the component (+**B**). At point "a" almost all of the magnetic domains are aligned and an additional increase in the magnetizing force will produce very little increase in magnetic flux. The material has reached the point of magnetic saturation. When **H** is reduced to zero, the curve will move from point "a" to point "b". At this point, it can be seen that some magnetic flux remains in the material even though the magnetizing force is zero. This is referred to as the point of retentivity on the graph and indicates the remanence (B_r) or level of residual magnetism in the material. (Some of the magnetic domains remain aligned but some have lost their alignment.) As the magnetizing force is reversed, the curve moves to point "c", where the flux has been reduced to zero. This is called the point of coercivity on the curve. (The reversed magnetizing force has flipped enough of the domains so that the net flux within the material is zero.) The force required to remove the residual magnetism from the material is called the coercive force (H_c) or coercivity of the material. As the magnetizing force is increased in the negative direction, the material will again become magnetically saturated but in the opposite direction (point "d"). Reducing **H** to zero brings the curve to point "e." It will have a level of residual magnetism equal to that achieved in the other direction. Increasing **H** back in the positive direction will return **B** to zero. Notice that the curve did not return to the origin of the graph because some force is required to remove the residual magnetism. The curve will take a different path from point "f" back to the saturation point where it with complete the loop.

From the hysteresis loop, a number of primary magnetic properties of a material can be determined.

(i) **Retentivity**, a measure of the residual flux density corresponding to the saturation induction of a magnetic material. In other words, it is a material's ability to retain a certain amount of residual magnetic field when the magnetizing force is removed after achieving saturation. The value of **B** at point "b" on the hysteresis curve.

40

(ii) **Residual Magnetism** or **Residual Flux**, the magnetic flux density that remains in a material when the magnetizing force is zero. Residual magnetism and retentivity are the same when the material has been magnetized to the saturation point. However, the level of residual magnetism may be lower than the retentivity value when the magnetizing force did not reach the saturation level.

(iii) **Coercive Force**, the amount of reverse magnetic field which must be applied to a magnetic material to make the magnetic flux return to zero. The value of **H** at point "c" on the hysteresis curve.

2.7   Mössbauer Spectroscopy

Since Mössbauer spectroscopy involves the resonant absorption of gamma radiation in the nucleus, it serves as a local prove. In the context of magnetism one learns about the internal magnetic field (and hence magnetic moment) at the local sites of the resonant nucleus. Careful analysis can also fell about the relative orientation of the magnetic moments. Mössbauer spectroscopy yields information on the magnetic properties of individual atoms rather than on assemblies of atoms as in conventional magnetization measurements. Mössbauer spectroscopy is used for the identification of magnetic field distribution of magnetic atoms in magnetic materials by the evaluation of the collected spectra. This is a very useful technique for studying the nature and number of nearest magnetic neighbors in magnetic alloys.

Mössbauer spectroscopy has also been used to determine the average direction of magnetization by using the well known fact that for the ^{57}Fe, The intenties of the six lines of the hyperfine spectra have an area ratio 3: Z: 1:1: Z: 3, Where $Z = \dfrac{4}{1 + \cot^2 \theta}$, θ being the angle between the direction of magnetic field at the nucleus and the direction of γ-ray emission [3.35]. In ^{57}Fe the strength of this magnetic field is H=33T [3.36] at room

temperature. The value Z varies from 0 for the axis magnetization in the sample phase to 4 for the axis of magnetization in sample plane.

Mössbauer spectroscopy is a technique which enables these energy levels to be investigated since the recoil free processes arising from the Mössbauer effect lead to the resonant absorption of γ-rays with an extremely precise energy. Hence, small changes in energy levels because of the hyperfine interactions between the nuclus and surrounding changes can be detected with the technique. A Mössbauer spectrum is characterized by the number, shape, position and relative intensity of the various absorption lines.

2.7.1   Mössbauer Effect

Nuclear transitions emitting gamma radiation, which are not preceded by phonon transitions. These zero-phonon gamma transitions, take place between the excited and ground state nuclear energy levels of the nucleus which is bound in a solid matrix as reported by Mössbauer [2.37]. Therefore, the nucleus is no longer isolated, but fixed with the lattice. In this situation the recoil energy may be less than the lowest quantized lattice vibration energy and consequently the γ-ray energy may be emitted without any loss of energy due to the recoil of nucleus. This is known as the Mössbauer effect. The frequency spread of such transitions which occure between nuclear excited states are solely determined by the energy uncertainty of the nuclear excited state involved. The Mössbauer γ-rays has a finite spread in energy which is quantized by a line width, defined as the full width at half maxima of maximum intensity and related to to the life time of the nuclear excited state. The line width restricts the number of isotopes in which the Mössbauer effect is observed.

The important parameters which can be measured by using Mössbauer spectroscopy are describing the interaction of the nucleus with the surrounding atomic electrons. These parameters give information about the nature of the chemical bonds, electric field gradient and magnetic ordering moments. The Hamiltonian for the interaction between the nucleus and the surrounding changes may be written as [2.38]

$$H=E_0+M_1+E_2+\dots\dots\dots\dots\dots\dots\dots \qquad (2.20)$$

42

Where E_0 represents electric monopole coulombing interaction between nuclear charges and the electron clouds which affects the nuclear energy levels, M_1 refers to magnetic dipole interaction between nuclear magnetic moments and the effective magnetic field at the nucleus and E_2 represents the electric quadrupole interaction between electric field gradient at the nucleus and the electric quardrupole moment of the nucleus. Higher order terms are usually very small and can be neglected.

This is most often achieved by oscillating a radioactive source with a velocity of a few mm/s and recording the spectrum in discrete velocity steps. Fractions of mm/s compared to the speed of light (3×10^{11}mm/s) gives the minute energy shifts necessary to observe the hyperfine interactions. For convenience the energy scale of a Mössbauer spectrum is thus quoted in terms of the source velocity, as shown in Fig2.11.
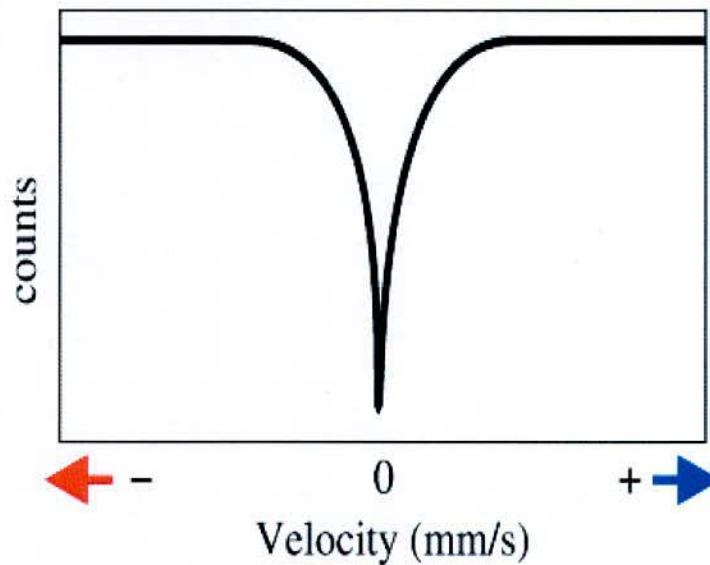
Fig2.10: Simple spectrum showing the velocity scale and motion of source relative to the absorber

In Fig2.11 the absorption peak occurs at 0mm/s, where source and absorber are identical. The energy levels in the absorbing nuclei can be modified by their environment in three main ways: by the Isomer Shift, Quadrupole Splitting and Magnetic Splitting.

In the above discussion we found that due to recoil of the emitting or absorbing nuclei, resonance absorption is not possible. But it is possible if the emitting and absorbing nuclei are bound in a crystal lattice. Then the whole crystal recoils, instead of just a single atom recoiling. In situation, the mass is so large that the recoil energy is negligibly small compared with $E_f - E_i$. Thus resonance absorption may occur resulting in the so called Mössbauer effect, which was observed for the first time in 1958 by German Physicist R.L. Mössbauer.

In solid as long as the energy of recoil of a nucleus during the emission or absorption of gamma quanta is less than the binding energy between atoms in crystal, there is no transfer of momentum to the individual atoms. However, there is a finite probability of the nuclear transition energy being transferred to atomic oscillators exciting the phonons. When the excitations of phonons does not take place , both the energy and momentum are distributed between the gamma quantum and the whole crystal as a unit making the recoil energy negligibly small as compared to the width of the γ-line. This makes possible to observe recoilless (zero-phonon) γ-resonance absorption.

2.7.1.1 Isomer Shifts

This shift, first observed in Mössbauer experiment by Kistner and Sunyar (1960) [2.37] is on account of the difference in the nuclear volume of the ground and excited states and the difference between the electron densities at the Mössbauer nucleus in different materials. The nuclear excited and ground states in the absence of hyperfine interaction except the electric monopole interaction are un split but their centers of gravity and shifted not the same source and absorber by an amount known as the isomer shift.

44

Isomer shift is not an absolute quantity since it represents the difference between the electric monopole interaction in the source and the absorber. Therefore, the zero velocity of the spectrum of a standard absorber is determined first and the isomer shifts of different absorbers expressed relative to that of the standard absorber. Thermal vibration of the nuclei will also shift the γ-ray energy. As these thermal vibrations are temperature dependent, the temperature of both the source and absorber should be considered when quoting isomer shifts.

Measurement of isomer shifts have been performed in a variety of compounds. Expression in velocity until the isomer shift is given by

$$v = c\ [\psi(0)_s^2 - \psi(0)_A^2] \tag{2.21}$$

where $\psi(0)^2$ is the difference of electron densities at the nuclear sites for the sources and absorbers used and c is a constant characteristic for the particular γ-transition and is independent of the chemical environment.

The IS arises from the fact that aa nucleus has a finite volume and S-electrons spend a fraction of their time inside the nuclear region. The nuclear charge thus interacts electrostatically with the S-electron charge. As a result of this interaction the nuclear energy levels get shifted by a small amount, the shift depends upon the chemical environment. Although, we cannot measure change directly, it is possible to compare values by mean of a suitable reference which can be either the γ-ray source or another standard absorber. The observed range of IS is within an order of magnitude of the natural line width of the transition i.e, 10^{-8} to 10^{-9} ev.

Let us consider that the absorber and source lattice are different is chemical composition so that electronic wave function at nuclei differ in the two lattices. This would cause differential shifts in the energy of the γ-rays from the source nuclei and the absorber nuclei. This difference in the energy can be written as [2.39]

$$IS = \Delta E_A - \Delta E_S$$

$$= (\frac{2\pi}{5})Ze^2(R_{ex}^2 - R_g^2)[|\psi(0)|_A^2 - |\psi(0)|_S^2]$$

$$= (\frac{2\pi}{5})Ze^2R^2(\frac{dR}{R})[|\psi(0)|_A^2 - |\psi(0)|_S^2] \qquad (2.22)$$

Where $dR = R_{ex} - R_g$ and $R = \frac{R_{ex} + R_g}{2}$, here R_{ex} and R_g are the nuclear radii of the excited and ground states, R is the average charge radius and $|\psi(0)|_A$ and $|\psi(0)|_S$ refer to the electron densities at the nuclei of absorber and the source respectively.

The expression shows that the IS is the product of two parameters

(i) dR/R , a nuclear parameter and

(ii) $|\psi(0)|_A^2 - |\psi(0)|_S^2$ an atomic or chemical parameter.

IS can be positive or negative, depending on whether dR/R is positive or negative, and

$$|\psi(0)|_A^2 > |\psi(0)|_S^2 \text{ or } |\psi(0)|_A^2 < |\psi(0)|_S^2$$

IS provides important information concerning the nature of the chemical bond because the outer electrons(valence electrons) would be must effectd by changes in chemical surrounding and consequently the changes in the outer S-electron densities would contribute must to IS. There is well defined range for IS for high spin complex. For an atom, the IS relative to iron metal are 0.8 to 1.5 mm/s for divalent iron and 0.2 to 0.5mm/s for trivalent iron[2.39-2.41]. A large change in IS is observed when the co-ordination number changes from 6 to 4. IS for octahedral Fe^{+3} is high spin complexes because in octahedral site co-ordination number is 6 whereas in tetrahedral site the co-ordination number is 4. As we know, increasing the sheared electrons at octahedral Fe^{+3} nucleus causing more IS at octahedral Fe^{+3} site that at tetrahedral Fe^{+3} site.

2.7.1.2 Electric Quadruple Splitting

The interaction of the quadruple moment of a nucleus with an electric field gradient (EFG) established at its site by the surrounding environment causes quadrupole splitting in nuclear levels [2.42-2.43]. An oblate (flattened) nucleus has a negative quadrupole moment while a prolate (elongated) one has a positive moment. Nuclei whose spin is up or ½ are spherical symmetric and have zero quadrupole moment and thus the ground state of ^{57}Fe with I=1/2 does not exhibit quadrupole splitting. While determining the isomer shift; it is assumed that the nuclear charges distribution is spherical. However, nuclei in states with a nuclear angular moment which are greater than ½ have in general non-spherical charge distribution which are characterized by a nuclear quadrupole moment. When the nuclear quadrupole moment experiences an asymmetric electric field produced by the arrangement of asymmetric electronic charge distribution and characterized by the electric field gradient (EFG),an electric quadrupole interaction occurs which gives rise to a splitting of the nuclear energy levels corresponding to different alignments of the quardrupole moment with respect to the principal axis of the nuclear quadrupole is fixed for a certain nucleus and hence the EFG can be determined from the Mossbauer Spectrum.

The valance electrons of the Mossbauer atoms and the asymmetry in the electronic structure contribute to the EFG and this is known as valence contributions. Lattice contribution is due to the asymmetric arrangement of Ligand atoms in non-cubic Lattices. Molecular orbits and the polarization of the core electrons also modify the EFG. For the EFG, the greatest contribution comes from the electrons on the ion. The polarizable nature of the electron cloud may change the EFG by increasing or decreasing it and is described quantitatively by the sternheimer antishelding factors [2.44]. For the open shell ion (non S-state) such as Fe^{+2}, the principal source of q; namely q_{val} comes from integrating over the valence electrons on the Mössbauer ion itself, plus a secondary contribution of q_{lat} from the rest of the crystal (usually assumed to be a sum over point charges).
Therefore

$$q = (1-R)q_{val} + (1-\gamma_\alpha)q_{lat} \qquad (2.23)$$

where Sternheimer factor R and γ_α denote the fraction of each EFG arising from deformed closed sub shells in the Mössbauer atom.

The quantum mechanical expression that descrives the interaction between a nucleus with quadrupole moment eQ and EFG q is given by the Hamiltonian operator

$$H=\frac{eqa}{4I(2I-1)}[3I_z^2 - I(I+1)+\frac{n}{2}(I_+^2 - I_-^2)] \tag{2.24}$$

Where I_+ and I_- are the raising and lowering operators for the conventional spin operators. For direct determination of quadrupole moment values, we discuss the determination of the quadrupole moment of the 3/2, 14.4 Kev state of Co^{57}. For the ferrous Fe^{+2} state, the EFG is predominantly because of lattice contribution in the expression

$$q=(1-R)q_{val} +(1-\gamma_\alpha)q_{lat} \tag{2.25}$$

$m_I=\pm 1/2$ and $m_I=\pm 3/2$. This is shown in Fig2.11, giving two line spectrum or 'doublet'.
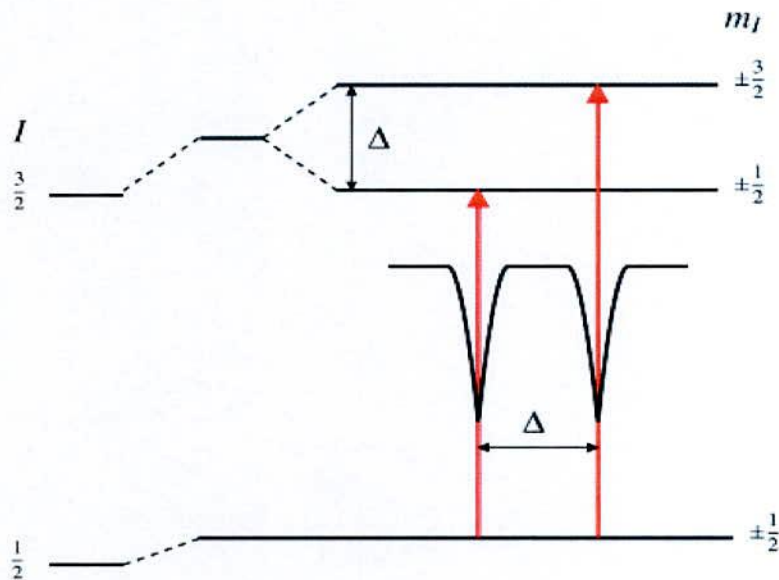
Fig. 2.11: Quadrupole splitting for a 3/2 to 1/2 transition. The magnitude of quadrupole splitting, Delta, is shown.

48

substates. Contribution for magnetic hyperfine field can come from all electrons that are present within the atom, the molecule and the lattice. The effects of magnetic hyperfine fields are observed in the Mössbauer spectra of magnetically ordered systems if the electron spin relaxation times are long. Magnetic splitting can arise due to magnetic hyperfine field and any external applied field and the field at the nucleus is a vector sum of two.

This magnetic field splits nuclear levels with a spin of I into (2I+1) substates. This is shown in Fig2.11 for ^{57}Fe. Transitions between the excited state and ground state can only occur where m_I changes by 0 or 1. This gives six possible transitions for a 3/2 to 1/2 transition, giving a sextet as illustrated in Fig2.11, with the line spacing being proportional to B effective magnetic field at the nucleus.
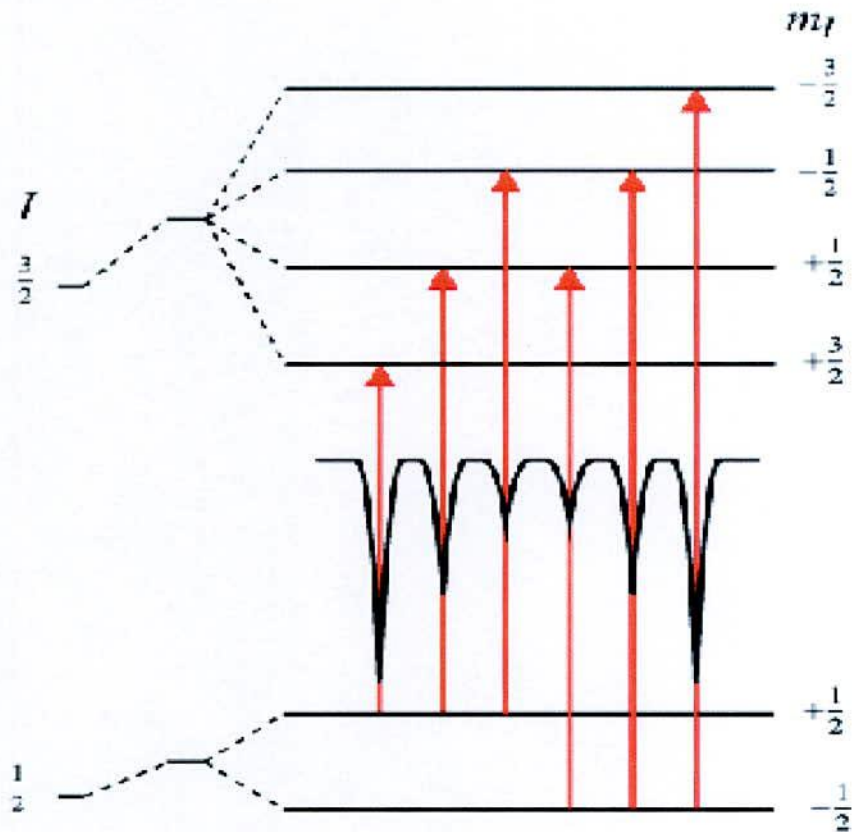
Fig. 2.12: Magnetic splitting of the nuclear energy levels

For ferric (Fe^{+2}) iron, the quadrupole splitting in $O-Fe_2O_3$ was studied. Since this ion is in the $^6S_{5/2}$ state; no contribution is expected from q_{val} and only q_{lat} must be considered. The Mössbauer spectrum shows a magnetic six-line patteren. The quadrupole interaction shifts the spectrum asymmetrically.

In the case of an isotope with a I=3/2 excited state, such as ^{57}Fe or ^{119}Sn, the excited state is split into two substates The magnitude of splitting, Delta, is related to the nuclear quadrupole moment, Q, and the principle component of the EFG, V_{zz}, by the relation

$$\Delta = eQV_{zz}/2. \tag{2.26}$$

2.7.1.3 Magnetic splitting

The hyperfine Hamiltonian for a nuclear magnetic dipole ia a magnetic field H is given by

$$H_M = -\mu.H \qquad (\text{Since } \mu = g\mu_N I)$$

$$H_M = -g\mu_N I.H \tag{2.27}$$

Where μ_N is the nuclear magnetron and g is the gyromagnetic ratio. The energy levels are

$$E_M = gM_N H M_I \qquad [M_I = I, I-1 \ldots\ldots\ldots] \tag{2.28}$$

This indicate that 2I+1 magnetic sublevels are equally spaced with a separation of $gM_N H$ between the levels.

When a nucleus experiences a magnetic field, a magnetic dipole interaction takes place between the nuclear magnetic moment and the magnetic field. This interaction splits the nuclear state (with I> 0) into two substates and the excited state with I=3/2 splits into four substates. The selection rules with $m_I=0,\pm1$ allows six possible transitions between these sets of excited and ground state leading to six-line Mössbauer spectrum.

The magnetic splitting is proportional to the magnetic field at the nucleus. The intensities of the absorption lines depend on the transitions probabilities between the different

49

The line positions are related to the splitting of the energy levels, but the line *intensities* are related to the angle between the Mössbauer gamma-ray and the nuclear spin moment. The outer, middle and inner line intensities are related by:

$$3 : \frac{4\sin^2\theta}{1+\cos^2\theta} : 1$$

meaning the outer and inner lines are always in the same proportion but the middle lines can vary in relative intensity between 0 and 4 depending upon the angle the nuclear spin moments make to the gamma-ray. In polycrystalline samples with no applied field this value averages to 2 but in single crystals or under applied fields the relative line intensities can give information about moment orientation and magnetic ordering as shown in Fig.2.11.

2.7.1.4 Magnetic Hyperfine Interaction

The internal magnetic field at the nucleus has its origin from the spin and radial and angular distribution of the electron density in the ato. The magnetic field is given by [2.45-2.46]

$$H = -\frac{8}{3}n\mu_B|\psi_\uparrow(0)|^2\,\overline{s} - 2\mu_B\langle\overline{l}\rangle\left\langle\frac{1}{r^3}\right\rangle - 2\mu_B\frac{\langle 3(\overline{r}.\overline{\Delta})\overline{r} - r^2\overline{s}\rangle}{r^5} \tag{2.29}$$

Where μ_B is Bhor magnetron, s and l are operators for the spin and orbital moment of the electron and $|\psi_\uparrow(0)|^2$ is the electron density at the nucleus with +1/2 spin projection.

The first term, in this expression is known as Fermi contact term which describes the contact magnetic interaction between the s-electrons and a nucleus, only S- electron contribute to the Fermi contact term since the S- electron have a non-zero charge density at the nucleus. The field resulting from this source is very large compared to that from other sources. The Fermi contact field mainly arises from the polarization of the spins of paired S-electrons by the unpaired 3d electrons via exchange attraction that emits between electrons of like spins [2.47-2.49]. The inner core electrons (1s and 2s) produce a large negative field, whereas 3s and 4s electron produce smaller positive fields resulting in a net negative field

51

almost of the nuclei [2.50]. The second term in the above expression is known as orbital current field and it is produce due to an interaction of the unquenched orbital moment of the electron with the nuclear magnetic moment.

The third term known as Dipolar field arises due to dipole-dipole interactions operation between the electron spin and the nuclear magnetic moment. For observing a well resolved Zeeman splitting in the Mössbauer spectrum, two conditions have to satisfied

$$\tau_0 > \tau_L \text{ And } \tau_s > \tau_L; \tag{2.30}$$

Where τ_0 the life time of the nuclear is excited state, τ_s is the electron spin correlation time and τ_L is the larmour precession time of the nucleus. The first conditions state that the Zeeman splitting must be larger than the natural line width. The second condition states the relationship between the spin correlation time and nuclear Larmour procession time. In paramagnetic system the spin correlation time is so small, of the order of 10^{-12} and 10^{-14} gu, That during on Larmour precession, the electron of spin undergoes several fluctuation and hence the nuclei will not experience any hyperfine field to precess around and hence no magnetic splitting will be absorbed. In magnetically ordered system, the stong exchange interaction helps to increase the spin correlations times, thus the direction of the hyperfine field is steady and the nucleus spin process round it to lift the degeneracy of the nuclear levels yielding hyperfine split spectrum.

Chapter - III

Experimental Procedure

Chapter-III Experimental Procedure

3.1 Methodology of Ferrite Preparation

The preparation of ferrites with optimum magnetic properties is a complex and difficult job to do. Knowledge and control of the chemical composition, homogeneity and microstructure are very crucial. The preparation of Polycrystalline ferrites with optimized properties has always demanded delicate handling and cautious approach. As the most of the properties needed for ferrite applications are not intrinsic but extrinsic, preparation of samples has to encounter added complexity. The ferrite is completely defined by its chemistry and crystal structure but also requires knowledge and control of parameters of its microstructure such as density, lattice parameters, porosity and their intra- and inter-granular distribution. It is well known that almost all ferrites decompose at the elevated temperature if we want to melt them under normal conditions. This happens because the oxygen splits off at higher temperature reducing Fe^{3+} and Fe^{+2}. This necessarily implies that ferrite preparation by melting, as in case of metals, is not possible. The normal methods of preparation of ferrites comprise of the conventional ceramic method or powder metallurgy, chemical co-precipitation method and sol-gel method.

3.1.1 Composition of the studied Ferrites System

A series of mixed ferrites of various compositions were fabricated by solid state reaction technique keeping in view of their ionic radial and valences for maintaining the charge neutrality.

In the present work, conventional ceramic method has been employed for a series of various compositions of Co-ferrites are synthesized, characterized and investigated. The powder preparation process are sintering facility available at Materials Science Division, Atomic Energy

53

Centre, Dhaka has been utilized in the preparation of samples. The following compositions were fabricated characterized and investigated thoroughly.

(i) $CoFe_2O_4$

(ii) $Co_{1-x}Cd_xFe_2O_4$ (where $x = 0.0.0.1, 0.3, 0.4$ and 0.5)
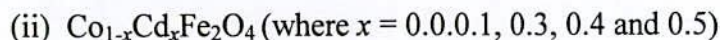
3.1.2 Method of Sample preparation

The sample preparation of Polycrystalline ferrites with optimum desired properties is still a complex and difficult task. ferrites with optimized properties have always demanded delicate handling and cautious approach in materials synthesis and appropriate knowledge of thermodynamics control of the chemical composition and homogeneity. There are several techniques to prepare ferrites, such as solid state reaction method [3.1], high energy ball milling [3.2], Sol gel method [3.3], chemical co-precipitation method [3.4], microwave sintering method [3.5], auto combustion method [3.6] etc for preparation of polycrystalline ferrite materials. In the present investigation solid state reaction has been employed for the preparation of Co-ferrite samples for its relative simplicity and availability. The overall preparation process generally comprised of the following four major steps.

(i) Preparing a mixture of materials.

(ii) Pre-firing the mixture to form ferrite at wet milling.

(iii) Pre-sintering and

(iv) Sintering.

3.1.3 Synthesis of Co-Cd Ferrites

There are many methods to prepare spinel ferrites like solid state, hydrothermal, solgel, auto combustion etc.

They are mainly divided into two groups:

(i) Conventional ceramic method i.e., solid state reaction method involves milling of reactants followed by sintering at elevated temperature range.

54

(ii) Non- Conventional method also called wet method. Among these processes there are sol-gel synthesis, chemical co-precipitation method, organic precursor method, reverse micelles method, co-spray, activated sintering etc.

3.1.4 Solid State Reaction Method

Polycrystalline ferrites are prepared normally by power metallurgy or ceramic technology. This means that ferrites attain their homogeneous compositions by reactions in the solid state and the shapes of the ferrite products are produced by pressing and subsequent sintering. A series of polycrystalline samples of mixed ferrites were prepared by the standard double sintering ceramic methods at the Materials Science Division, Atomic Energy Centre, Dhaka. In this method high purity oxide (99.99%) such as Fe_2O_3, Co_3O_4, and CdO of E-Mark of Germany were weighted precisely according to their molecular weight. The weight percentage of the oxide to be mixed for various samples was calculated by using formula:

$$\text{Weight \% of oxide} = \frac{M.wt \cdot of\ oxide \times required\ weight\ of\ the\ sample}{Sum\ of\ Mol.wt.of\ each\ oxide\ in\ a\ sample}$$

The constituent in required stoichiometric proportions of materials were troughly mixed using ceramic morter and pestle for 4 hrs and then ball milled in a planetary ball mill in ethyl alcohol media for 2hrs with stainless steel balls of different sizes in diameter Fig.3.1. The slurry was dried and the powder was pressed into disc shape. The disc shaped sample was pre-sintered at 950°C for 5hrs. The sample was then cooled down to room temperature at the same rate as that of heating. After that samples were crushed again and subsequently wet ball milled for 6hrs hours in distilled water to reduce it to small crystallites of uniform size. In order to produce chemically homogeneous and magnetically better material this prefired lump material was crushed. These oxide mixtures were milled thoroughly for 4-6 hours to obtain homogeneous mixture.

The mixture was dried and a small amount of saturated solution of polyvinyl alcohol (PVA) were added as a binder and pressed into pellet and toroid shape respectively under pressure 1.75 ton-cm^{-2} and 1.2 ton-cm^{-2} using hydraulic press Fig. 3.2. The prepared samples (Fig 3.3) were sintered at 1050°C-1200°C for 2-3hrs with a microprocessor controlled muffle furnace. The samples were polished in order to remove any oxide layer formed during the process of sintering.

Cylindrical container with integral bottom and removable lid

Grinding media tumbling as mill turns

Slurry containing supension of particles being sized

Wear-resistant mill lining

Rubber-coated rollers connected by a belt and pulley to a drive motor
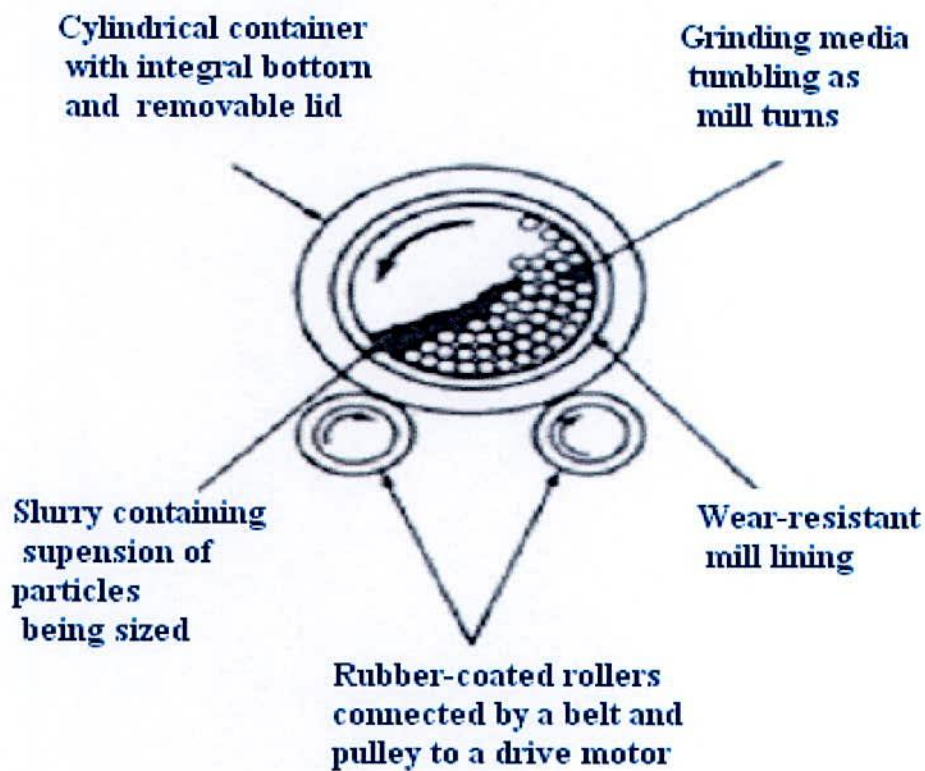
Fig. 3.1 Rubber-lined mill with stainless-steel balls

Fig.3.2 Hydraulic press used to make different shaped samples.
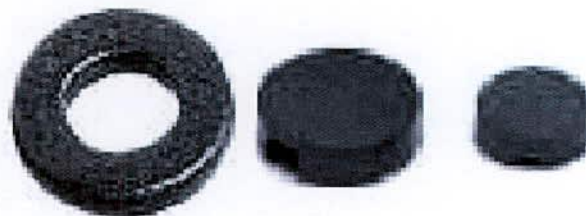
Fig.3.3 Toroid and disk shape sample.

3.1.4.1 Pre-firing the Mixture to form Ferrite at wet milling

The extend of this work in this step varies greatly depending on the starting materials, when component oxides are used, the corresponding step involves a mere mixing of the oxides by wet milling. Prolonged wet grinding of the powder mixture in steel ball mills produces good mixing and a smaller particle size, which in turn decreases the porosity of the final product. To avoid iron contamination, mixing is done in a rubber-lined mill with stainless-steel balls and a fluid such as distilled water or acetone/ethanol is used to prepare the mixture in to slurry.

The following block diagram in Fig. 3.4 represents the method employed for the Co- ferrites:
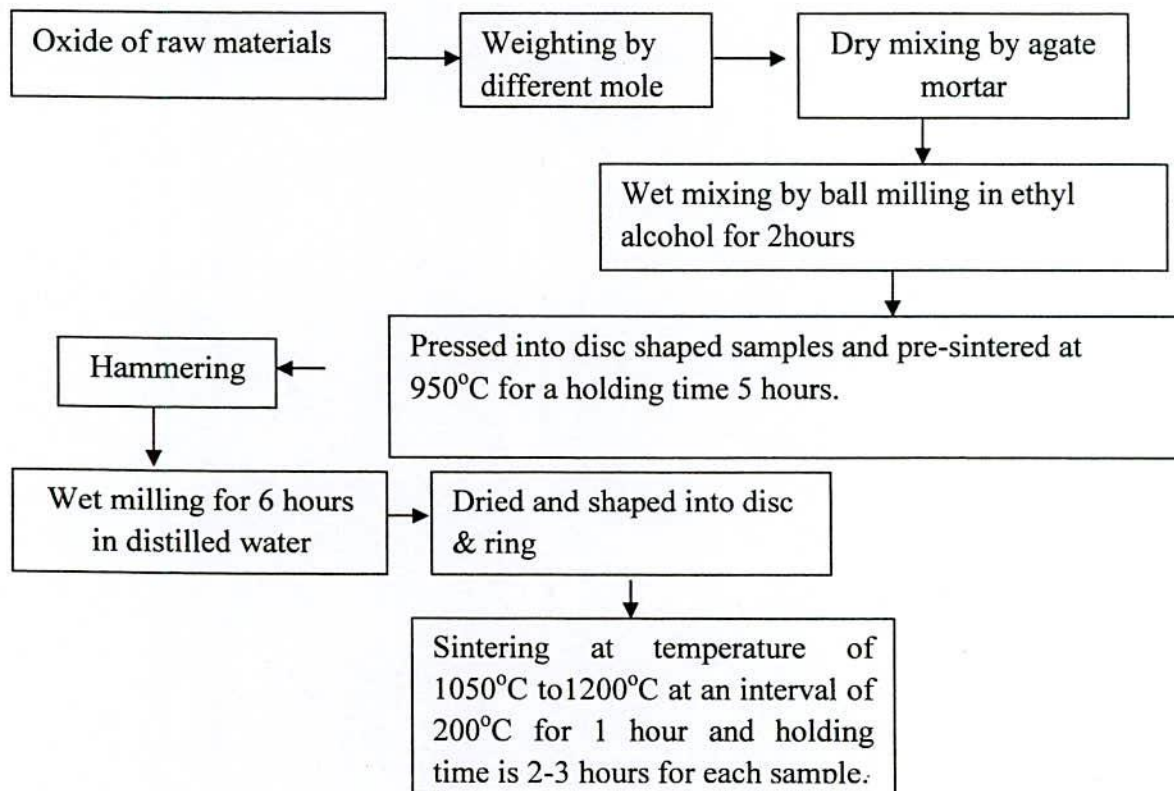
Fig.3.4: Flow chart of ferrite sample preparation technique by usual ceramic method.

Ferric oxide Fe_2O_3 and whatever oxides MO are required are taken in powder form with the cations in the ratio corresponding to that in the final product. Metal carbonates may also be used; during the later firing, CO_2 will be given off and they will be converted to oxides

3.1.4.2 Pre-sintering the Mixture to form Ferrite

The pre-sintering is very crucial because in this step of sample preparation a ferrite is formed from its component oxides. The slurry prepared in step (1) is dried, palletized and then transferred to a porcelain crucible for pre-firing at temperature between 900°C and 1200°C. This was performed in a furnace named Gallen Kamp at Materials Science Division, Atomic Energy Centre, Dhaka. This is done in air, and the temperature goes up to about 1200°C down to 200°C in about 20hours of time. Solid-state reactions take place between the component oxides in this stage, leading to the formation of ferrites actually achieved by counter diffusion. This means that the diffusion involves two or more species of ions which move in opposite direction initially across the interface of two contacting particles of different component oxides. During the pre-sintering stage, the reaction of Fe_2O_3 with metal oxide (MO or M'_2O_3 where M is divalent and M' is the trivalent metal atom) takes place in the solid state to form spinel according to the reactions [3.7]:

$$MO + Fe_2O_3 \rightarrow MO. Fe_2O_3 \text{ (spinel)}$$

$$2M'_2O_3 + 4Fe_2O_3 \rightarrow 4M'Fe_2O_4 \text{ (spinel)} + O_2$$

For Co-ferrite,

$$2Co_3O_4 \rightarrow 6CoO + 3O_2$$

$$CoO + Fe_2O_3 \rightarrow CoFe_2O_4$$

For Co-Cd ferrite,

$$(1-x) CoO + xCdO + Fe_2O_3 \rightarrow Co_{1-x}Cd_xFe_2O_4$$
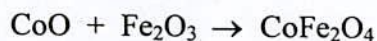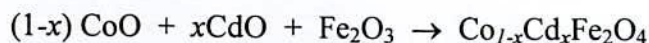
(Where x = 0.0, 0.1, 0.3, 0.4 and 0.5)

As far as the final composition of the ferrite is concerned step (2) is most crucial because subsequent steps would not change the composition substantially. However, the 'raw' ferrite thus formed has two defects its composition is not homogeneous and it contains pores. In order to produce chemically homogeneous, dense and magnetically better material of desired shape and size, sintering at an elevated temperature is needed.

3.1.4.3   Converting the ferrites into powder and pressing the powder

These undesirable features of the raw ferrites are eliminated in the following two steps:

(i) **Grinding:** The ferrite produced via pre-sintering is usually in the lump form. In this step, it is first ground into powder in a steel ball mill. Grinding eliminates intra particle pores, homogenizes the ferrite, reduces the particle size to << 1μm and promote mixing of any un-reacted oxides.

(ii) **Pressing or Extrusion:** The dry powder is mixed with an organic binder and pressed in to compacts of desired shapes either by the conventional method in a die-punch assembly or by hydrostatic or isostatic compaction. Most shapes, such as toroidal cores, are pressed (at 1-10 ton/cm^2, 14-140MPa), but rods and tubes are extruded.

3.1.4.4 Sintering

Sintering is the final and a very critical step of preparing a ferrite with optimized properties. The sintering time, temperature and the furnace atmosphere play very important role on the magnetic property of final materials. Sintering commonly refers to processes involved in the heat treatment by which a mass of compacted powder is transformed into a highly densified object by heating it in a furnace below its melting point. Ceramic processing is based on the sintering of powder compacts rather than melting/ solidifications/cold working (characteristic for metal), because:

(i)   Ceramics melt at high temperatures

(ii)   As solidified microstructures cannot be modified through additional plastic deformation and re-crystallization due to brittleness of ceramics

(iii)   The resulting course grains would act as fracture initiation sites

(iv)   Low thermal conductivities of ceramics (< 30 - 50 W/ mK) in contract to high thermal conductivity of metals (in the range 50 – 300 W / mK) cause large temperature gradients, and thus thermal stress and shock in melting-solidification of ceramics.

Sintering is the bonding together of a porous aggregate of particles at high temperature. The thermodynamic driving force is the reduction in the specific surface area of the particles. The sintering mechanism usually involves atomic transport over particle surfaces, along grain boundaries and through the particle interiors. Any un-reacted oxides form ferrite, inter diffusion occurs between adjacent particles so that they adhere (sinter) together, and porosity is reduced by the diffusion of vacancies to the surface of the part. Strict control of the furnace temperature and atmosphere is very important because these variables have marked effects on the magnetic properties of the product. Sintering may result in densification, depending on the predominant diffusion pathway. It is used in the fabrication of metal and ceramic components, the agglomeration of ore fines for further metallurgical processing and occurs during the formation of sandstones and glaciers. Sintering must fulfill three requirements:

(a) to bond the particles together so as to impart sufficient strength to the product

(b) to densify the grain compacts by eliminating the pores and

(c) to complete the reactions left unfinished in the pre-sintering step

The theory of heat treatment is based on the principle that when a material has been heated above a certain temperature, it undergoes a structural adjustment or stabilization when cooled at room temperature. The cooling rate plays an important role on which the structural modification is mainly based.

Why do need Sintering?

The principle goal of sintering is the reduction of compact porosity. Sometimes the initial spaces between compacted grains of ceramics are called "voids", to differentiate term from the isolated spaces = pores, which occur in the final stages of sintering. The sintering process is usually accompanied by other changes within the materials, some desirable and some undesirable. The largest- changes occur in;

(i)   To bind the particles together so as to impart sufficient strength to the products.

(ii)   To densify the green compacts by eliminating the pores

(iii)   To homogenizer the materials by completing the relation left un pressed in the pre-sintering step

(iv)   To make strength of elastic modulus

(v)   To make hardness and fracture tough

(vi)   To make homogeneous distribution of grain number, grain size and shape.

(vii)   To improve the average pore size and shape

(viii) To get a stable chemical composition and crystal structure

Sintering is a widely used but very complex phenomenon. The fundamental quantification of change in pore fraction and geometry during sintering can be attempted by several techniques, such as: dilatometry, buoyancy, gas absorption, porosimitry indirect methods (e.g. hardness) and quantitative microscopy etc. The description of the sintering process has been derived from model experiments (e.g. sintering of a few spheres) and by observing powdered compact behavior at elevated temperatures. The following phenomena were observed:

(i)   Increase of inter- particle contact area with time.

(ii)   Rounding- off of sharp angles and points of contacts

(iii)   In most cases the approach of particle centers and overall densification

(iv)   Decreases in volume of inter connected pores.

(v)   Continuing isolation of pores

(vi)   Grain growth and decreases in volume of isolated pores.

3.2   X-ray Diffraction (XRD)

X-rays are the electromagnetic waves whose wavelength is in the neighborhood of 1Å. The wavelength of an X-ray is that the same order of magnitude as the lattice constant of crystals and it is this which makes X-ray so useful in structural analysis of crystals. X-ray diffraction (XRD) provides precise knowledge of the lattice parameter as well as the substantial information on the crystal structure of the material under study. X-ray diffraction is a versatile nondestructive analytical technique for identification and quantitative determination of various crystalline phases of powder or solid sample of any compound. When X-ray beam is incident on a material, the photons primarily interact with the electrons in atoms and get scattered. Diffracted waves from different atoms can interfere with each other and the resultant intensity distribution is strongly modulated by this interaction. If the atoms are arranged in a periodic fashion, as in crystals, the diffracted waves will consist of sharp interference maxima (peaks) with the same symmetry as in the distribution of atoms. Measuring the diffraction pattern therefore allows us to deduce the distribution of atoms in a material. It is to be noted here that, in diffraction experiments, only X-rays diffracted via elastic scattering are measured.

The peaks in an X-ray diffraction pattern are directly related to the atomic distance. Let us consider an incident X-ray beam interacting with the atoms arranged in a periodic manner as shown in two dimensions in Fig. 3.5. The atoms, represented as spheres in the illustration, can be viewed as forming different sets of planes in the crystal. For a given set of lattice planes with an inter-plane distance of d, the condition for a diffraction (peak) to occur can be simple written as

$$2d \sin n\theta = n\lambda \, , \tag{3.1}$$
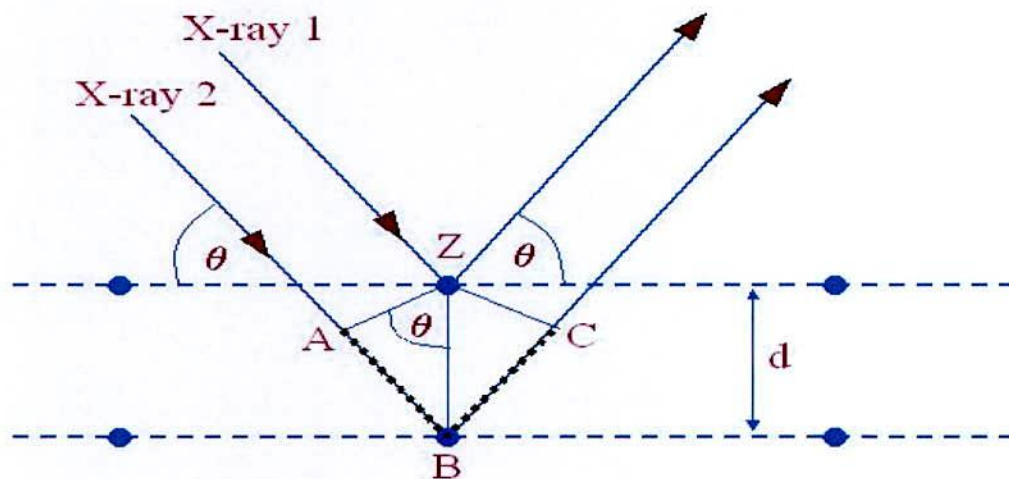
Fig. 3.5 Bragg's diffraction pattern

which is known as Bragg's law. In the equation, λ is the wavelength of the X-ray, θ is the scattering angle, and n is an integer representing the order of the diffraction peak. The Bragg's Law is one of the most important laws used for interpreting X - ray diffraction data. From the law, we find that the diffraction is only possible when $\lambda < 2d$ [3.9].

In the present work, A PHILIPS PW 3040 X' pert PRO X-ray diffractometer was used for the lattice parameter to study the crystalline phases of the prepared samples in the Materials Science Division, Atomic Energy Centre, Dhaka. Fig. 3.6 shows the block diagram of X' pert XRD system.

The powder diffraction technique was used with a primary beam powder of 40 kV and 30mA for Cu-K$_\alpha$ radiation. A nickel filter was used to reduce Cu-K$_\beta$ radiation and finally Cu-K$_\alpha$ radiation was only used as the primary beam. The experimental has been performed at room

temperature. A 2θ scan was taken from 15° to 75° to get possible fundamental peaks of the samples with the sampling pitch of 0.02° and time for each step data collection was 1.0 sec. Both the programmable divergence and receiving slits were used to control the irradiated beam area and output intensity from the powder sample, respectively. An anti scatter slit was used just after the tube and in front of the detector to get parallel beam only. All the data of the samples were stored in the computer memory and later on analyzed them using computer "software" X' PERT HJGHS CORE". For XRD experiment each sample was set on a glass slide and fixed the sample by putting adhesive typed the two ends of the sample.
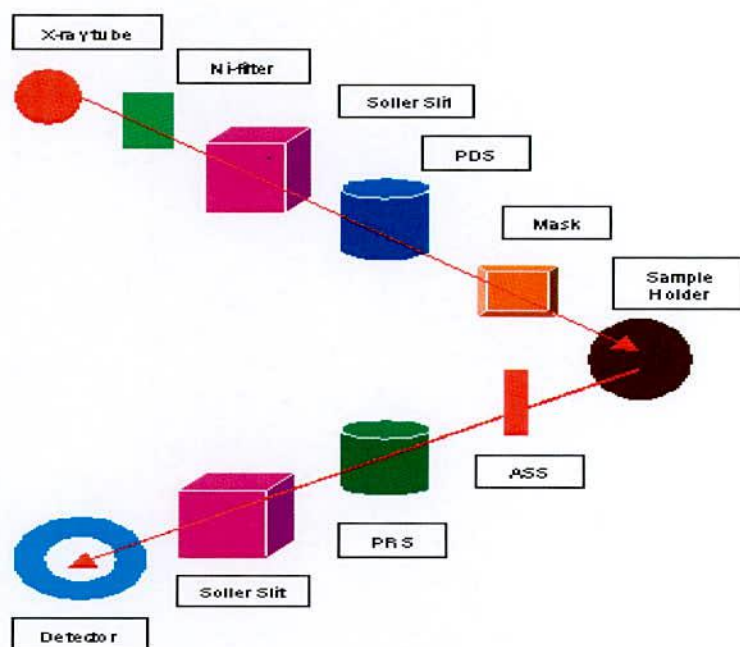
Fig. 3.6 Block diagram of the PHILIPS PW 3040 X'Pert PRO XRD system.

For each composition, the cylindrical samples of weight more than 2 gm are converted into powder. For XRD experiment each sample was set on a glass slide and fixed the sample by putting adhesive tape at the two ends of the sample X-ray diffraction patterns were carried out to confirm the crystal structure. Instrumental broadening of the system was determined from θ−2θ

scan of standard Si. At (311) reflection's position of the peak, the value of instrumental broadening was found to be 0.07°. This value of instrumental broadening was subtracted from the pattern. After that, using the X-ray data, the lattice constant (a) and hence the X-ray densities were calculated.

3.2.1 Different Parts of the PHILIPS X' Pert PRO XRD System

Fig 3.7 shows the inside view of the X'- pert PRO XRD system. A complex of instruments of X- ray diffraction analysis has been established for both materials research and specimen characterization. These include facilities for studying single crystal defects, and a variety of other materials problems.
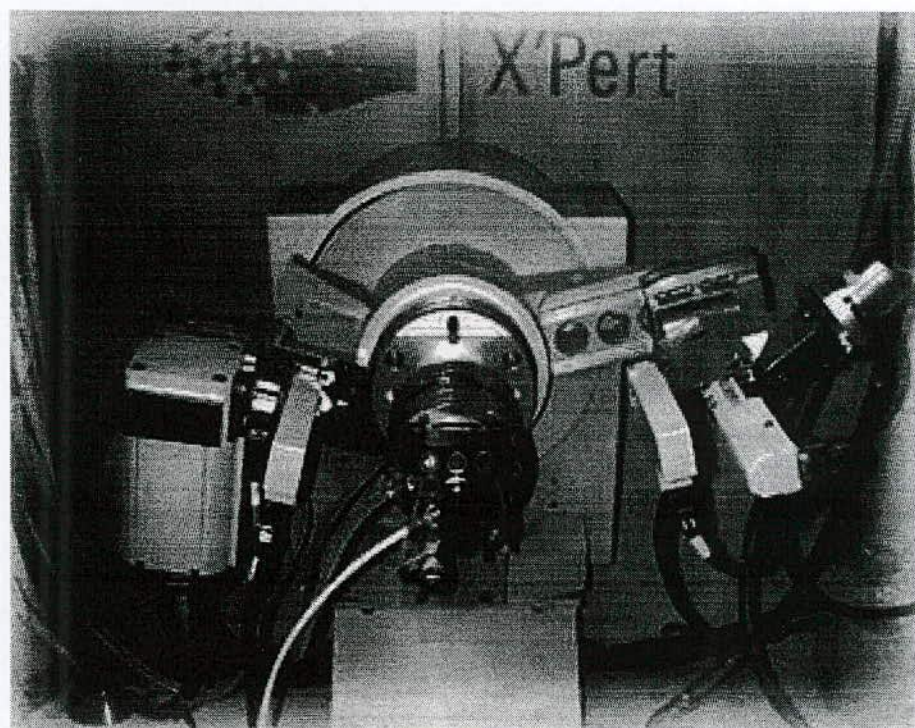
Fig. 3.7 Internal arrangement of a PHILIPS X' Pert PRO X-ray diffractometer

The PHILIPS X' Pert PRO XRD system comprised of the following parts.

(i) "Cu-Tube" with maximum input power of 60 kV and 55 mA

(ii) "Ni- Filter" to remove Cu-K$_\alpha$ component

(iii) "Solar slit" to pass parallel beam only

(iv) "Programmable Divergent slits"(PDS) to reduce divergence of beam and control irradiated beam area

(v) "Mask" to get desired beam area

(vi) "Sample holder" for powder sample.

(vii) "Anti Scatter slit" (ASS) to reduce air scattering back ground.

(viii) "Programmable Receiving slite" (PRS) to control the diffracted beam intensity and

(ix) "Solar slite to stop scattered beam and pass parallel diffracted beam only.

3.2.2 Interpretation of the XRD data

The XRD data consisting of θ_{hkl} and d_{hkl} values corresponding to the different crystallographic planes are used to determine the structural information of the samples like lattice parameter and constituent phase. Lattice parameters of Co-ferrites samples were determined. Normally, lattice parameter of an alloy composition is determined by the Debye-Scherrer method after extrapolation of the curve. We determine the lattice spacing (interplaner distance), d using these reflections from the equation which is known as Bragg's Law.

$$2d_{hkl} \, Sin\theta = \lambda$$

$$\text{i.e. } d_{hkl} = \frac{\lambda}{2\sin\theta} \, , \tag{3.2}$$

where λ is the wavelength of the X-ray, θ is the diffraction angle and n is an integer representing the order of the diffraction.

The lattice parameter for each peak of each sample was calculated by using the formula:

$$a = d_{hkl} \times \sqrt{h^2 + k^2 + l^2} \, , \tag{3.3}$$

67

where h, k, l are the indices of the crystal planes. We get d_{hkl} values from the computer using software "X'- Pert HJGHS CORE". So we got ten 'a' values for ten reflection planes such as a a_1, a_2 a_3 ..... etc. Determine the exact lattice parameter for each sample, through the Nelson-Riley extrapolation method. The values of the lattice parameter obtained from each reflected plane are plotted against Nelson-Riley function [3.10]. The Nelson-Riley function F (θ), can be written as

$$F(\theta) = \frac{1}{2}\left[\frac{\cos^2\theta}{\sin\theta} + \frac{\cos^2\theta}{\theta}\right],$$
(3.4)

where θ is the Bragg's angle. Now drawing the graph of 'a' vs F(θ) and using linear fitting of those points will give us the lattice parameter 'a_0'. This value of 'a_0' at F(θ) = 0 or θ = 90° .These 'a_0's are calculated with an error estimated to be ± 0.0001Å.

3.2.3 X-ray Density and Bulk Density

X-ray density, ρ_x was also calculated usual from the lattice constant. The relation between ρ_x and 'a' is as follows,

$$\rho_x = \frac{ZM}{Na^3},$$
(3.5)

where M is the molecular weight of the corresponding composition, N is the Avogadro's number (6.023X10^{23} mole^{-1}), 'a' is the lattice parameter and Z is the number of molecules per unit cell,(Z = 8 for the spinel cubic structure). The bulk density was calculated considering a cylindrical pellet of mass (m) and volume (V) of the pellets using the relation

$$\rho_B = \frac{m}{V} = \frac{m}{\pi r^2 h},$$
(3.6)

where m is the mass of the pellet sample, r is the radius and h is the thickness of the pellet.

3.2.4 Porosity

Porosity is a parameter which is inevitable during the process of sintering of oxide materials. It is noteworthy that the physical and electromagnetic properties are strongly dependent on the porosity of the studied samples. Therefore an accurate idea of percentage of pores in a prepared sample is prerequisite for better understanding of the various properties of the studied samples to correlate the microstructure property relationship of the samples under study. The porosity of a material depends on the shape, size of grains and on the degree of their storing and packing. The difference between the bulk density ρ_B and X-ray density ρ_x gave us the measure of porosity. Percentage of porosity has been calculated using the following relation [3.11]

$$P = (1 - \frac{\rho_B}{\rho_x}) \times 100\% \tag{3.7}$$

3.3 Permeability Measurement

From the frequency dependence of complex permeability, evolution of permeability and magnetic loss component at different stages of ferrite sample as affected by thermal treatment at different temperature was determined using toroids shape sample prepared with insulating Cu wire. The 4192 LF Impedance analyzer directly measure the value of inductance, L and loss factor.

$$D = \tan\delta \tag{3.8}$$

From inductance the value of real part of complex permeability, μ' can be obtained by using the relation

$$\mu' = \frac{L}{L_0}, \tag{3.9}$$

where L is the inductance of the toroid and L_0 is the inductance of the coil of same geometric shape in vacuum, L_0 is determined by using the relation,

$$L_0 = \frac{\mu_0 N^2 S}{\pi \bar{d}} \qquad (3.10)$$

Here μ_o is the permeability of the vacuum, N is the number of turns (here N = 5), S is the cross-sectional area of the toroid shaped sample, S = dh, where, $d = \frac{d_1 \sim d_2}{2}$ $\bar{d}$ is the average diameter of the toroid sample given as

$$\bar{d} = \frac{d_1 + d_2}{2} , \qquad (3.11)$$

Where, d_1 and d_2 are the inner and outer diameter of the toroid samples.

3.3.1 Agilent Precision Impedance Analyzer (Agilent, 4192A)

The Agilent Technologies 4294A precision impedance analyzer greatly supports accurate impedance measurement and analysis of a wide variety of electronic devices (components and circuits) as well as electronic and non-electronic material Fig :3.8. We made use of the excellent experimental facilities available at the Materials Science Dvission, Atomic Energy center, Dhaka. Moreover, the 4294A's high measurement performance and capable functionally delivers a powerful tool to circuit design and development as well as materials research and development (both electronic and nonelectronic materials) environments:

- Accurate measurement over wide impedance range and wide frequency range

- Powerful impedance analysis functions

- Ease of use and versatile PC connectivity

The following are application examples;

- Impedance measurement of two terminal components such as capacitors, inductors, ferrite beads, resistors, transformers, crystal/ceramic resonators, multi-chip modules or array/network components.

70

Semiconductor components

- C – r characteristic analysis of varac for diodes.
- Parasitic analysis of a diode, transistor or IC package terminal/leads.
- Amplifier input/output impedance measurement.
- Impedance evaluation of printed circuit boards, relays, switches, cables, batteries etc.
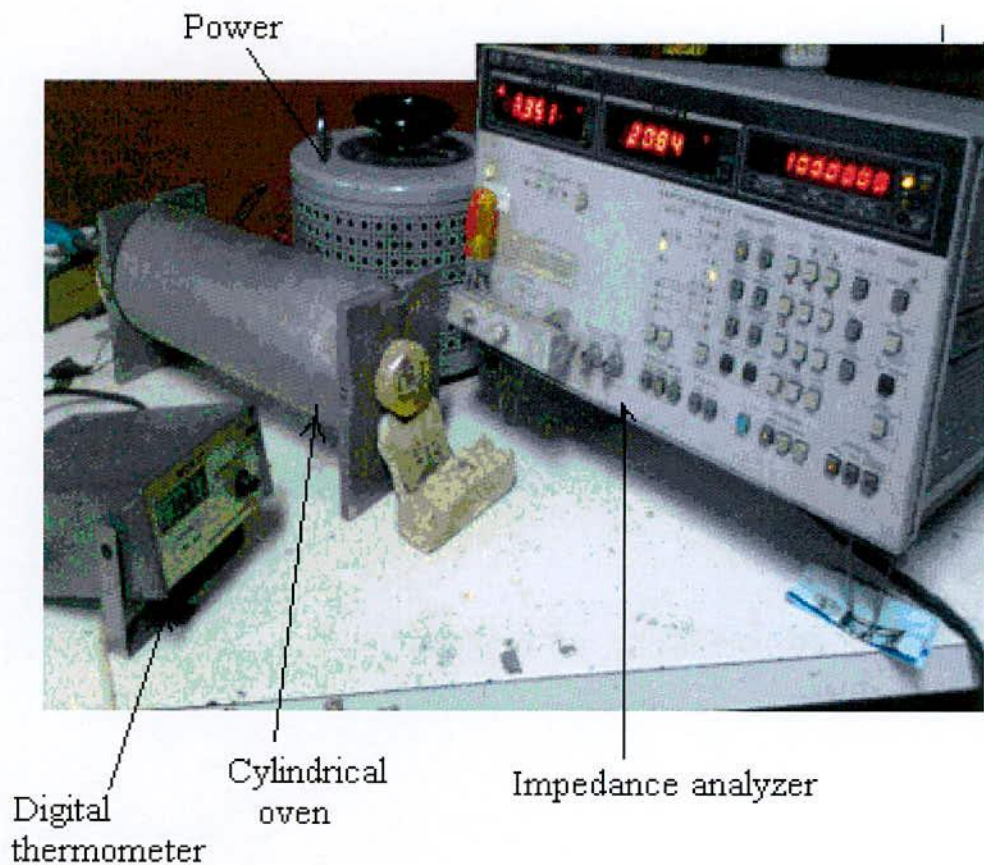
Fig.3.8 Impedance Analyzer Model-Hewlett-Packard 4192A

Dielectric materials

- Permittivity and loss tangent evaluation of plastics, ceramics, printed circuit boards and other dielectric material

Magnetic materials

- Permeability and loss tangent evaluation of ferrite, amorphous and other magnetic materials.

Semiconductor material

- Permittivity, conductivity and C – V characteristics of semiconductor materials.

3.3.1 Curie Temperature

Curie temperature is a measure of exchange force in ferrimagnetics. It is the temperature at which the thermal energy kT tending to disorder the system just wins over the exchange energy tending to order the system magnetically. At this temperature, ferromagnetic substance thus changes over to a paramagnetic substance.

Curie temperature measurement is one of the most important measurements because it provides substantial information on magnetic status of the substance in respect to the strength of exchange interaction. Above Curie temperature spontaneous magnetization vanishes and ferromagnetic materials behave like paramagnetic materials. So the determination of Curie temperature accurately is of great importance. The temperature dependence properties of ferrite materials depend upon its sublattice distribution and spin orientations of the metal ions and we can predict about the sublattice magnetization by measuring the Curie temperature.

There are several processes of measuring the Curie temperature; these are

    (i)   by measuring magnetization against temperature

    (ii)   by measuring variation of initial permeability against temperature

(iii)   by measuring susceptibility against temperature

(iv)   by measuring the variation of resistivity of the sample against temperature

In our present research work, we measured the Curie temperature of the samples by observing the variation of initial permeability of the ferrite samples with temperature and magnetization against temperature.

3.3.3 Measurement of Curie temperature by observing the Variation of Initial Permeability with Temperature

For ferromagnetic materials in particular, for ferrite it is customary to determine the Curie temperature by measuring the permeability as a function of temperature. According to Hopkinson effect [3.12] which arises mainly from the intrinsic anisotropy of the material has been utilized to determine the Curie temperature of the samples. According to this phenomenon, the permeability increases gradually with temperature and reaching to a maximum value just before the Curie temperature.

Curie temperature measurements were done by using Hewlett Packard 4192A LF Impedance Analyzer shown in Fig. 3.8 Impedance parameters absolute value of impedance ($|Z|$), absolute value of admittance ($|Y|$), phase angle (θ), resistance I, reactance (X), conductance (G), susceptance (B), inductance (L), capacitance (C), dissipation (D) and quality factor (Q). Measurement range of $|Z|$/R/X is 0.1mΩ to 1.2999 MΩ, $|Y|$/G/B is 1 ns to 12.999 s; θ is -180° to +180°; L is 0.1mH to 1.000 kH; C is 0.1PF to 100.0 mF, D is 0.0001 to 19.999; Q is 0.1 to 1999.9. All have a basic accuracy of 0.1% and resolution of $4\frac{1}{2}$ digits. Number of display digits dependence on measuring frequency and OSC level setting. We made use of the excellent experimental facilities available at the Materials Science Division, Atomic Energy Centre, Dhaka.

The temperature dependent permeability was measured by using induction method. The specimen formed the core of the coil. The number of turns in each coil was 5. We used a constant frequency (100 kHz) of a sinusoidal wave, AC signal of 100mV. HP 4192A impedance analyzer with continuous heating rate of ≈ 5 K / min with very low applied ac field of $\approx 10^{-3}$Oe. By varying temperature, inductance of the coil as a function of temperature was measured. Dividing this value of L_o (inductance of the coil without core material), we got the permeability of the core i.e. the sample. When the magnetic state inside the ferrite sample changes from ferromagnetic to paramagnetic, the permeability falls sharply. From this sharp fall at specific temperature the Curie temperature was determined. For the measurement of Curie temperature, the sample was kept inside a cylindrical oven with a thermocouple placed at the middle of the sample. The thermocouple measures the temperature inside the oven and also of the sample.

The sample was kept just in the middle part of the cylindrical oven in order to minimize the temperature gradient. The temperature of the oven was then raised slowly. If the heating rate is very fast then the temperature of the sample may not follow the temperature inside the oven and there can be misleading information on the temperature of the samples. The thermocouple showing the temperature in that case will be erroneous. Due to the closed winding of wires the sample may not receive the heat at once. So, a slow heating rate can eliminate this problem. The cooling and heating rates are maintained as approximately $0.5°C$ min^{-1} in order to ensure a homogeneous sample temperature. Also a slow heating ensures accuracy in the determination of Curie temperature. The oven was kept thermally insulated from the surroundings. The temperature was measured with a digital thermometer attached close to the sample and put inside the furnace where the temperature fluctuation is almost negligible. Then the permeability versus temperature curve was plotted from which the Curie temperature was calculated.

3.3.4 Mechanisms of Permeability

Mechanisms of permeability can be explained as the following way: a demagnetized magnetic material is divided into number of Weiss domains separated by block walls. In each domain all the magnetic moments are oriented in parallel and the magnetization has its saturation

value M_s. In the walls the magnetization direction changes gradually from the direction of magnetization in one domain to that in the next. The equilibrium positions of the walls results from the interactions with the magnetization in neighboring domains and from the influence of pores; crystal boundaries and chemical in homogeneities which tend to favor certain wall positions.

3.3.5 Techniques of Measurements of Permeability

Measurements of permeability normally involve the measurements of the change in self inductance of a coil presence of the magnetic core. The behavior of a self inductance can now be described as follows. Suppose we have an ideal lossless air coil of inductance L_0. On insertion of magnetic core with permeability μ, the inductance will be μL_0. The complex impedance Z of this coil can be expressed as,

$$Z = R + jX = j\omega L_0(\mu' - j\mu''),$$ (3.12)

where the resistive part is

$$R = \omega L_0 \mu',$$ (3.13)

and the reactive part is

$$X = \omega L_0 \mu''$$ (3.14)

The radio frequency (RF) permeability can be derived from the complex impedance of a coil Z (Eqn. 3.12). The core is usually toroidal to avoid demagnetization effects. The quantity L_0 is derived geometrically.

3.3.6 Frequency Characteristics of Ferrite Samples

The frequency characteristics of the cubic ferrite sample i.e. the permeability spectra were investigated using Wayne Kerr Impedance Analyzer of Model No.6500B provide the value of inductance, L and loss factor, $D = \tan\delta$. The measurements of inductances were taken in the frequency range of 1 kHz to 120 MHz. The values of measured parameters obtained as a

function of frequency and the real (μ') and imaginary part (μ'') of permeability and the loss factor are calculated. μ' is calculated by using the Eq^n.3.9 and Eq^n.3.10 and μ'' is calculated by using the following equation

$$\mu'' = \mu' \tan\delta \qquad (3.15)$$

3.4   Magnetization measurement

Magnetization in ferrite samples originate due to the difference in the magnetic moments for the two sub-lattices. The larger the difference, the greater is the resultant magnetization, because of the anti-parallel arrangements of the moments in two sub-lattices. The magnetic moment of each sub-lattice arises due to the presence of magnetic ions such as Fe^{2+}, Fe^{3+}, Mn^{2+}, Cu^{2+}, Ni^{2+}, Co^{2+} etc. In our case, only iron ion has magnetic moment since Mg and Zn are non-magnetic. Different ions occupy different 2sites. So, as a whole, the two sub-lattices have their individual resultant magnetic moments. The differences in magnetic moment between the two sub-lattices give rise to net magnetic moment which in turn yields magnetization. In the present study magnetization has been performed using a Vibrating Sample Magnetometer (VSM).

3.4.1 Vibrating Sample Magnetometer (VSM)

The principle of VSM is the measurement of the electromotive force induces by magnetic sample when it is vibrate at a constant frequency in the presence of a static and uniform magnetic field. A small part of the (10-50mg) was weighed and made to avoid movements inside the sample holder. Fig.(3.9) shows Vibrating Sample Magnetometer (VSM) of Model EV7 system. The magnetic properties measurement system Model EV7 is a sophisticated analytical instrument configured specially for the study of the magnetic properties of small samples over a broad range of temperature from 103K to 800k and magnetic field from-20KO_e to +20KO_e. Vibrating Sample Magnetometer is a versatile and sensitive method of measuring magnetic properties developed by S. Foner [3.13] and is based on the flux change in a coil when the sample is vibrated near it.

Fig. 3.9 Vibrating Sample Magnetometer

The VSM is designed to continuously measure the magnetic properties of materials as a function of tempertature and field. IIn this type of magnetometer, the sample is vibrated up and down in a region surround by several pickup coils. The magnetic sample is thus acting as a time-changing magnetic flux, varying magnetic flux is accompanied by an electric field and the field induces a voltage in pickup coils. This alternating voltage signal is processed by a control unit system, in order to increase the signal to noise ratio. The result is a measure of the magnetization of the sample.

3.4.2 Principle of VSM

If a sample is placed in a uniform magnetic field, created between the poles of a electromagnet, a dipole moment will be induce. If the sample vibrates with sinusoidal motion a sinusoidal electrical signal can be induced in suitable placed pick-up coils. The signal has the same frequency of vibration and its amplitude will be proportional to the magnetic moment, amplitude, and relative position with respect to the pick-up coils system. Figure 3.10 shows the block diagram of vibrating sample magnetometer.
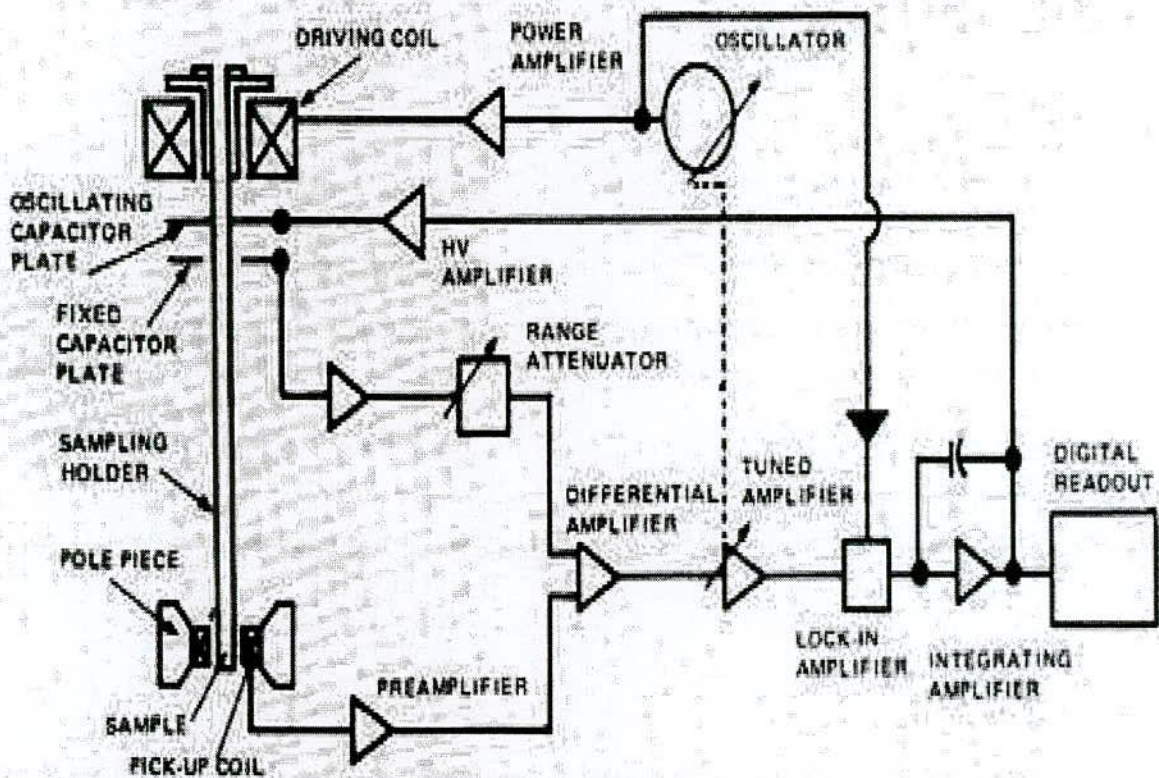

Fig.3.10: Block diagram of a Vibrating Sample Magnetometer

The sample is fixed to a sample holder located at the end of a sample rod mounted in a electromechanical transducer. The transducer is driven by a power amplifier which itself is driven by an oscillator at a frequency of 90 Hz. So, the sample vibrates along the Z axis perpendicular to the magnetizing field. The latter induce a signal in the pick-up coil system that is fed to a differential. The output of the differential amplifier is subsequently fed into a tuned amplifier and an internal lock in amplifier that receives signal supplied by the oscillator.

The output of this lock-in amplifier, or the output of the magnetometer itself, is a DC signal proportional to the magnetic moment of the sample being studied. The electromechanical transducer can move along X, Y and Z directions in order to find the saddle point. Calibration of the vibrating sample magnetometer is done by measuring the signal of a pure Ni standard of known saturation magnetic moment placed in the saddle point. The basic instrument includes the electromechanical system and the electronic system (including a personal computer). Laboratory electromagnets or superconducting coils of various maximum field strengths may be used.

3.5   Experimental Procedure for Mössbauer Spectrometer

3.5.1 Instrumentation

Mössbauer measurement can be made in two different geometries, transmission and scattering configurations. In the present work only transmission geometry was used. In transmission type measurements, the intensity of γ-rays transmitted through a thin absorber are measured with the help of a suitable detector like proportional counter. γ-ray source is driven electromagnetically by a transducer so as to Doppler shift the energy spectrum is obtained by counting transmitted γ-rays by small and known amounts. The absorption Mössbauer spectrum is obtained by counting transmitted γ-rays as a function of the source to absorber velocity.

Figure 3.11 shows a schematic diagram of a simple Mössbauer spectrometer. The source velocity is controlled by a transducer which is oscillated with constant acceleration. A waveform generator sends a reference waveform (triangular in the spectrometers at Liverpool) to the drive

amplifier, via a Digital to Analogue Converter. This signal is sent to the vibrator where it is converted to a mechanical oscillation of the drive shaft and source. A small coil within the vibrator provides a feedback signal to correct any deviations from the reference waveform.
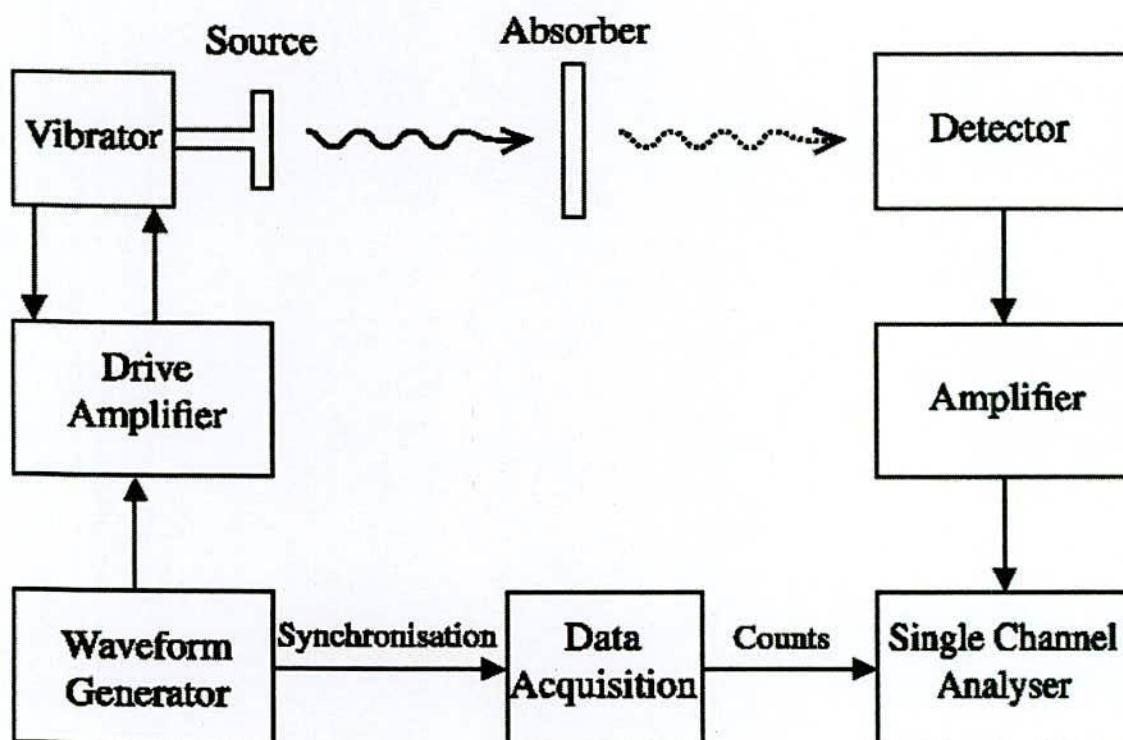
Figure 3.11: Mössbauer spectrometer schematic.

The detector is a proportional counter containing a 90% argon and 10% methane gas mixture. It uses an applied bias voltage of -2.0keV to -2.5keV and has 65% detection efficiency for 14.41keV gamma-rays. The pulse magnitude from the detector is directly proportional to the γ-ray energy and is sorted by a single channel analyzer after amplification. This allows the selection of the Mössbauer γ-ray from any other radiation emitted from the source.

The detector counts and source velocity are synchronized by a microprocessor system. The counts accumulate in 576 channels for one complete cycle, which contain two complete spectra: one for positive acceleration and one for negative acceleration of the source. As the acceleration is constant the time interval is equal for all velocity intervals, hence each channel records for the same amount of time. During analysis the full spectrum is folded around a center point to produce a single spectrum. This increases the number of counts (and hence gives better statistics) and flattens the background profile produced by the difference in intensity of the source radiation as the source moves relative to the absorber and detector.

The work reported here is based on Mössbauer spectroscopy of 14.4KeV γ-rays. For this ^{57}Co embedded in Rh matrix was used as the source. It emits 14.4KeV γ-radiation nuclear level decay scheme depicted in Fig.3.12. The half life of the source is 270 days.
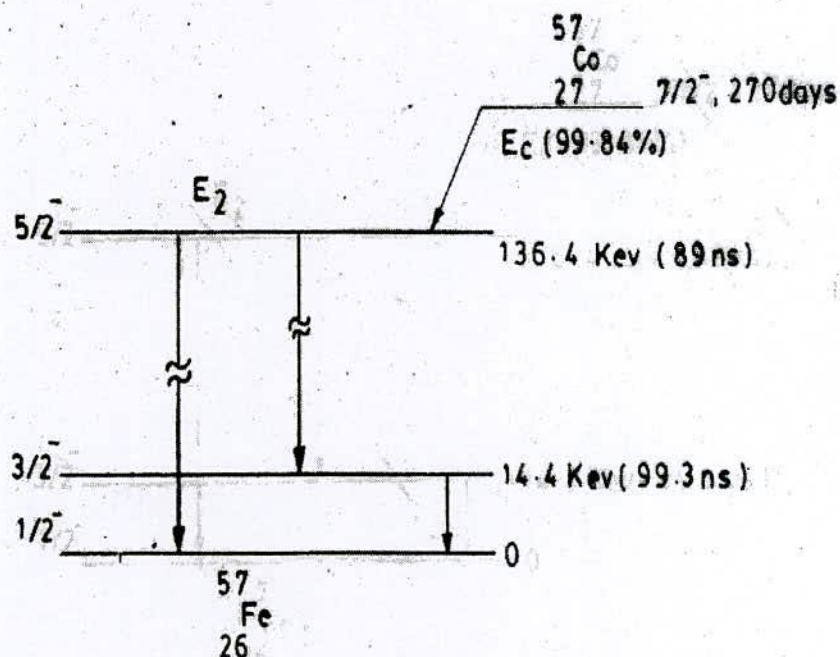
Fig.-3.12. Nuclear Level Decay of ^{57}Co to ^{57}Fe leading to 14.4 keV Mössbauer γ- ray

3.5.2 Velocity Drive System

In order to provide a Doppler motion to the source with respect to stationary observer or vice-versa a velocity drive system is used. In the present work Doppler motion is given to the source. For this an electromechanical system is used. It comprises of a velocity transducer and its related electronics [3.14]. It works fairly linear by up to a velocity of ±25mm/s. To run this in constant acceleration mode this is connected to computer and a power amplifier. Triangular wave is fed as a reference signal to one of the transducer coils acting as a pick up coil. Also due to transducer motion a signal is induced at this pick up coil subtracts from the reference generating an error signal, which is amplified, integrated and then applied to a complimentary circuit to push pull power amplifier which drives the coil. In this way self sustained motion of the drive is obtained. Pulses of a repetition rate equal to that of the frequency of a triangular wave formed from the leading edge of the square wave obtained by differentiation of the triangular wave. These pulses are used to start and stop signals for scanning of 512 channels. Here synchronization is achieved with the help of computer.

3.5.3. γ-source

A good Mössbauer source should have high recoil free electrons, long life time and narrow line width. In the present work, Mössbauer studies using ^{57}Fe have been reported. The γ-rays of 14.4KeV emitted by it are used. Characteristics are as follows Matrix: Rhodium; Matrix size: 8mm diameter; Matrix thickness: 6 μm; Source strength: 10mCi and half life: 270 days.

3.5.4. γ-rays Detection System

Three types of detectors are used in Mössbouer spectroscopy the proportional counter, the scintillation detector and the solid state detector. For the energy region from 1 to 2okeV a proportional counter gives good performance with a high efficiency and a fairly good resolution. In this system Krypton filled proportional counter has been used. The counter consists of an

outer cylinder at ground potential and a center wire anode at a high positive potential ($\approx 1500V$) precisely 1700V in our case.

Table-3.1 Properties of ^{57}Fe isotopes

Isotope Abundance (%)	2.19
Transition energy (keV)	14.39
Spin and Parity I_g	$\dfrac{I^-}{2}$
I_e	$-\dfrac{3^-}{2}$
Excited state half life (sec)	9.8×10^{-8}
Internal conversion Co-efficient	9.00
Cross-section(cm^{-2})	2.43×10^{-18}
Magnetic moment μ_g (nm) μ_e (nm)	0.09024 -0.154
Quadrupoles moment Q_g(barns) Q_e(barns)	0.0 0.285
Natural width(keV)	4.655×10^{-12}
Observable width W_g (mm/s)	0.194
Recoil energy E_g (eV)	1.956×10^{-3}
Recoil free fraction of ^{57}Fe in Rh matrix (at 300k)	0.72

A γ-ray entering the counter ionizes the Krypton gas and forms in pairs. The electrons will accelerate to the anode and form other ion pairs by collision with the gas atoms. Multiplications factors as high as 10^5 can be obtained, and the anode current will be proportional to the γ-ray energy. To prevent a continuous electrical discharge in the counter, a quenching gas,

such as metheane, is added which dissipates the energy by dissociation. For higher γ-ray energies (> 20 keV) the scintillation counter is used. The solid state detector has extremely good energy resolution (600Ev at 14.4keV), but it cooled below 120^0k. For 14.4KeV γ-rays a proportional counter gives good performance with a high efficiency and a fairly good resolution. Proportional counter has got a very poor efficiency for 122 KeV and 136 KeV γ-rays. During this work, we have used a Krypton filled proportional counter which yielding 20% energy resolution. For further routing the signal to detect it, a preamplifier and a signal channel analyzer were used.

3.5.5 Pre-amplifier and Amplifier

The signal from the proportional counter is only 2mV. In order to select proper energy pulses using a single channel analyzer and to feed them to a multichannel analyzer for storage, pulses of -2V height are required. This would need a high gain amplifier. The proportional counter output is at an impedance of ~1MΩ. This has to be reduced to a few ohms in order to reduce the noise level. For this purpose the proportional counter output is fed to a preamplifier first, and its output is then fed to the amplifier [3.15]. The pre-amplifier serves as an impedance matching device.

3.5.6 Single Channel Analyzer

In order to select 14.4KeV pulses of γ-rays a single channel analyzer is used. Since height of the detector pulse is proportional to the γ-energy, a pulse height discriminator (or analyzer) is employed. It yields the output pulse only if the linear input pulses fall between prescribed upper and lower levels, the so-called window. Further details of the circuit performance may be found in reference [3.16]

3.5.7 Data Storage system

The spectrum reported in this work has been recorded in constant acceleration mode and so the data have been collected in multi scaling mode. For this a multi channel analyzer (MCA) has been used. This MCA works in time scaling mode and each channel opens for a constant

84

dwell time ranging from 0.2 msec to 2 msec. It has in all 1024 channels and has an option of using a minimum of 128 or integral multiple numbers of channels. The memory storage is magnetic type. We have used 512 channels. Synchronization is to be maintained between velocity amplitude of the drive and the channel number of MCA. The data are collected into groups. First group of 256 channels pertains to positive Doppler velocities and the second group of remaining 256 channels which is mirror image of the first pertains to negative Doppler velocities. The representative spectrum of ^{57}Fe absorber is shown in Fig-3.13.
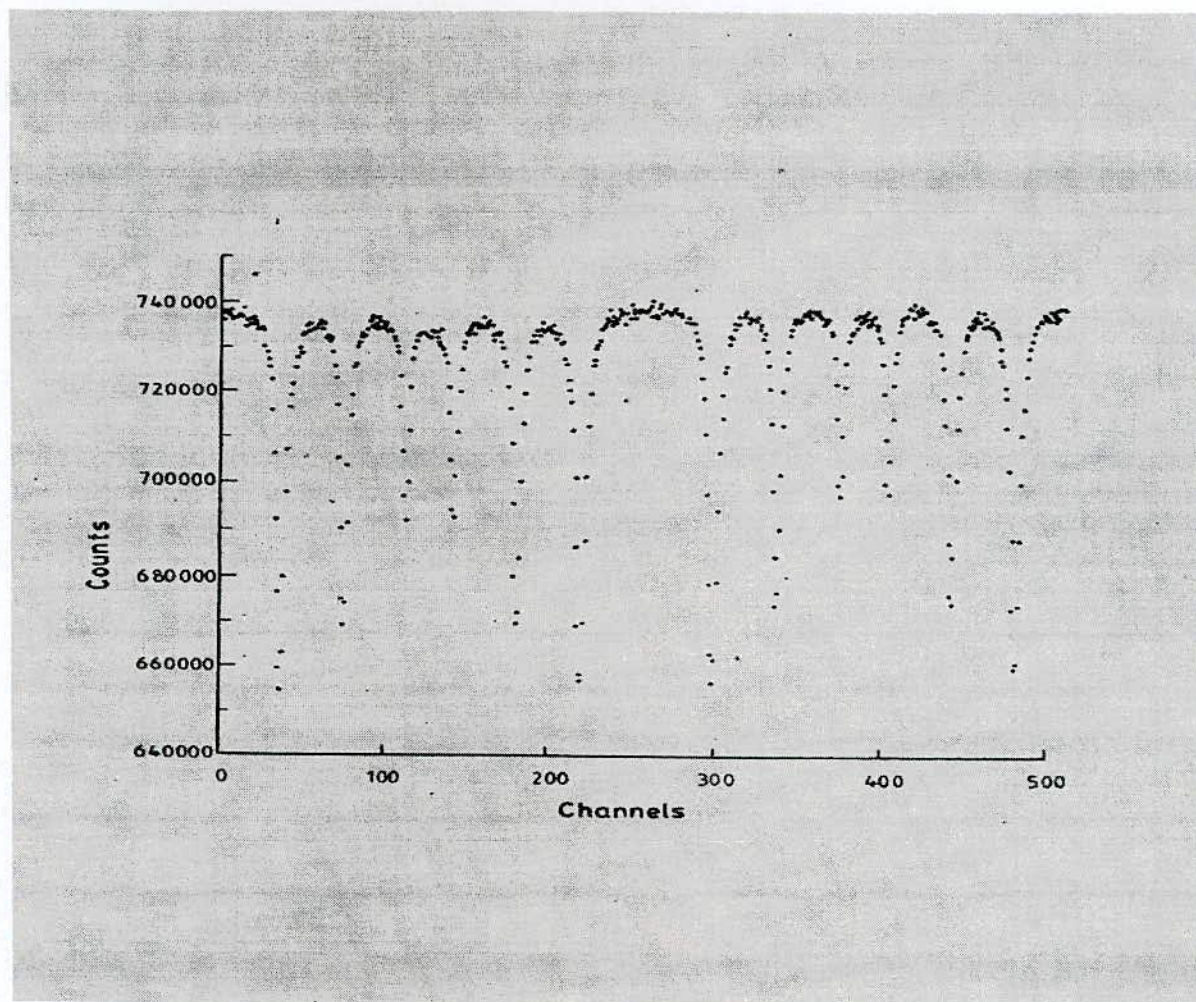
Fig-3.13: Room temperature Mössbauer transition spectrum for relative counts vs Channels of ^{57}Fe absorber.

3.5.8 Description of work done

Using the above Mössbauer set-up, with ^{57}Co as source and Natural Iron(^{57}Fe) as absorber, a Mössbauer spectrum is observed. For this we have used an exactly similar single channel analyser as discussed. Absorber is placed informet of the source at a distance of 10 cm. Velocity of the drive is set to 0.3 cm/s. Then using the MCA, counts are obtained in 512 channels. Then a graph between no. of counts versus velocity is plotted. In order to calculate the velocity per channel standard velocity between peaks are given in literature as in Fig-3.14. Using these values, velocity per channel is calculated.
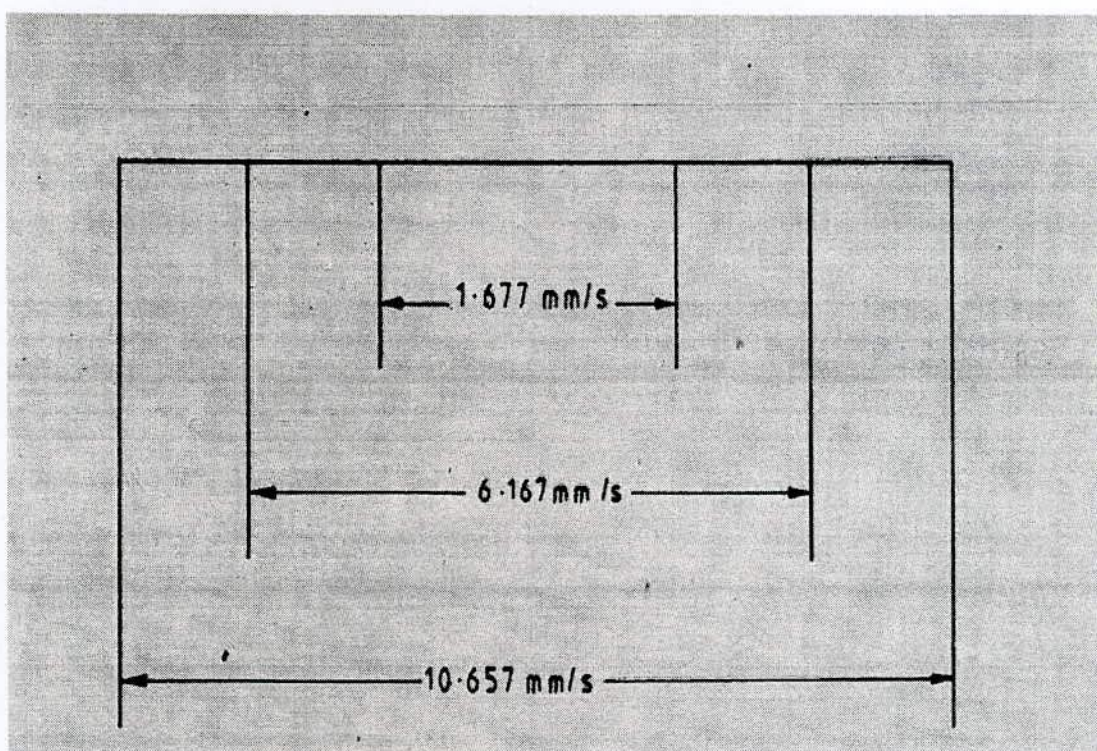
Fig-3.14: Standard velocity between peaks of ^{57}Fe absorber.

3.5.9 Calibration of ^{57}Fe absorber sample for measurement of Mössbauer parameters

Using the Mossbauer set-up spectrum for ^{57}Fe absorber is obtained. The number of counts versus velocity of the source is plotted in fig.3.15. Energies corresponding to the velocities are also denoted in the same figure. We see that there are are two groups of spectra which are mirror image of each other, containing six lines each.
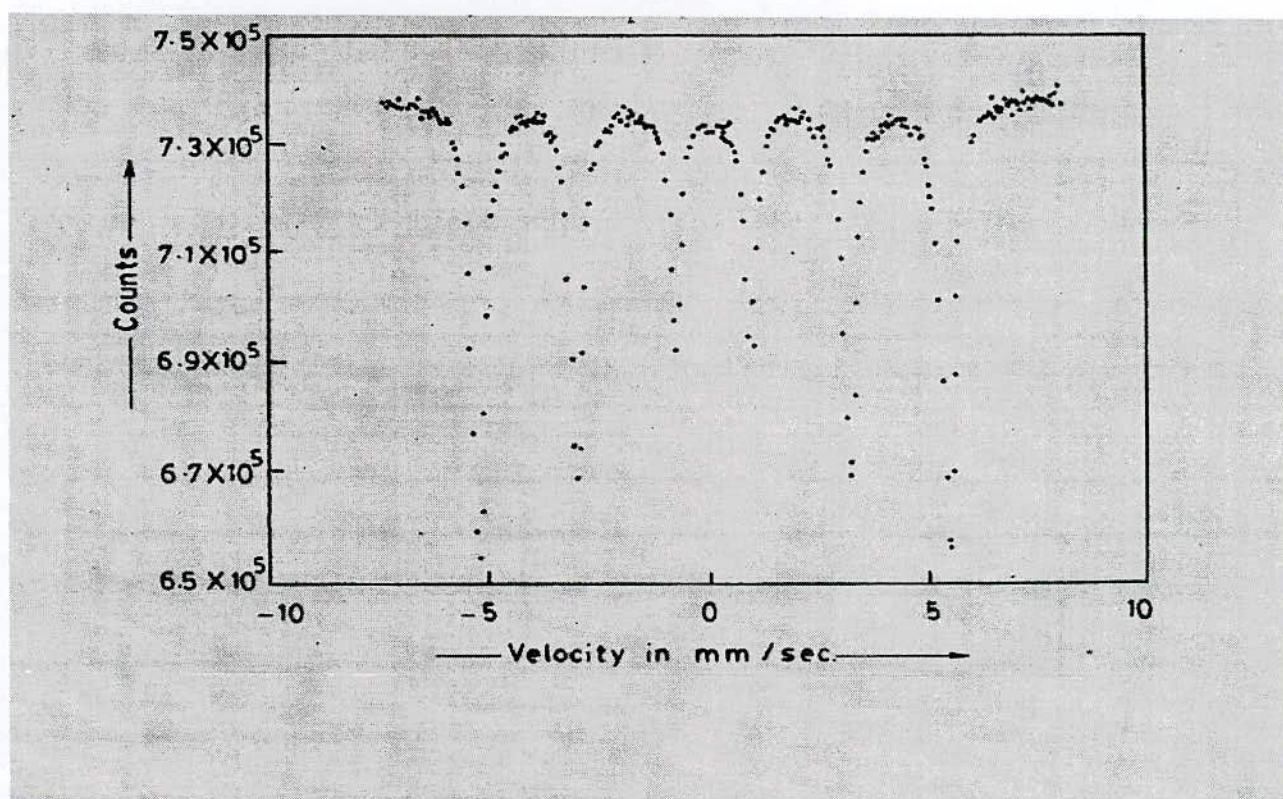
Fig- 3.15: Room temperature Mössbauer transition spectrum for relative counts versus velocity of ^{57}Fe absorber.

In the case of ^{57}Fe, there is in fact internal magnetic field acting at ^{57}Fe nucleus. This causes the upper $-\frac{3}{2}$ level to split to four levels and the lower $-\frac{1}{2}$ level splits into two levels.

Using the selection $\Delta m = 0, \pm 1$, for transition to occur, one gets six possible transitions. The source in Rh-matrix is a single line source. Hence in order to match the source energy to each of the six allowed energy difference, in Iron metal absorber; one has to give six different velocities to the source. This is automatically achieved in constant acceleration mode.

3.5.10 Computer Analysis of the Data

A non-linear variable matrices minimization technique is used iteratively to optimize the parameters of the theoretical function of minimizing χ^2 for the spectral data. First using the calibration spectrum of ^{57}Fe recorded at the same derive setting at which the sample spectrum is recorded, one linearizes the data and the two groups-(mirror images of each other) are folded resulting in improved statistics. The parabolic effect, a consequence of the proximity between the source and detector is eliminated through folding of the spectrum. The folded data is then used for analysis. The fitting is done with the following parameters: central shift, quadrupole splitting, internal hyperfine field, line width, site population and intensity ratios of the component in the magnetic pattern. Finally the experimental spectrum and the fitted function are plotted on a monitor to decide about the goodness of fit.

Chapter - IV

Results and Discussion

Chapter-IV

Results and Discussion of Co$_{1-x}$Cd$_x$Fe$_2$O$_4$ Ferrites

4.0 Introduction

Ferrites continue to be very attractive materials for technological applications due to their combined properties as magnetic conductors (ferrimagnetic) and electrical insulators. Co-ferrite posses an inverse spinel structure and the degree of inversion depends upon the heat treatment [4.1]. CoFe$_2$O$_4$ contains an isotropic magnetic ion Co^{+2}. The electrical and dielectric properties of materials substantially depends on the method of preparation [4.2], and heat treatment during Preparation [4.3] which controls the microstructure forming high resistive boundaries between the constituents grains. It has been demonstrated that the inversion is not complete in CoFe$_2$O$_4$ and the degree of inversion sensitively depends on the thermal treatment and method of preparation condition [4.4].

CdFe$_2$O$_4$ are generally assumed to be normal spinel with all Fe^{3+} ions on B-sites and all Cd^{+2} ions on A -sites [4.5-4.6]. The presence of a small fraction Cd^{+2} at tetrahedral sites enhances the hopping mechanism between $Fe^{+2} \Leftrightarrow Fe^{3+}$. Cd substituted mixed ferrite is interesting from applications point of view and has not been studied much in detail. The magnetic properties of ferrites such as permeability, magnetization, coercive field, Curie temperature are affected by composition as well as by the type of substitution, cation distribution and method of preparation. The partial replacement of nonmagnetic Cd ions in Co- ferrite is expected to weaken the magnetic coupling resulting in decrease of Curie temperature. A few reports are available on mixed Co-Cd ferrites [4.7-4.9]. The aim of the present thesis work is to investigate in detail the effects of substitution of Cd^{2+} ions covering a wide range of concentration on the structural, magnetic properties and Mössbauer spectroscopic analysis of Co$_{1-x}$Cd$_x$Fe$_2$O$_4$ferrites.

When magnetic dilution of the sublattices is introduced by substituting nonmagnetic ions in the lattice, frustration and/or disorder occurs leading to collapse of the collinearity of the ferromagnetic phase by local spin canting exhibiting a wide spectrum of magnetic ordering e.g. antiferromagnetic, ferromagnetic , re-entrant spin glass, spin glass and cluster spin glass [4.10,

89

4.11]. Small amount of site disorder i.e. cations redistribution between A and B sites is sufficient to change the super-exchange interactions which are strongly dependent on thermal history i.e. on sintering temperature, time and atmosphere as well as heating/cooling rates during materials preparation. The magnetic properties of ferrites such as permeability, complex permeability, magnetization, Curie temperature are affected by composition as well as by the type of substitution, cation distribution and method of preparation [4.12-4.13]. A systematic line broadening effect in the Mössbauer spectra was observed and was interpreted as originating from different Cd ion dependencies of the magnetic hyperfine field at various iron sites. The isomer shift indicated that the iron ions were ferric at the tetrahedral [A] and the octahedral [B]. The quadrupoles shift showed that the orientation of the magnetic hyperfine field with respect to the principal axes of the electric field gradient was random. As a comparative study, Mössbauer spectroscopy was employed in this work to evaluate $Co_{1-x}Cd_x Fe_2O_4$ following different periods of ball-milling. Like nonmagnetic Cd forms a divalent ion, and also has a strong preference for the A-sites.

4.1   X-ray Diffraction

4.1.1 Phase Analysis

Structural characterization and identification of phases are prior to the study of ferrite properties. X-ray diffraction (XRD) studies of the samples were performed by using Philips X' PERT PRO X-ray Diffractometer using Cu-K_α radiation in the range of $2\theta = 15°$ to $65°$ in steps of $0.02°$. The X-ray diffraction (XRD) patterns for the series of samples $Co_{1-x}Cd_xFe_2O_4$ ($x = 0.0$, 0.1, 0.3, 0.4 and 0.5) sintered at $1075°C$ for 2 hours is shown in Fig. 4.1. All the samples show good crystallization with well defined diffraction lines. A phase analysis using X-ray diffraction technique was performed to confirm the formation of single-phase cubic spinel structure with no extra lines corresponding to any other crystallographic phase. The results obtained from XRD pattern for all the samples of $Co_{1-x}Cd_xFe_2O_4$ with the (hkl) values corresponding to the diffraction peaks of different planes (111), (220), (311), (222), (400), (422), (511), and (440) which represent either odd or even indicating the samples are spinel cubic phase. The peaks are

found to shift slightly towards the lower d-spacing values which indicate that the lattice parameters are increasing with the increase of Cd content.
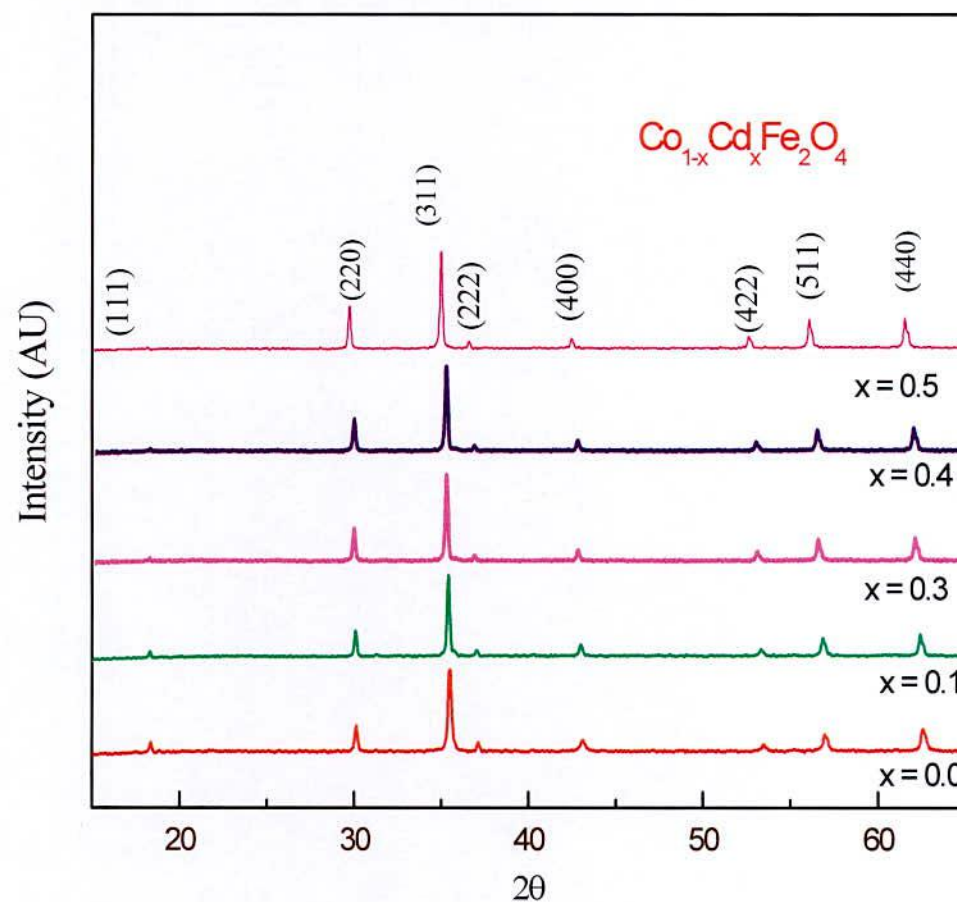
Fig.:4.1: X-ray diffraction patterns of $Co_{1-x}Cd_xFe_2O_4$ ferrites sintered at 1075^0C for 2 hrs.

The reflections also demonstrate the homogeneity of the studied samples. Therefore single phase spinel structure is confirmed for all the samples with increasing trend of the lattice parameter as the Cd content is increased. Using XRD data, the lattice parameter "a" and hence the X-ray densities were calculated.

4.1.2 Lattice Parameters

The accurate lattice parameter from the calculated lattice paramerter 'a' corresponding to each plane of XRD pattern using Nelson-Riley function [4.14]

$$F(\theta) = \frac{1}{2}[\frac{\cos^2\theta}{\sin\theta} + \frac{\cos^2\theta}{\theta}] \tag{4.1}$$
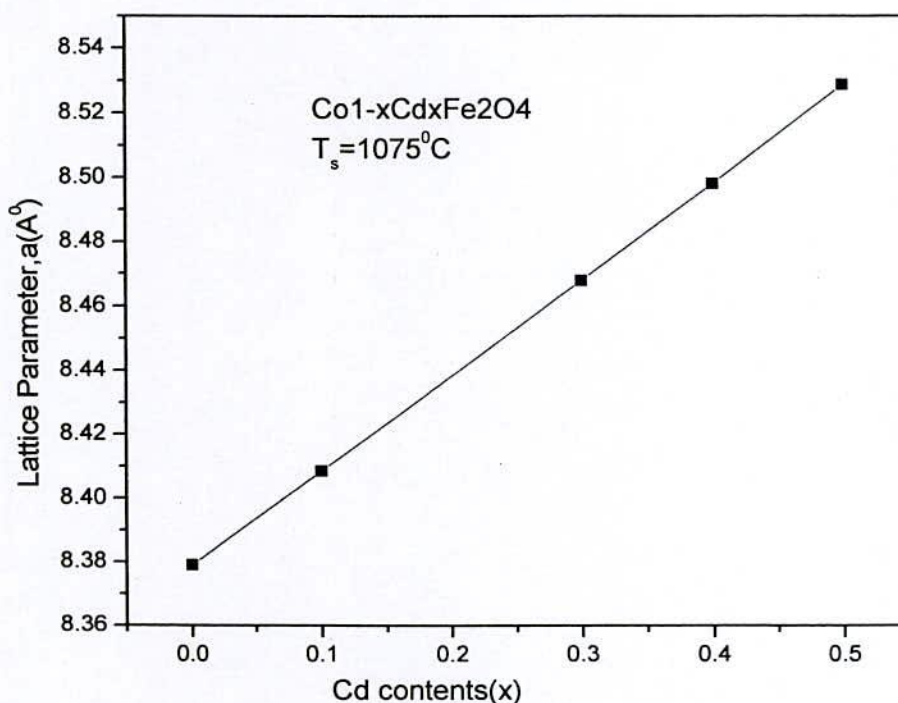
Fig.4.2: Variation of lattice parameter 'a' as a function of Cd content(x) of $Co_{1-x}Cd_xFe_2O_4$ ferrites.

where θ is the Bragg's angle, by extrapolating the lattice parameter values to $F(\theta) = 0$ or $\theta = 90°$. Variation of lattice parameter 'a' as a function of Cd content x is shown in Fig. 4.2 and also shown in Table - 4.1. From Fig. 4.2, it is observed that the lattice parameter increases linearly with increasing Cd content obeying Vegard's law [4.15]. This enhancement of lattice parameter is attributed to Cd^{2+} with larger ionic radius (0.97Å) which replaces Co^{2+} having smaller ionic

92

radius (0.72 Å) [4.16-4.17]. It is well known that the distribution of cations on the octahedral B-sites and tetrahedral A-sites determines to a great extent the physical, electrical and magnetic properties of ferrites. There exists a correlation between the ionic radius and the lattice constant, the increase of the lattice constant is proportional to the increase of the ionic radius [4.18]. Similar results for Co-Cd ferrite system have been reported by A. M. Abdeen et.al [4.19], A. R. Shitre et.al [4.17], O. M. Hemeda et.al [4.16], A.A. Ghani et.al [4.20]. The unit cell is expected to expand its size by expansion of the lattices resulting in increase of lattice parameter gradually.

4.1.3 Density and Porosity

Variation of density with Cd content is shown in Fig. 4.3. The bulk density, d_B, was calculated by usual mass and dimensional consideration whereas X-ray density, d_x, was calculated from the molecular weight and the volume of the unit cell for each sample by using the eq^n (3.6) and eq^n (3.5). The calculated values of the bulk density and X-ray density of the present ferrite system are listed in Table - 4.1.

The X-ray density and bulk density increase significantly with the increasing Cd-content. This may be due to the higher atomic weight and density of Cd are 112 and 8.9 g/cm^3 respectively Compared to Co of which corresponding values are 58.9 and 8.6 g/cm^3 respectively [4.21]. Therefore an increase of density with increasing Cd^{2+} is obviously expected. It is observed that the enhancement of density is significant up to low content of Cd i.e, x= 0.1 which means that small addition of Cd accelerates profoundly the ferritization process and mass transport mobility of cations. The result signifies that small amount of Cd has pronounced effect on the densification of the $CoFe_2O_4$ when it is substituted by Cd.

Moreover, due to lower melting point of CdO, sintering mechanism is accelerated resulting in an enhancement of density of the prepared samples. It is worthwhile to mention that density play an important role on the magnetic properties especially on the structure sensitive extrinsic property such as permeability, porosity changes slightly with Cd content and is shown in Table - 4.1. It is observed that porosity decreases monotonically with increasing Cd content in contrast

93

with bulk density which shows reverse behavior. This porosity which is intrinsic for any oxide materials plays an important role in deciding the magnetic and electrical properties.
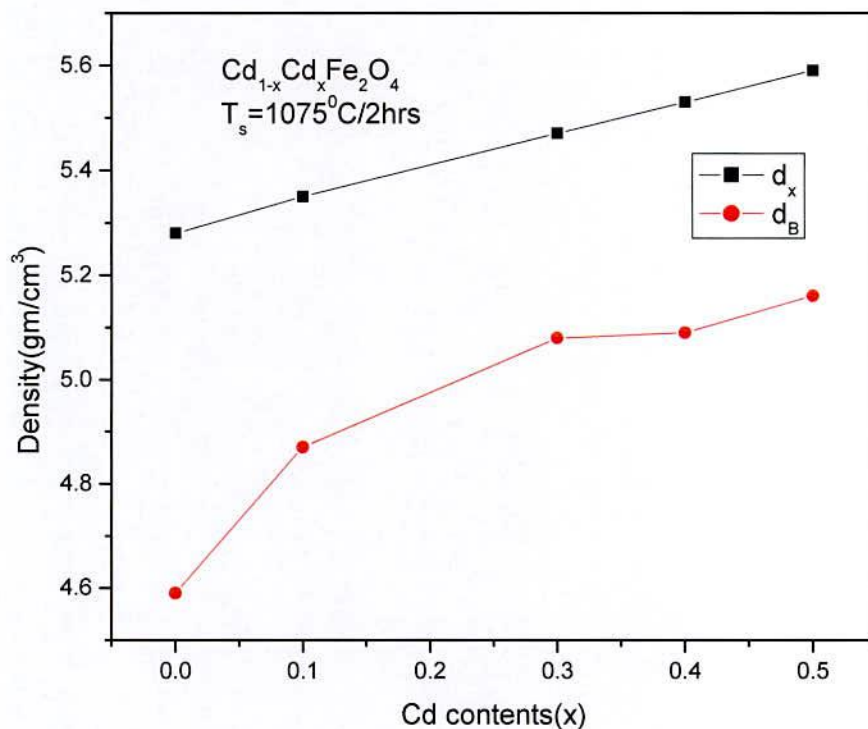
Fig. 4.3: Variation of density with Cd content (x) of $Co_{1-x}Cd_xFe_2O_4$ ferrites.

Table - 4.1 Data of the lattice parameter (a), X-ray density (d_x), bulk density (d_B), porosity (P %), Curie temperature (T_c) of $Co_{1-x}Cd_xFe_2O_4$ samples sintered at 1075°C in air for 2hrs.

Cd content (x)	a_o (Å)	d_x (g/cm^3)	d_B (g/cm^3)	P%	T_C (K)
0	8.379	5.28	4.59	13.9	723
0.1	8.409	5.35	4.87	8.8	658
0.3	8.468	5.47	5.08	7.3	515
0.4	8.498	5.53	5.09	8.0	462
0.5	8.529	5.59	5.16	7.6	393

4. 2. Magnetic properties

4.2.1 Temperature Dependence of Initial Permeability

Fig. 4.4 shows the temperature dependence of initial permeability (μ') for the toroid shaped samples $Co_{1-x}Cd_xFe_2O_4$ ferrites, where x = 0.0, 0.1, 0.3, 0.4, and 0.5 sintered at 1075^0C for 2 hrs, which is measured at a constant frequency (100 kHz) of an AC signal by using Impedance Analyzer. It is observed that the initial permeability increases with the increase in Cd content while it falls abruptly close to the Curie point. This is because Cd in these compositions not only increases the magnetic moment but also lowers anisotropy, K_1 [4.22]. On the other hand, permeability increases with the decrease of K_1 as the temperature increases according to the relation $\mu' \infty \dfrac{M_s^2 D}{\sqrt{K_1}}$ [4.23, 4.24].

It is observed from Fig. 4.4 that the permeability falls sharply when the magnetic state of the ferrite samples changes from ferromagnetic to paramagnetic. When the anisotropy constant reaches to zero just below the Curie temperature, μ' attains its maximum value and then drops off sharply to minimum value at the Curie point. The sharpness of the permeability drop at the Curie point can be used as a measure of the degree of compositional homogeneity [4.25] which has also been confirmed by X–ray diffraction that no impurity phases could be detected.
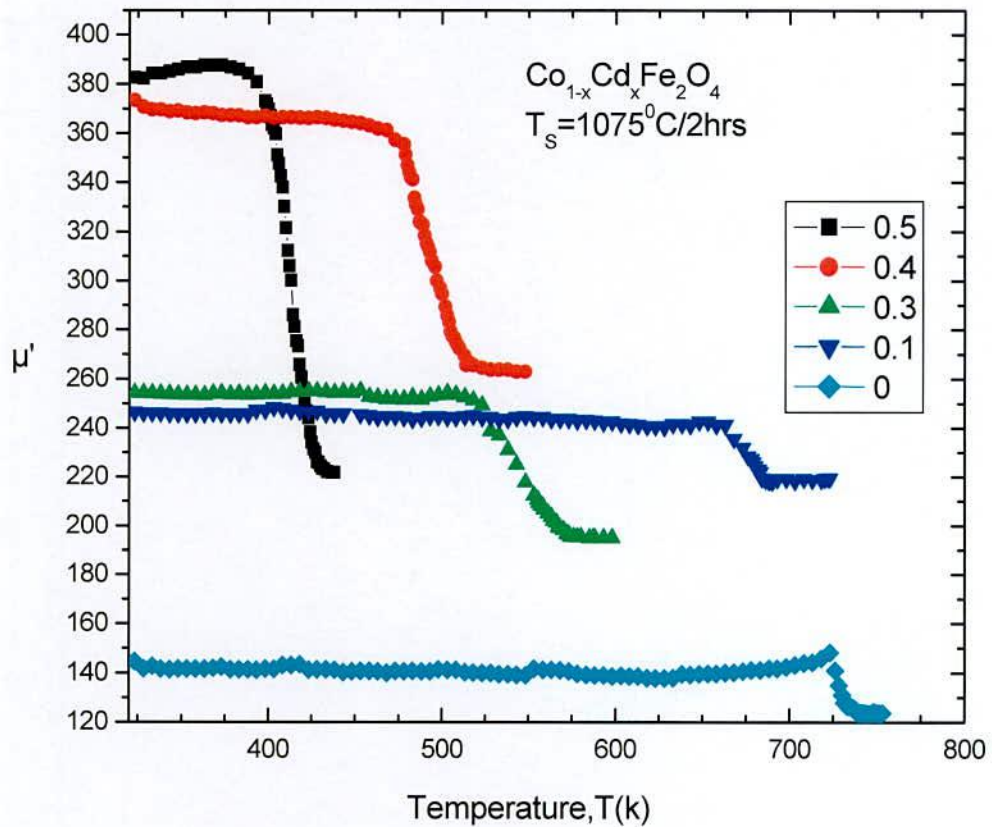
Fig. 4.4   Temperature dependence of real part of initial permeability, μ' of $Co_{1-x}Cd_xFe_2O_4$ ferrites sample sintered at 1075^0C for 2 hrs.

The μ'- T plot does not show any secondary maximum that may occur due to formation of magnetite (Fe_3O_4) by Fe^{2+} ions, there by indicating the single phase formation of the samples. This observation is supported by XRD patterns as well as the initial permeability versus temperature measurement. It is well known that anisotropy constant decreases considerably with temperature. In most cases, anisotropy decreases from a high value (at lower temperature) to zero near T_c [4.23]. It is observed that for the sample x = 0.0, the μ' increases with temperature to a maximum value just below the T_c which is the manifestation of Hopkinson effect. This occurs, because the crystal anisotropy becomes almost zero near T_c [4.23- 4.17]. Since anisotropy decreases faster than magnetization on heating, the initial permeability expectantly increasing with temperature tends to infinity just below the T_c and then abruptly falls to low value when the

96

samples become paramagnetic. The μ - T graph is smooth indicating that the temperature dependence of anisotropy is well compensated due to the substitution of Cd for Co resulting in decrease of anisotropy energy for the sample. It is also reflected in the value of permeability that μ has attained a value as high as $\mu \approx 385$ compared with $\mu \approx 145$ for the pure $CoFe_2O_4$ ferrite. The slight thermal hysteresis in permeability is also due to anisotropy effect in these samples.

4.2.2   Compositional dependence of Curie temperature

Fig. 4.5 shows the variation of Curie temperature T_c with Cd content of $Co_{1-x}Cd_xFe_2O_4$ ferrites and the values are taken during heating the sample. T_c of the studied sample was determined from μ'-T curve. The temperature corresponding to the peak value of $\frac{d\mu'}{dT}$ has been taken as the Curie temperature of the sample. The T_c values are shown in Table - 4.1. T_c is the transition temperature above which the ferrite material losses its magnetic properties. The Curie temperature gives an idea of the amount of energy required to break up the long-range ordering in the ferromagnetic material. The Curie temperature mainly depends upon the strength of A-B exchange interaction.

From Fig. 4.5 it is observed that Curie temperature linearly decreases with increasing Cd content. The non-magnetic Cd^{2+} ions replaced the magnetic Fe^{3+} ions on A-sites and thus the number of Fe^{3+} decreases on A-sites. This tends to decrease the strength of A-B exchange interactions. The decrease of T_c is due to the weakening of the A-B exchange interaction as well as due to increase of lattice parameter with Cd^{2+} content which increases the distance between the magnetic cations. A linear dependence of T_c with Cd content is observed upto $x = 0.5$. The linear decrease of T_c with x content is attributed to the progressive weakening of J_{AB} exchange interactions resulting from substitution of nonmagnetic Cd in the tetrahedral (A-site) occupancy.
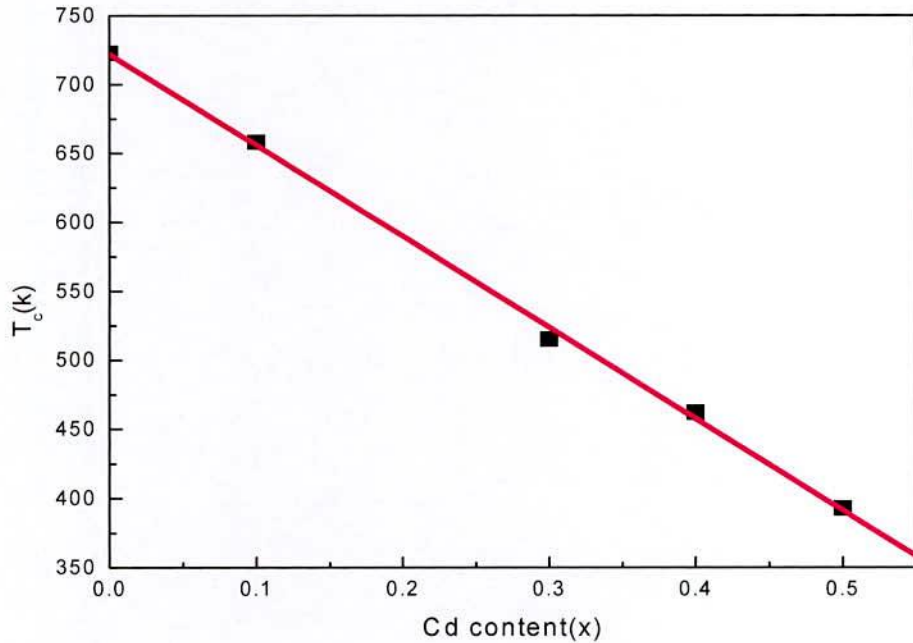
Fig. 4.5 Variation of Curie temperature, T_c with Cd content (x) of $Co_{1-x}Cd_xFe_2O_4$ ferrites.

A linear fitting of the Curie temperature with x gives an empirical relation for the samples. From this empirical relation Curie temperature of pure Co-ferrite is found to be 723K. Our experimental value of the Co-ferrite is 723K, the literature values are 735K [4.13], 793K [4.26] and 860K [4.30, 4.31]. The difference in determined T_c values by various authors are due to the deviation of the cation distributions as affected by thermal history of the samples as well as method of sample preparation.

4.2.3 Frequency Dependence of Initial Permeability

Initial permeability of polycrystalline ferrite is an important factor in the application of some devices. So, the optimization of the dynamic properties such as complex permeability in the high frequency range requires a precise knowledge of the magnetization mechanisms involved. The magnetization mechanisms contributing to the complex permeability, $\mu = \mu' - i\mu''$,

where, μ' is the real permeability (in phase) and μ" the imaginary permeability (90° out of phase). The real permeability μ' describes the stored energy expressing the component of magnetic induction while imaginary permeability μ" represent the loss of electric and magnetic energy. Complex permeability has been determined as a function of frequency, f upto 120 MHz at room temperature for all the samples of $Co_{1-x}Cd_xFe_2O_4$ (where x = 0.0, 0.1, 0.3, 0.4, and 0.5), ferrites by using the conventional technique based on the determination of the complex impedance of a circuit loaded with toroid shaped sample. Fig-4.6 (a, b, c) represents the results of the real part of the permeability, μ', and Fig-4.7(a, b, c) imaginary part, μ'' as a function of frequency for the whole series of ferrite sample sintered at 1075^0C for different time 1 hours,2 hours and 4 hours respectively.

All the measurements have been done using Wayne Kerr Impedance Analyzer (Model No. 6500B) in the frequency range of 1 kHz–120 MHz at room Temperature. From figs.4.6(a, b, c) it was noticed that the real part of the complex permeability remains fairly unchanged over a large range of frequency (up to 10MHz), rises slightly to reach a maximum and then decreases rapidly to very low at very high frequency. We can call this real part of the permeability, μ' as initial permeability. It is clearly evident from this figure that the initial permeability μ' increases with the increase of Cd content up to x=0.5. Again the increase of permeability with Cd content is connected with increased magnetization density, grain size and possible reduction of anisotropy energy with the addition of nonmagnetic Cd.

From Fig 4.7(a, b, c), the imaginary component, μ'' first rises and then increases quite abruptly making a peak at certain frequency (called resonance frequency, f_r) where the real component, μ' is falling sharply. It is observed from the fig-4.8 that the higher the permeability lowers the resonance frequency of the material. This phenomenon is attributed to the ferromagnetic resonance [4.28]. Resonance frequency (f_r) was determined from the maximum of imaginary permeability of ferrites. The resonance frequency peaks are the results of the absorption of energy due to matching of the oscillation frequency of the magnetic dipoles and the applied frequency. Since the starting point of resonance frequency determines the upper limit of the

operational frequency of any device, it predicts that the operational frequency range of the samples was stable up to about 7MHz and the permeability dispersion initiated above 7MHz.
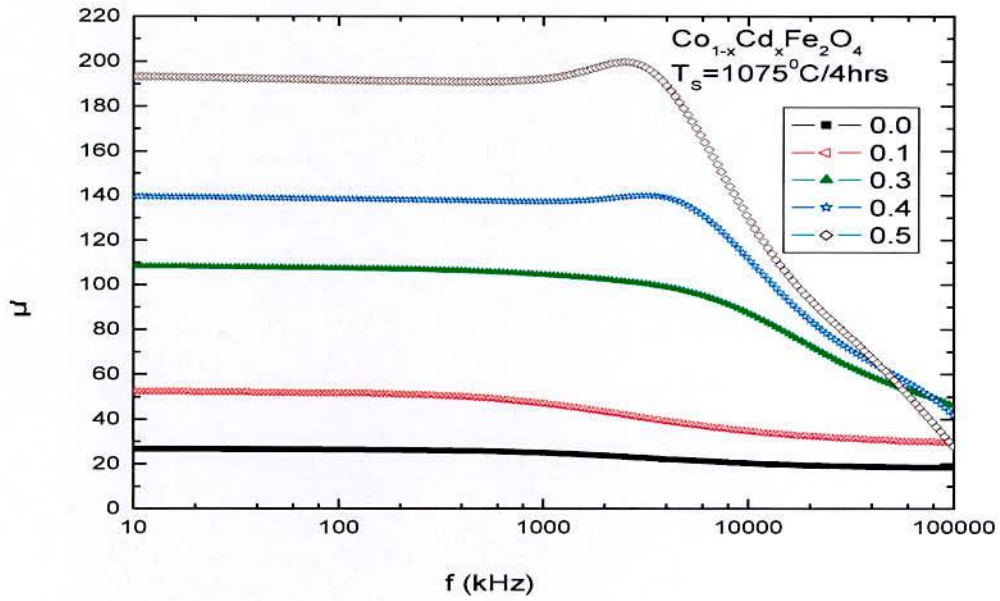

(a)
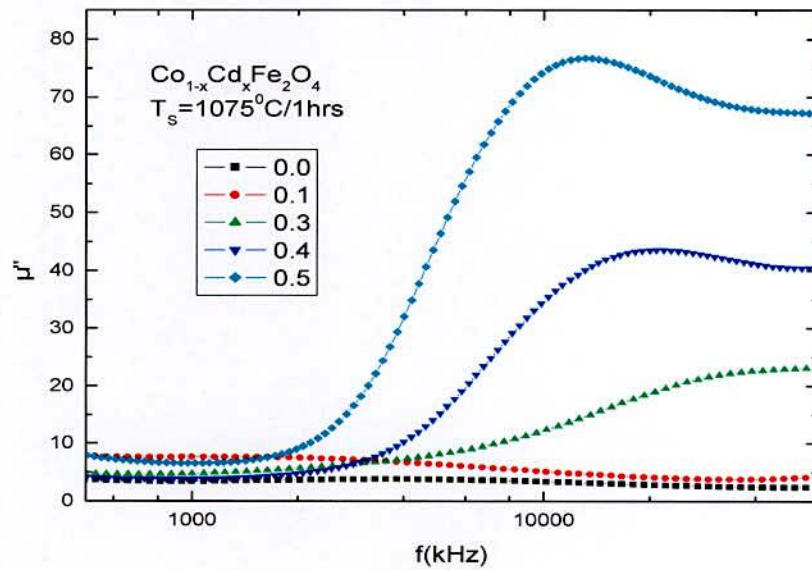

(b)

100
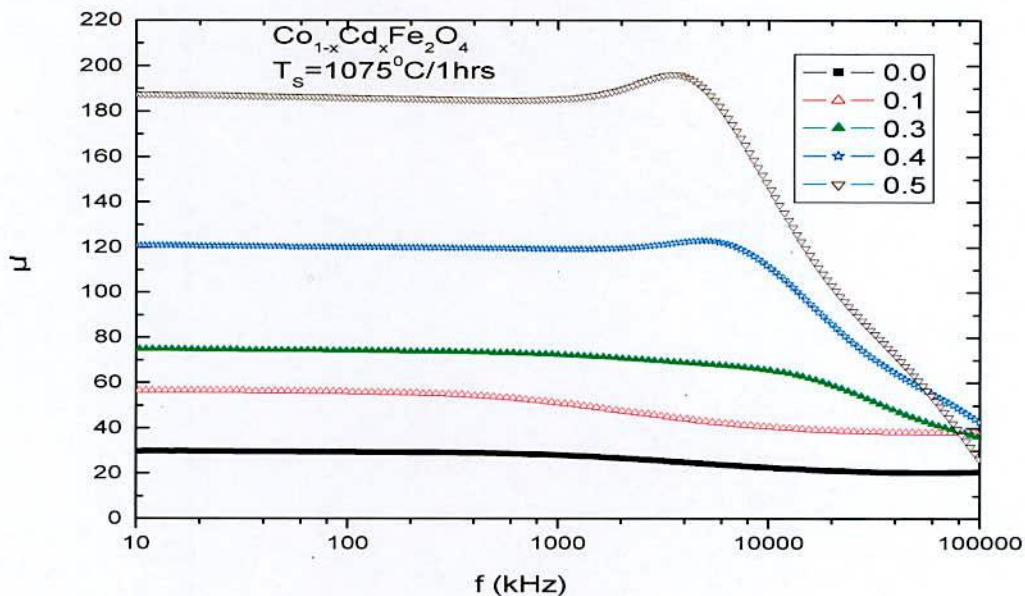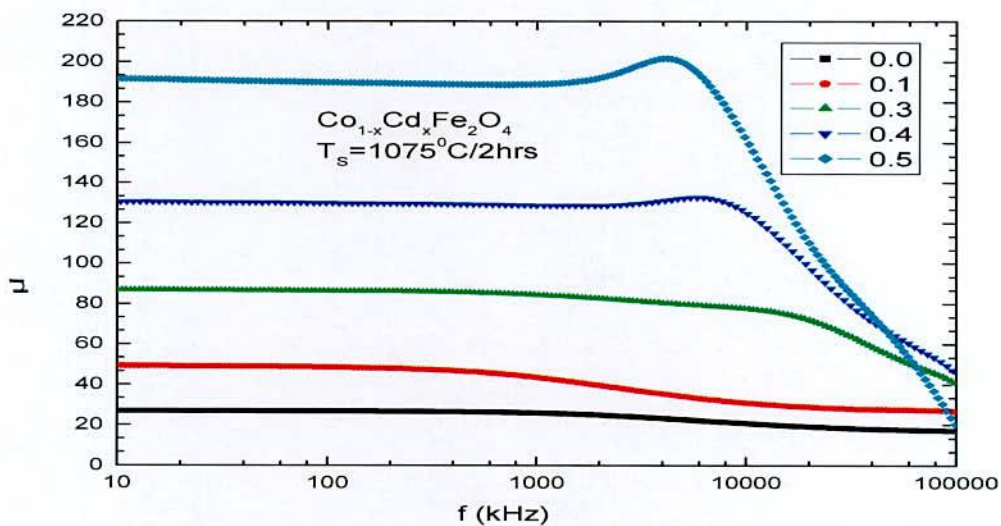
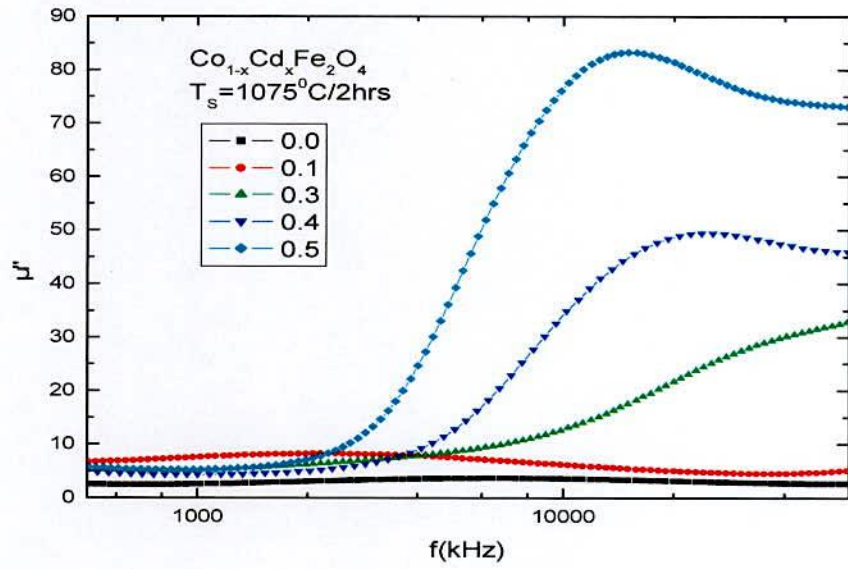(c)
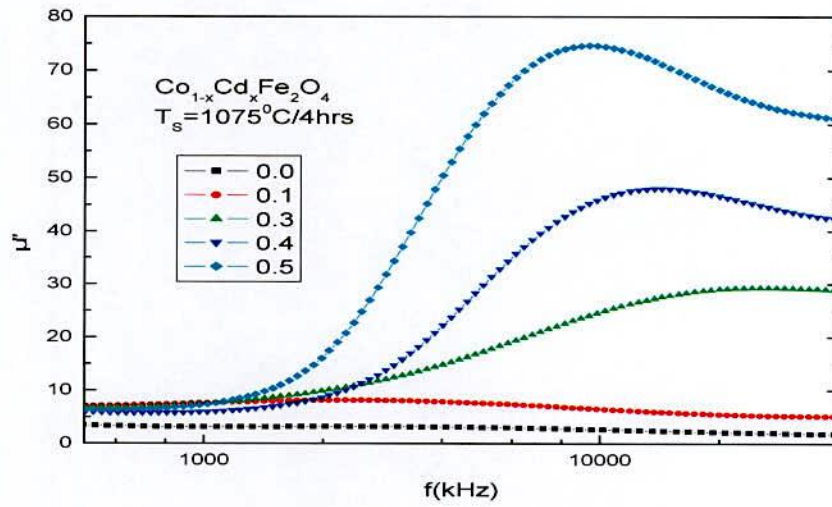
Fig. 4.6 Frequency dependence of the real part of the permeability, μ' of $Co_{1-x}Cd_xFe_2O_4$ ferrites sintered at 1075°C for (a) 1hour (b) 2 hours and (c) 4 hours.

(a)

(b)

(c)

Fig. 4.7   Frequency dependence imaginary part of the permeability, μ'' of $Co_{1-x}Cd_xFe_2O_4$ ferrites sintered at 1075°C for (a) 1hour (b) 2 hours and (c) 4 hours.
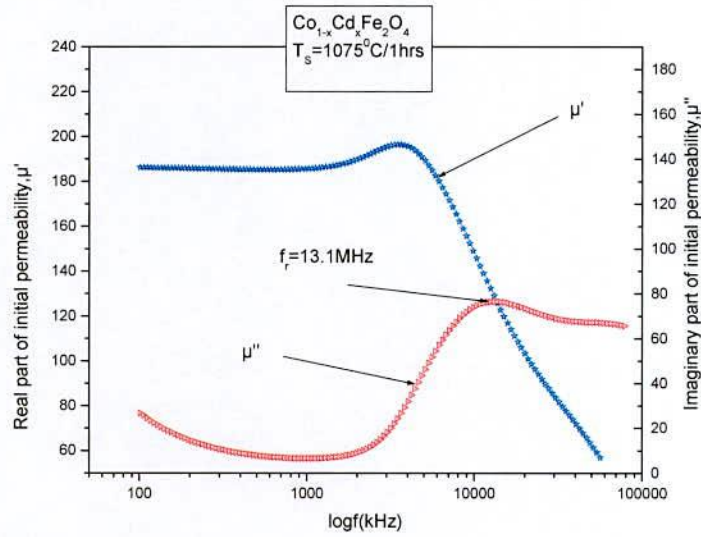
Fig.4.8 Variation of real and imaginary part of initial permeability with frequency $Co_{1-x}Cd_xFe_2O_4$ ferrites where x=0.5 sintered at 1075^0C for 1 hour.

4.2.4 Compositional Dependence of Initial Permeability

Permeability of polycrystalline ferrites is related to the spin rotation and domain wall motion [4.28]. Spin rotation and domain wall motion are related as $\mu = 1 + \chi_w + \chi_{spin}$ where, χ_w is the domain wall susceptibility, χ_{spin} is the intrinsic rotational susceptibility. The domain wall susceptibility and the intrinsic rotational susceptibility are given by the following equations

$$\chi_w = \frac{3\pi M_s^2 D}{4\gamma} \tag{4.2}$$

$$\chi_{spin} = \frac{2\pi M_s^2}{K} \tag{4.3}$$

Where, M_s, K, D and γ are the saturation magnetization, total anisotropy, average grain diameter, and domain wall energy, respectively. Properties of ferrites are dependent on their compositions, additives and microstructures. It is well known that the magnetic properties are

103

greatly influenced by the microstructures; the larger the grain sizes, the higher the saturation magnetization and larger initial permeability. Ferrites with lower initial permeability and saturation magnetization are suitable for microwave applications.
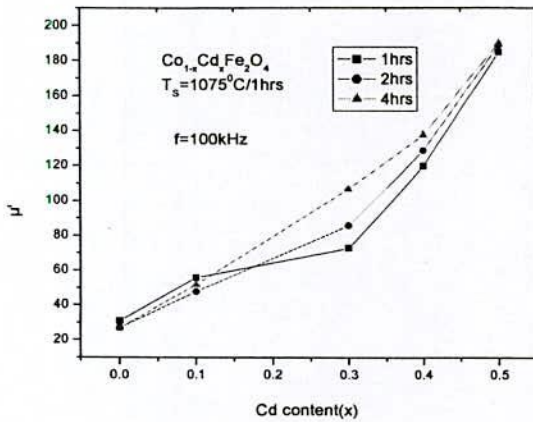
Fig.4.9: Real part of complex permeability of $Co_{1-x}Cd_xFe_2O_4$(x = 0.0, 0.1, 0.3, 0.4, 0.5) as a function Cd content (x) sintered at 1075^0C for different time.
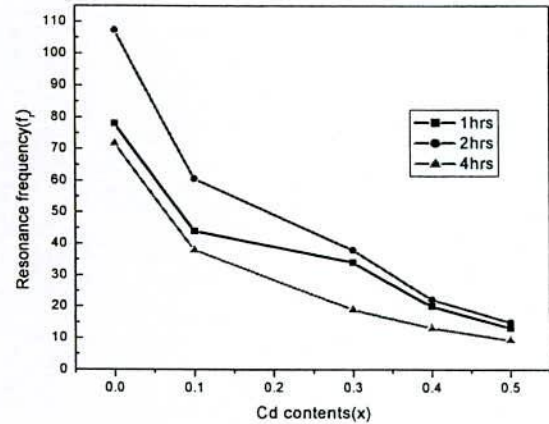
Fig.4.10: Resonance frequency of $Co_{1-x}Cd_xFe_2O_4$(x = 0.0, 0.1, 0.3, 0.4, 0.5) as a function Cd content (x) sintered at 1075^0C for different time.

Fig-4.9 shows that the variation of initial permeability (at 100kHz) with Cd content of $Co_{1-x}Cd_xFe_2O_4$ ferrites at constant sintering temperature 1075^0C varying sintering time 1hr, 2hrs and 4hrs while the resonance frequency decreases with Cd content (x) as shown in fig.4.10 and we have also studied the effect of sintering time on the permeability of Co-Cd ferrites. Here we found that the real part of complex permeability almost constant for x=0.0 and 0.1 while increases for x=0.3, 0.4 and 0.5 with sintering time shown in Fig-4.11.The increase in permeability with sintering time can be attributed to the increase in density and grain size and decrease in porosity with sintering time. The large grain diminishes the grain boundary, thereby the domain walls can move easily, which leads to higher permeability. Moreover, the increase in sintering time leads to decrease in the internal stress and crystal anisotropy, which cause a decrease in the magnetic anisotropy. Hence the hindrance to the movement of the domain walls reduces, which increases the value of the initial permeability (4.29).
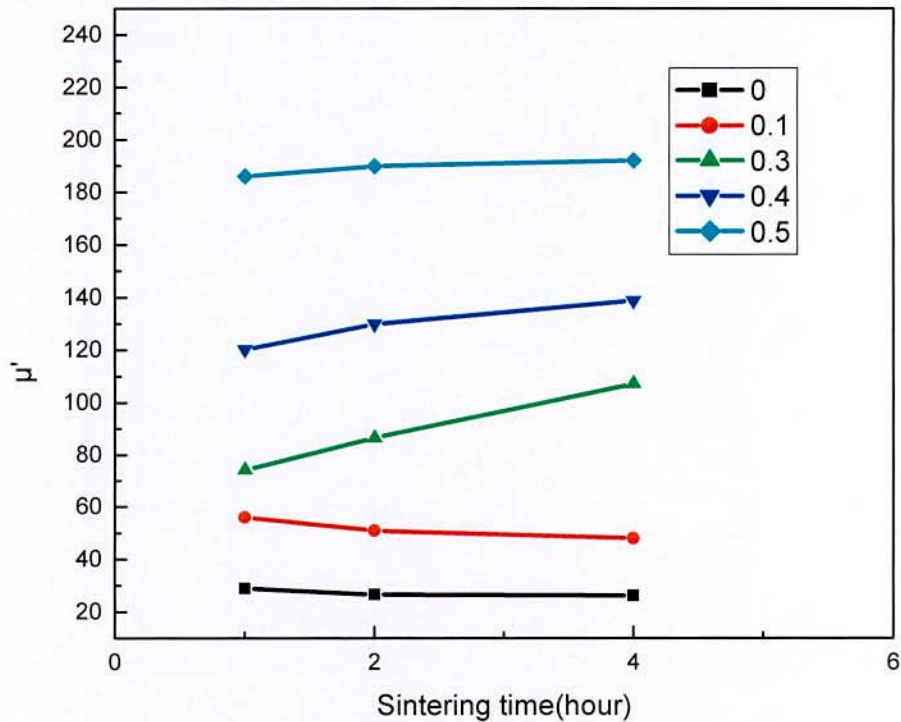
Fig.4.11: Sintering time dependent real permeability of $Co_{1-x}Cd_xFe_2O_4(x = 0.0, 0.1, 0.3, 0.4, 0.5)$ ferrites.

A comparative study of the complex permeability of $Co_{1-x}Cd_xFe_2O_4$ ferrites with frequency sintered at 1075^0 C for 1hr, 2hrs and 4hrs has been shown in Fig. 4.11. Fig 4.11 shows that samples sintered at 1075^0 C for 4 hours have higher permeability than that sintered at 1075^0 C for 1 hour and 2 hour.

Therefore, permeability increases with increasing of annealing time. It is clear that, if pores can be suppressed or located at the grain boundaries, the permeability may be increased with grain size. The relationship between grain size and permeability would generally be linear only if the grains growth petty much at the same time and rate. It is also observed that the higher the permeability of the material, the lower frequency of the onset of ferromagnetic resonance. This really confirm with Snoek's limit $f_r \mu' =$ constant (4.30), where f_r is the resonance frequency for domain wall motion above which μ' decreases. This means that there is effective limit to the product of resonance frequency and the permeability so that high frequency and high

105

permeability are mutually incompatible. The resonance frequency of Snoek's limit $f_r\mu'$ along with the permeability of the samples are shown in Table-4.2

Table-4.2: Data for real permeability (μ'), resonance frequency (f_r) and Snoek's limit ($f_r\mu'$) of $Co_{1-x}Cd_xFe_2O_4$ ferrites.

| Cd, Content (x)	Sintering Time, t=1hrs			Sintering Time, t=2hrs			Sintering Time , t=4hrs		
	Permeability (μ') at 100kHz	Resonance frequency f_r(MHz)	Snoek's limit ($f_r\mu'$ = const.)	Permeability (μ') at 100kHz	Resonance frequency, f_r(MHz)	Snoek's limit (f_r = const.)	Permeability (μ' at 100kHz	Resonance frequency, f_r(MHz)	Snoek's limit (f_r μ' = const.)
0.0	29	78	2418	27	107.4	2818	27	71.8	1940
0.1	56	44	2464	48	60.62	2910	52	38	1976
0.3	73	34	2482	86	38	3268	107	19	2033
0.4	120	20	2400	129	22.2	2863	138	13.1	1807
0.5	185	13.1	2423	189	15	2835	190	9.38	1782

4.2.5 Frequency Dependence of Relative Quality Factor

Fig. 4.12 (a, b, c) represents the frequency dependence of relative quality factor (RQF) of Co-Cd ferrites sintered at 1075^0C for different annealing time. The quality factors were calculated from the magnetic loss tangent measured on the coil wound toroidal shaped samples. The variation of RQF with frequency shows a similar trend of the samples. The RQF increases with the rise in frequency showing a sharp maximum and then starts decreasing with the further increase in frequency. It is seen that RQF deteriorates beyond 1.02MHz i.e, the loss tangent is minimum up to 1.02MHz and then it rises rapidly. The loss is due to lag of domain wall motion with the applied alternating magnetic field and is attributed to various domain defects [4.31], which include non-uniform and non-repetitive domain wall motion, domain wall bowing, localized variation of flux density, and nucleation and annihilation of domain walls. This happens at the frequency where the permeability begins to drop. This phenomenon is associated with the ferromagnetic resonance within the domains [4.32] and at the resonance maximum

106

energy is transferred from the applied magnetic field to the lattice in the rapid decreases in RQF. From the Fig -4.12, it is also noticed that the relative Q-factor of the samples increases with the increase in Cd content(x). Highest value of the relative Q-factor of Co-Cd ferrites was recorded at x = 0.5. Peaks corresponding to the maxima in Q-factor were shifted towards the higher frequency side with the increase in Cd content(x) to the samples shown in fig.-4.13.
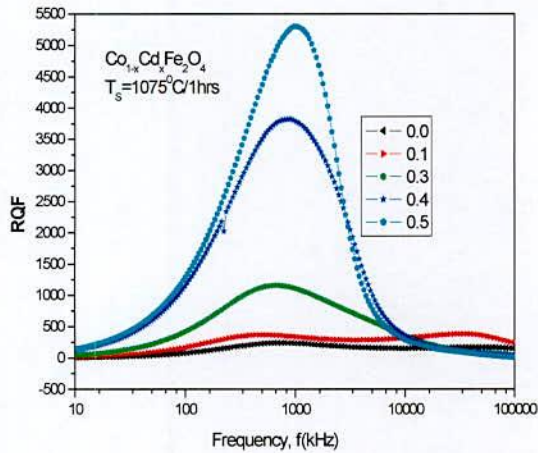
(a)
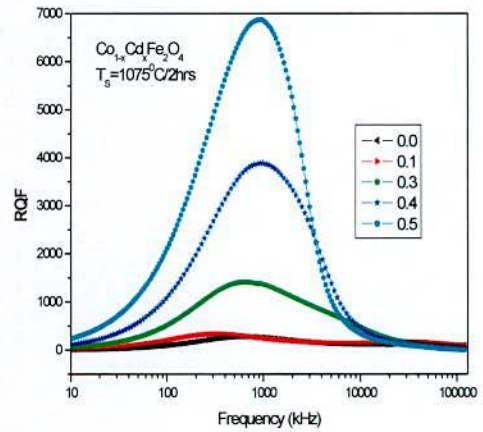
(b)
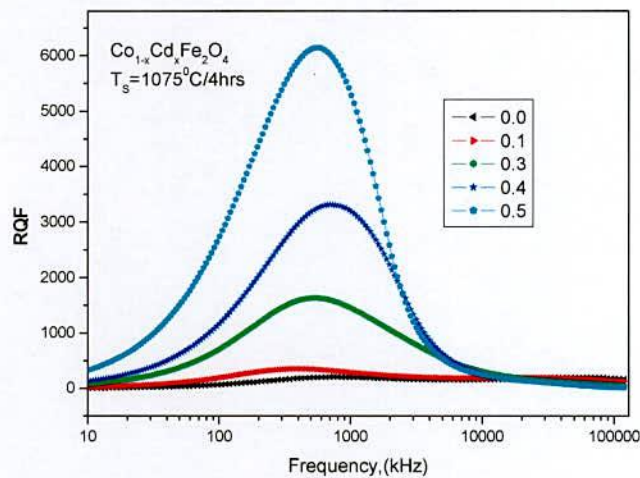
(c)

Fig.4.12 Variation of Relative Quality Factor (RQF) with frequency of $Co_{1-x}Cd_xFe_2O_4$ ferrites sintered at 1075^0C for different annealing time (a) 1 hour (b) 2 hours and (c) 4 hours.

107
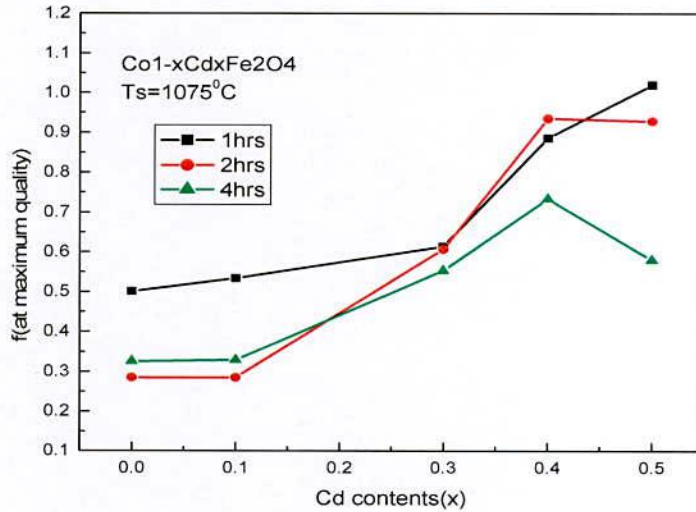
Fig.4.13   Variation of frequency, f (at maximum quality) with Cd content (x) of Co_{1-} $_xCd_xFe_2O_4$ ferrites sintered at 1075^0C for different annealing time.

4.2.6   Variation of Saturation Magnetization at Room Temperature

The magnetic properties measured by vibrating sample magnetometer (VSM) at room temperature for $Co_{1-x}Cd_xFe_2O_4$ (x = 0.0, 0.1, 0.3, 0.4, 0.5) ferrites sintered at 1075^0C for 2 hours. The room temperature magnetic hysteresis (M-H) loop of the samples has been measured and is presented in Fig-4.14. The hysteresis loops show a little hysteresis effect. The magnetization under applied magnetic field for the as–prepared samples exhibits a clear hysteretic behavior. It is observed that the magnetization increases sharply at very low field (H< $1kO_e$) which corresponds to magnetic domain reorientation and thereafter increases slowly up to saturation magnetization defined as the maximum possible magnetization of a material.
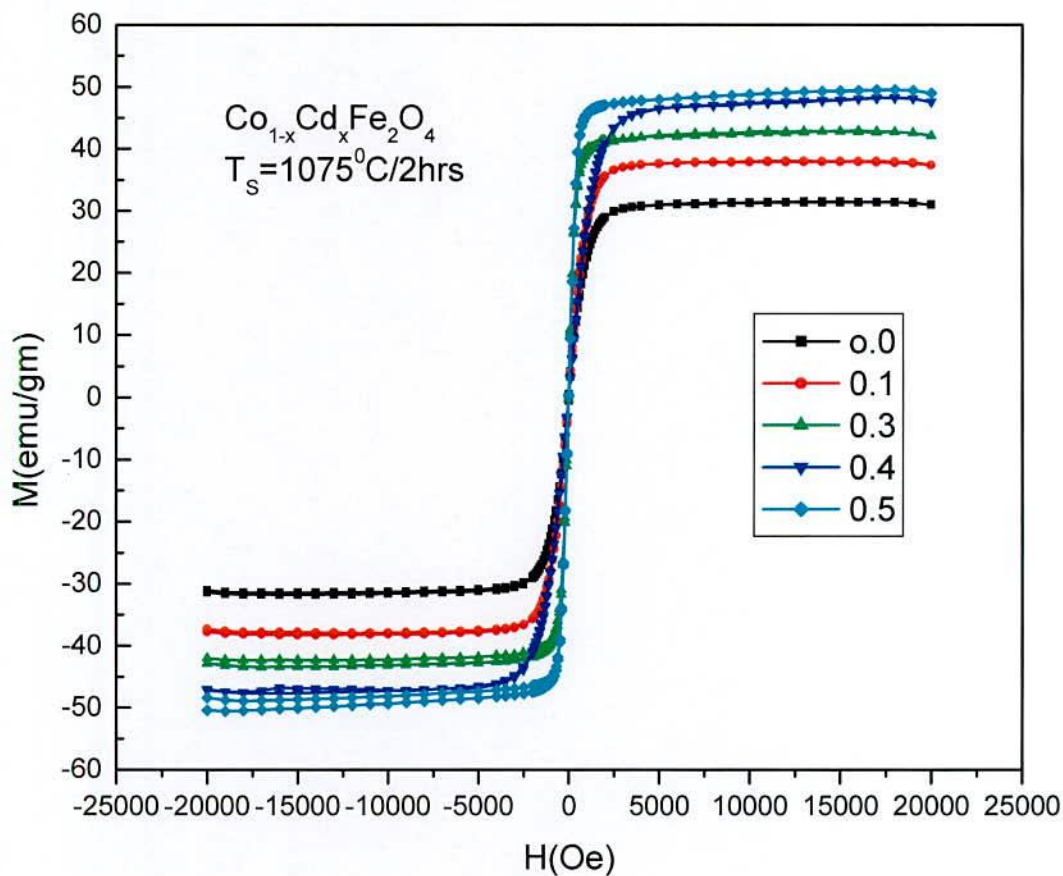
Fig.4.14: Variation of magnetization at room temperature as a function of applied field on
Co$_{1-x}$Cd$_x$Fe$_2$O$_4$ ferrites sintered at 1075^{0}C for 2hours.

The room temperature saturation magnetization (Ms) as a function of field of the samples has been measured and is presented in Fig-4.15. It is observed that saturation magnetization is saturated with an applied field of H=3.0kO$_e$ The saturation magnetization (M$_s$) of the Co$_{1-x}$Cd$_x$Fe$_2$O$_4$ ferrites as a function of Cd content at room temperature is shown in Fig. 4.15 and Table - 4.3. It is observed that saturation magnetization, increases with the increase of Cd

content. The observed variation in saturation magnetization can be explained on the basis of cation distribution and the exchange interactions between A and B sites, respectively.
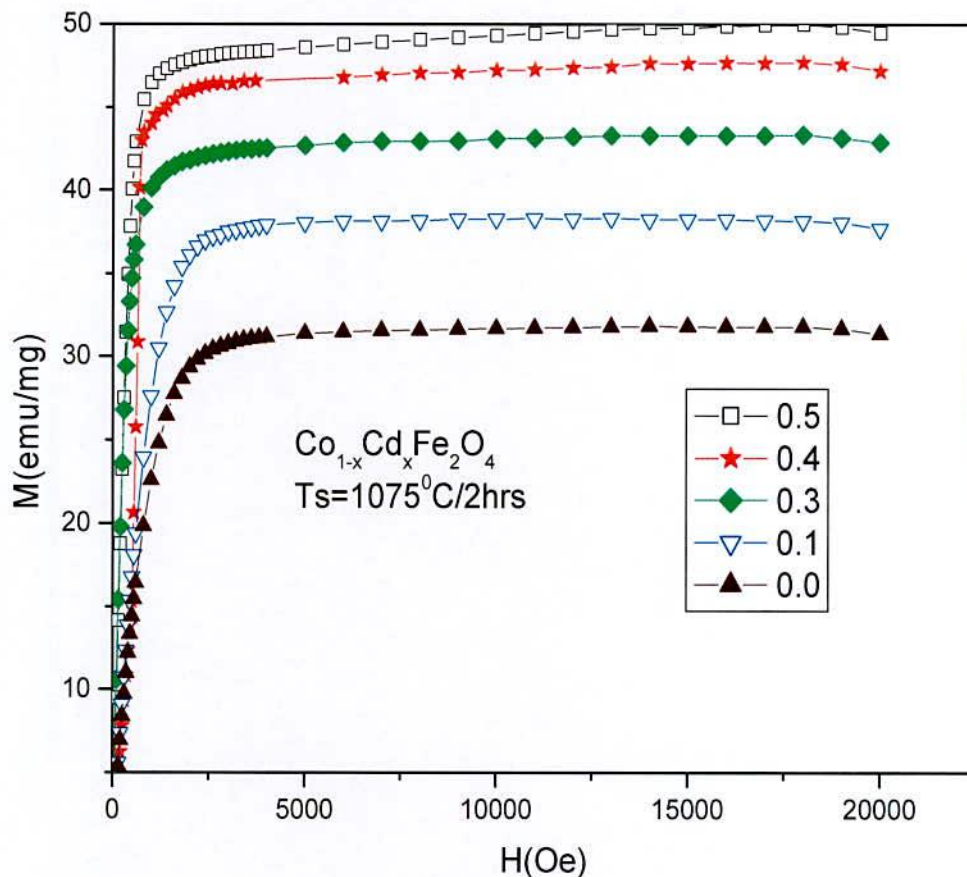
Fig.4.15: The Magnetization (M) versus the applied magnetic field (H) curves of $Co_{1-x}Cd_xFe_2O_4$ ferrites sintered at 1075^0C for 2hours.

From these values of saturation magnetization, the magneton number i.e., saturation magnetization per formula unit in Bohr magneton, n_B was calculated using the relation [4.33]

$$n_B = \frac{MMs}{\mu_B N} ,$$

(4.4)

where M is the molecular weight of the ferrite sample, M_s is the saturation magnetization emu/gm, N the Avogradro's number and μ_B the Bohr magneton. The value of M_s, n_B (experimental, theoretical) is shown in Table - 4.3. It is observed that saturation magnetization, increases with the increase of Cd content.

Initial increase of magnetization is attributed to the preferential occupation of A-sites by Cd^{2+}, thus displacing an equal amount of Fe^{3+} from A-sites to B-sites leading to the difference in magnetization between the B sublattice and the A sublattice, $M = M_B - M_A$ in the antiferromagnetic coupling. This enhancement of magnetization with increasing cadmium content is explained based on Neel's two sublattice model [4.34].
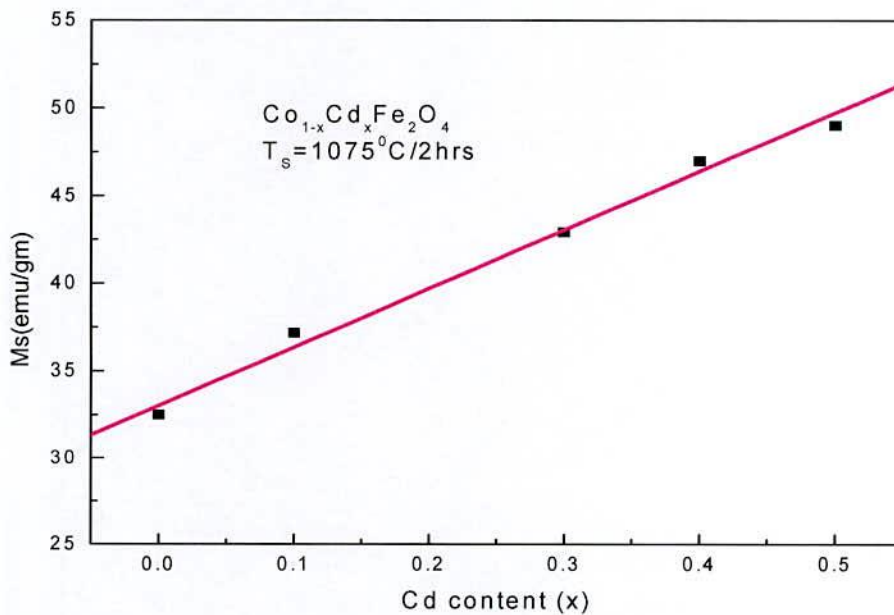
Fig.4.16: Saturation magnetization (M_s) of $Co_{1-x}Cd_xFe_2O_4$ as a function of Cd content (x) at room temperature.

Magnetic moment of any composition depends on the distribution of Fe^{3+} ions between A and B sub lattices since Cd^{2+} is nonmagnetic having zero net magnetic moment and that of

111

Fe^{3+} is $5\mu_B$. The replacement of x amount of Cd^{2+} ions (Cd^{2+} occupies A-sites) for Co^{2+} can give rise to (1-x) Fe^{3+} ions on A-sites and (1+x) Fe^{3+} ions on B-sites and considering that all Co^{2+} occupies B-sites with magnetic moment of $3\mu_B$. The cation distribution then takes the following form; $(Cd_xFe_{1-x})_A[Co_{1-x}Fe_{1+x}]_B$. The Cd^{2+} substitution leads to increased Fe^{3+} ions on B-sites and consequently magnetization of the B-sites increases while that of A-sites decreases resulting in an increase of net magnetization M= M_B - M_A. The existence of canted spin gives rise to the Yafet-Kittel angle (α_{Y-K}), which compares the strength of A-B and B-B exchange interactions [4.35]. Y-K angles are calculated at 298K using the following formula

$$n_B = M_B(x)\cos \alpha_{Y-K} - M_A(x),\qquad(4.5)$$

Where α_{Y-K} is the canted angle.. It is observed that α_{Y-K} angles for the samples are non zero; i.e Y-K has a small value. This means that the cation distribution is not exactly as proposed by theory. Increase in Y-K angles for the samples with Cd content is attributed to the increased favour of triangular spin arrangements on B-sites leading to the reduction in the A-B exchange interaction and subsequent decrease in magnetization [4.36, 4.37]. Almost Cd^{2+} substituted ferrites have shown a similar type of canting behavior above a certain limit of their content [4.38 - 4.39]. Hence in the present system of ferrites, frustration and randomness increases as Cd content increase in the Co-ferrites and shows significant departure from Neel's collinear model.

Table- 4.3 Data of saturation magnetization (M_s), theoretical and experimental magnetic moment (n_B) and Yafet–Kittel angle (α_{Y-K})

Cd content (x)	Saturation Magnetization Ms (emu/g)	Magnetic Moment n_B (μ_B)		Yafet–Kittel angle
		theoretical	experimental	α_{Y-K}
0	32.5	3	1.3	38
0.1	37.2	3.7	1.54	42
0.3	42.92	5.1	1.86	51
0.4	47	5.8	2.06	54
0.5	49	6.5	2.2	58

4.2.7 Variation of Magnetization with Temperature

The effect of temperature on magnetic material can be determinate by the magnetic properties of the materials. Rising the temperature of a solid, result in the increase of the thermal vibrations of atoms, with this the atomic magnetic moments are free to rotate. This phenomenon the atoms tend to randomize the directions of any moments that may be aligned. From fig. 4.16, it is observed that with increasing temperature, the saturation magnetization diminishes gradually and abruptly drops to zero at what called the Curie temperature (T_c). The Curie point of a ferromagnetic material is the temperature above which it loses its characteristic ferromagnetic ability. At temperatures below the Curie point the magnetic moments are partially aligned within magnetic domains in ferromagnetic materials. As the temperature is increased from below the Curie point, thermal fluctuations increasingly destroy this alignment, until the net magnetization becomes zero at and above the Curie point.
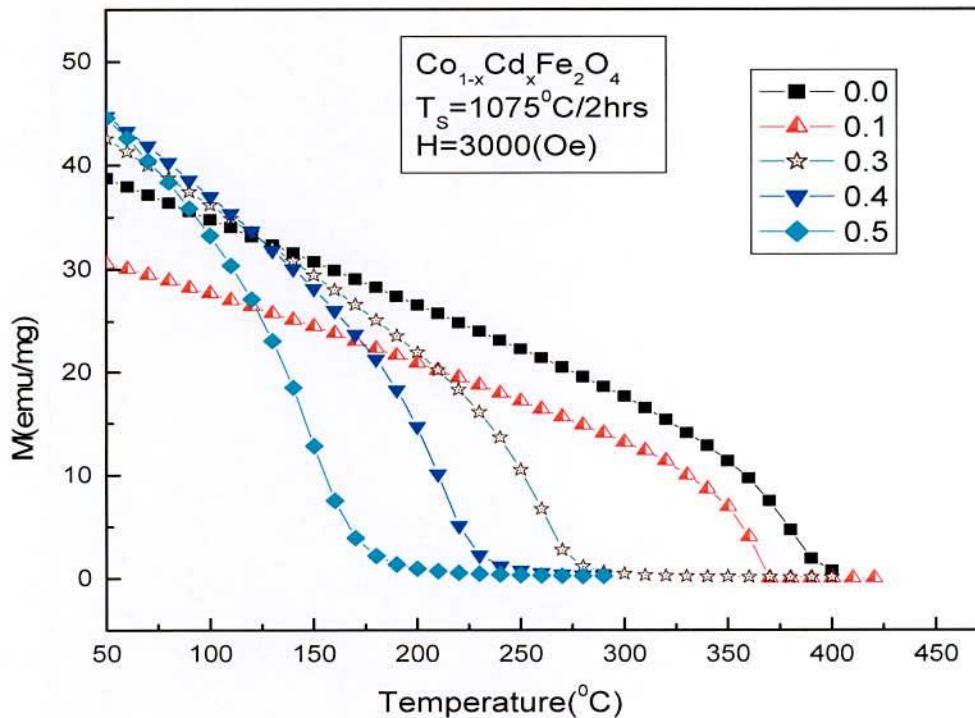

Fig.4.17: Temperature dependence of magnetization of $Co_{1-x}Cd_xFe_2O_4$ ($x = 0.0, 0.1, 0.3, 0.4, 0.5$) with an applied field 3000 Oe

113

Above the Curie point, the material is purely paramagnetic. At temperatures below the Curie point, an applied magnetic field has a paramagnetic effect on the magnetization, but the combination of paramagnetism with ferromagnetism leads to the magnetization following a hysteresis curve with the applied field strength.

4.3   Experimental Results and Analysis of Mössbauer for Co-Cd Ferrites

Mössbauer spectroscopy is used for the identification of magnetic field distribution of magnetic atoms in Co-Cd ferrite. Structural and magnetic changes in $Co_{1-x}Cd_xFe_2O_4$ as induced by high – energy ball-milling were investigated by Mössbauer spectroscopy. The as-prepared powder displays sharp peaks expected for a well-crystallized cubic spinel. In the absence of magnetic order, Mössbauer spectra from Fe ions on either A- or B-sites of the spinel would show one or a set of doublets with particular values of isomer shift and quadrupole splitting. On the other hand, magnetically ordered Fe ions would yield sextents of six absorption lines each, reflecting hyperfine magnetic splitting. The line widths are often sensitive sample crystallinity and compositional effect. The Mössbauer spectroscopy technique in constant-acceleration mode has been used to study hyperfine structure of soft ferrites with composition $Co_{1-x}Cd_xFe_2O_4$ (x = 0.0, 0.1, 0.3, 0.4, 0.5, 0.6 & 0.7).

The experiments were performed at room temperature in transmission geometry, using [57]Co in a rhodium matrix. Pure [57]Fe thin foil has been used as the reference material for Standarization of results. The data are collected into two groups. Each group is of 256 channels and the second group gives a mirror image spectrum of the first group. We linearize the data and the two groups are folded resulting in improved statistics. The parabolic effect in the base line is caused by the periodic parabolic displacement of the source, get cancelled as a result of the folding. The fitting is done in terms of the Mössbauer parameters of Isomer shift (IS), quadrupole splitting(E_Q), hyperfine magnetic field (H_{hf}), line width is measured by full width half maximum (FWHM) and percentage of absorption of the components in magnetic pattern.

In this case of ^{57}Fe there is an magnetic field acting at ^{57}Fe nuclei. This causes the upper - $\frac{3}{2}$ level to split to two levels. Using the selection rule $\Delta m = 0, \pm 1$ for transitions to occur, we get six possible transitions, In order to match the source energy to each of six different velocities of the source. This is automatically achieved in constant acceleration mode. Room temperature Mössbauer spectra, typical of Co-Cd ferrites, are obtained and the changes in the spectra corresponding to the different compositions of the system $Co_{1-x}Cd_xFe_2O_4$ are shown in Fig-4.17(a, b, c & d) and Fig-(e, f, g).

A comparison of the spectrum of pure iron with those of the ferrites of different compositions shows the shift in the spectral lines and their broadening. This is caused by the change in the number of nearest neighbor iron atoms and also there inter atomic distances. The numerical values of IS, E_Q, FWHM, H_{hf} and absorption percentage are shown in Table-4.4

The coulombic interaction after the energy separation between the ground state and the excited state of the nuclei, thereby causing a slight shift in the position of the observed centroid of the spectrum, which are different for various Co-Cd ferrites with different compositions give rise to isomer shifts. The velocity scale is calibrated by a room temperature measurement on a thin natural iron foil sample. The IS's given relative to the centroid of this spectrum as shown in Table-4.4. IS of all the samples are given relative to the centroid of this spectrum. The centroids for the ferrites are calculated relative to the centroid of these spectra from the centroids of the velocity scale of a thin ^{57}Fe foil sample. The IS's of the iron atom in Co-Cd ferrites with composition $Co_{1-x}Cd_xFe_2O_4$ is observed to be in the range 0.176 to 0.35 mm/s, indicating the isomer shift values for all samples are typical of the high – spin Fe^{3+} ions [4.40]. Small effect on the isomer shifts values which indicates that the s- electron change distribution of the Fe^{+3} Ions change with Cd substituting.
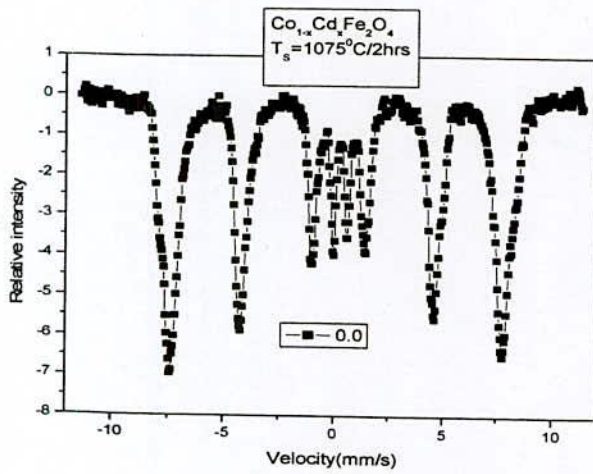
(a)
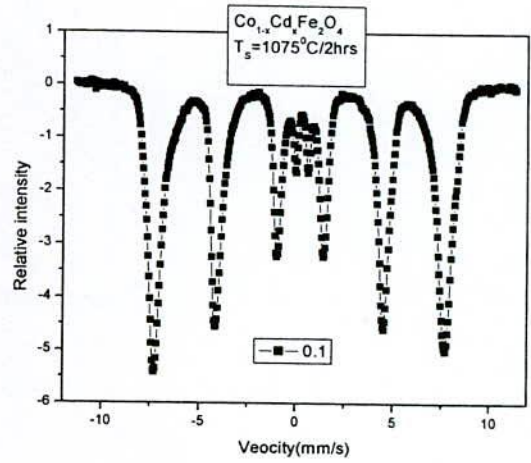
(b)
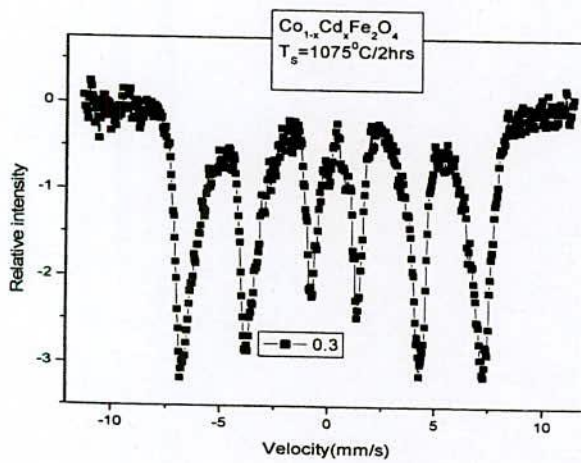
(c)
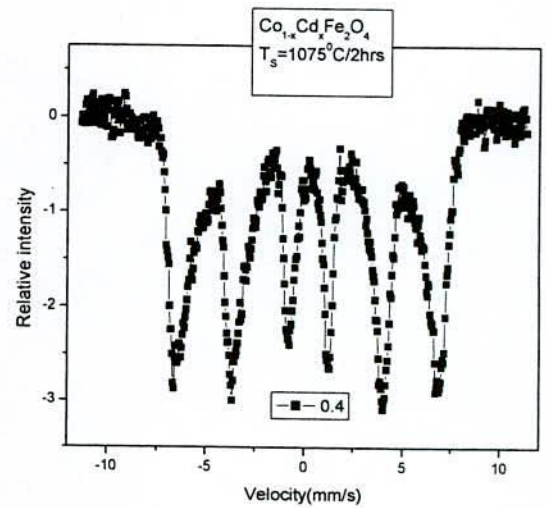
(d)

Fig-4.18(a, b, c, d) Room temperature Mössbauer spectra of $Co_{1-x}Cd_xFe_2O_4$ (x = 0.0, 0.1, 0.3, 0.4) ferrites sintered at 1075^0c for 2 hours.

116
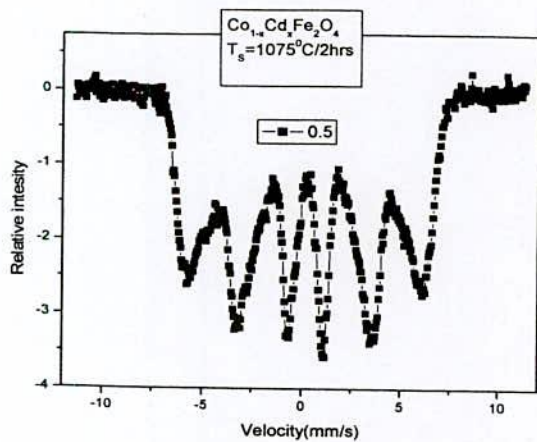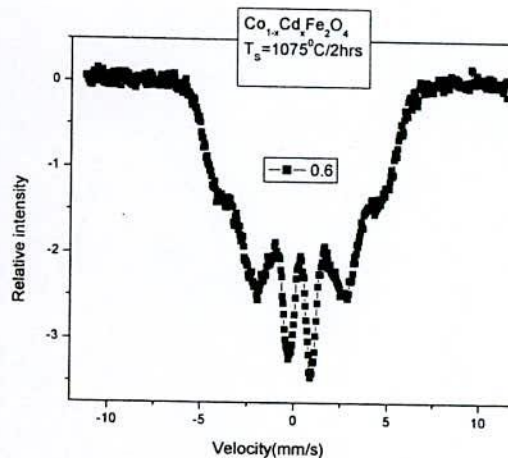
(e)   (f)
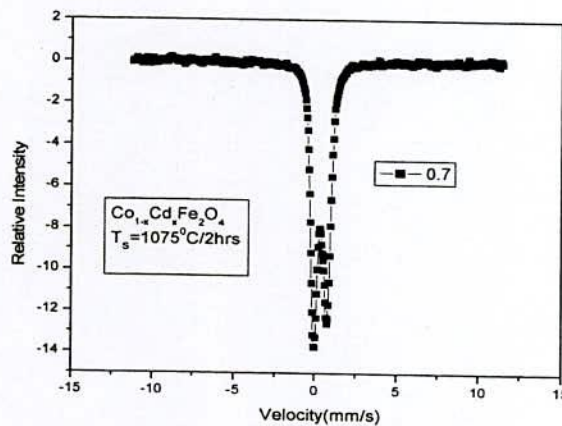
(g)

Fig-4.19(e, f, g) Room temperature Mössbauer spectra of $Co_{1-x}Cd_xFe_2O_4$ (x = 0.5, 0.6, 0.7) ferrites sintered at 1075^0c for 2 hours.

Quadrupole splitting is the electric quadrupole interaction between the quadropole moments of the nuclei and the electric field gradient at the nucleus due to the symmetric distribution of changes on the ions. This provides information on the nature chemical bonds. The E_Q of Fe - atom in the ferrites with composition $Co_{1-x}Cd_xFe_2O_4$ is observed in the range -0.889 to 0.754 mm/s as shown in Table-4.4 The observed trend of the Mössbauer line wide and the average quadrupole splitting point to a gradual

decrease in structural disorder with increase of Cd- content. In the extreme case Cd=0.7 shown in Fig-4.18(g), the amount of Fe has a ratio of 3:2 between the doublet and the two magnetic spectra.

Absorption percentage, as compared with pure iron, decrease in $Co_{1-x}Cd_xFe_2O_4$ ferrites. These absorption percentage decreases with increasing Cd content. These results are shown in table-4.4. The effect of change in the composition of $Co_{1-x}Cd_xFe_2O_4$ ferrites system on the transition line width as measured by FWHM is also shown in Table-4.4. The experimental FWHM of pure ^{57}Fe foil is 0.18mm/s, FWHM of the ferrites broadening is 6 to 11 times up to x=0.5(Cd content). FWHM and absorption percentage gradually decreases with increasing nonmagnetic Cd^{+2} ions concentration. Such observation suggests the ferromagnetic character decreases on increasing Cd^{+2} ions. Using the standard result, the experimental spectra for the Co-Cd ferrites samples of different composition have been obtained by the best fit for the distribution of the hyperfine field.

The results of average magnetic hyperfine field (H_{hf}) of the Co-Cd ferrites sample with composition $Co_{1-x}Cd_xFe_2O_4$ are shown in table-4.4. The general trend of decreasing the hyperfine fields value is presumably due to the weaking of A-B exchange interaction caused by the substitution of magnetic Co^{+2} ions, which also results in a decrease of the curie temperature. As indicated, the samples exhibit typical relaxation spectra in room temperature and could be analyzed in terms of the superposition of two sextent and a quadrupole split central line. The Mössbauer phenomenon and the hyperfine interactions have characteristic compositional depends on Cd^{+2} ions and the spectrum observed in any situation depends on whether the properties of the nuclear environment or the position of the nucleus are changing relative to this Cd-content. The hyperfine H_{hf} decreases with increasing Cd-content as shown in Fig-4.19.

It is well known that the internal hyperfine magnetic field at the Fe nucleus is antiparallel to the atom's magnetic moment. Consequently, Fe ions with antiparallel moments contribute to the external peak, and Fe ions with parallel moments contribute to the sextet corresponding the other peak shown in Fig-4.17(a, b, c, d) and Fig-4.18 (e)

In the range of $0 \leq 0.6$ is observed ferromagnetic behavior extent but $x \geq 0.6$ in Fig 4.18(f, g) we have paramagnetic doublet at room temperature. It is attributed by site preference,

118

since Cd^{+2} ions prefer the A-sites and the Cd^{+2} substitution leads to increased Fe^{+3} ions on B-sites and consequently magnetization of the B- sites increases while that of A-sites. The existence of canted spin causes the reduction in magnetization in B-sites, which is turn reduced the supper transferred hyperfine field [4.41], so the addition of Cd^{+2}, ions finally reduces AB interaction with increases in Cd concentration.
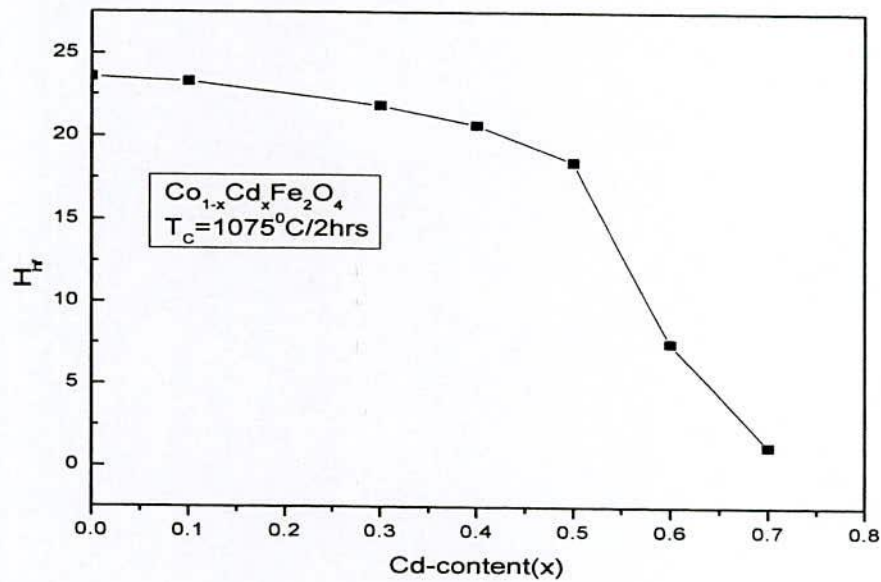
Fig-5.20 Variation of internal hyperfine field due to change in Cd- content in $Co_{1-x}Cd_xFe_2O_4$ ferrites sintered at 1075^0C for 2 hours.

The physical origin of this spin arrangement is from the canting of the spins in the B-sublattice due to weaking of the intersublattice interaction J_{BB} on nonmagnetic Cd-substitution in the A-sublattice. As in the case of spinels, J_{BB} is antiferromagnetic, the B-sublattice splits into two sublattices forming YK angle between the direction of the spins resulting in a decrease of net B-sublattice magnetization. This happens because the replacement of large Fe^{+3} ions by smaller Cd^{+2} ions reduce the influence of the internal hyperfine field at nearest Fe^{+3} sites through transferred hyperfine field.

119

Such observation suggests that the ferromagnetic to paramagnetic state with reduction H_{hf} on increasing Cd^{+2} ions concentration.

Table: 4.4 Numerical values of Isomer shifts (IS), Quadrupole splitting (E_Q), hyperfine field (H_{hf}), Full width half maximum (FWHM) and Absorption percentage of $Co_{1-x}Cd_xFe_2O_4$ ferrites sintered at 1075^0C for 2 hours.

Cd Contents(x)	IS,mm/s ±0.005	E_Q mm/s ±0.005	H_{hf} Tesla $\pm0.1T$	FWHM mm/s, ±0.01	Absorption%
Pure ^{57}Fe	....	0.058	33	0.18	11.38
0.0	0.20	0.754	23.58	1.954	7.17
0.1	0.176	0.666	23.31	1.866	5.5
0.3	0.28	0.347	21.86	1.554	4.3
0.4	0.20	0.355	20.69	1.421	3.3
0.5	0.178	0.044	18.48	1.154	3.7
0.6	0.31	-0.534	7.51	0.71	3.36
0.7	0.35	-0.889	1.24	0.70	13.8

CHAPTER - V

Conclusions

Conclusions

5.0   Conclusions

The synthesis, characterization and detail study of structural, magnetic properties and Mössbauer spectroscopic analysis have been carried out on $Co_{1-x}Cd_xFe_2O_4$ (where x=0.0, 0.1, 0.3, 0.4 and 0.5) ferriets samples using standard double sintering ceramic method, sintered at 1075^0C for 1hr, 2hrs and 4hrs. Powder X-ray difractometry of the ferrite samples revels the single phase cubic spinel structure , as well as defined reflections are observed without any ambiguity variation of lattice parameter with Cd content obeys Vegard's law and the linear variation of x-ray densities with Cd content suggest that the substituted atom preferentially occupies tetrahedral (A) site. The bulk density is lower than the X-ray density increases monotonically with increasing Cd content signifying that the non magnetic ion has a pronounced effect on the densification of the ferrites. Currie temperature decreases linearly with the addition of Cd ions. This is due to the fact that the replacement of Fe^{+3} ions by Cd^{+2} ions the A- sites results in the decrease of strength of A- B super exchange interaction. Thus, the number of Fe^{3+} ion decreases at the A- site which tends to decrease the strength of A-B exchange interaction of the type $Fe_A^{+3} - O^{-2} - Fe_B^{+3}$. These decrease the linkages between the magnetic ions that determine the magnitude of the Curie temperature.

The initial permeability increases with Cd content and sintering time has little effect on permeability. The increase of permeability with Cd content is connected with increased magnetization, density, grain size and possible reduction of anisotropy energy with the addition of nonmagnetic Cd. The resonance shifts towards the lower frequency, as the permeability of the samples increases which really confirms with Snoek's relation. Highest value of the relative quality factor of $Co_{1-x}Cd_xFe_2O_4$ ferrites at x = 0.5 peaks corresponding to the maxima in Q-factor were shifted towards the higher frequency side with the increase in Cd^{+2} content.

Saturation magnetization and magnetic moment are found to increase Cd upto x = 0.5. Cd substitution in the Co-ferrites leads to increase of Fe^{+3} ions on the B-sites and consequently decreases Fe^{+3} ions A-sites. So, the net magnetization increases accordingly up to x = 0.4-0.5

based on Neel's two sub lattice collinear model. The decrease in the magnetic moment after x>0.4 indicates the possibility of a non-collinear spin canting effect in the system. The existence of canted spin gives rise to Yafet-Kittle angle (α_{Y-K}) which compress the strength of A-B_θ and B-B exchange interaction. The increase in Y-K angles for the samples with Cd-content (x > 0.4) is attributed to the increased preference of triangular spin arrangement on B- sites due to frustration of B-B exchange interaction. An increase in initial permeability has also been found with increasing Cd content. Saturation magnetization (M_s) increases with increasing Cd-content with a value of M_s= 32.5emu/g for x = 0.00 compared with M_s = 49 emu/g for x = 0.5.

The Mössbauer spectra for the samples clearly show Lorentzian shaped lines in sextet broad distribution of magnetic hyperfine field (H_{hf}) as compared to pure [57]Fe foils up to x=o.5 but x $\geq$ 0.6 doublet broad distribution of magnetic H_{hf}. The isomer shift of $Co_{1-x}Cd_xFe_2O_4$ ferrites to the pure Fe standard are in the range 0.18 – 0.35 mm/s indicating the Fe^{+3} ions. The average magnetic H_{hf} of the Co-Cd ferrites decreases due to the weakening of A-B exchange interaction caused by the substitution of magnetic Co^{+2} with non-magnetic Cd^{+2} ions, which also results in a decrease of the Curie temperature, our observation the replacement of large Fe^{+3} ions by smaller Cd^{+2} ions reduce the influence of the internal hyperfine field at nearest Fe^{+3} sites through transferred hyperfine field.

References

References

Chapter I

[1.1]   B. D. Culity and C. D. Graham; "Introduction to magnetic materials",2nd edition, A. Willey & Son Publication, 2009, U. S. A.

[1.2]   S. Hilpert, Ber. Deutseh. Chem. Ges. BD2, 42 (1909) 2248.

[1.3]   J. L Snoek; "New developments in Ferromagnetism & Antiferromagnetism"; Annales de physique,3(1948)137.

[1.4]   J. Smith and H. P. J. Wijn, "Ferrites", Wiley LONDON, (1959), p-140

[1.5]   A. Balayachi, J. L. Dormann, and M. Nogues, "Critical analysis of magnetically semi-disordered systems: critical exponents at various transitions", J. Phys.: Condens. Matter 10 (1998) 1599.

[1.6]   M. A. Hakim, M. Manjurul Haque, M. Huq, Sk. Manjura Hoque and P. Nordblad, "Re-entrant Spin Glass and Spin Glass Behaviour of Diluted Mg–Zn Ferrites", CP1003, Magnetic Materials, International Conference on Magnetic Materials (ICMM-2007) AIP, P-295.

[1.7]   H. Martinho, N. O. Moreno, J. A. Sanjurjo, C. Rettori, D. L. Huber, S. B. Oseroff, W. Ratcliff, S. W. Cheong, Phys. Rev.B64 (2001) 024408

[1.8]   M. H. Mahmoud, A. M. Abdallas, H. H. Hamdelv, W. M. Hikal, S. M. Taher, J. C Ho; "Mossbauer Spectroscopic evaluation of high-energy ball-milled $CdFe_2O_4$"; J. Magn. Mater. 263(2003) 269-274.

[1.9]   S. M Prup, B. Topsoc; J . Appd. Phys.11 (1976) 63

[1.10] J. M. Daniels, A. Rosencwaiy; Can. J. Phys. 48 (1970) 381

[1.11] J. K. Srivastava, K. Muralecdharan, R. vijayaraghavan; Phys. Left 24 (1984) 482.

[1.12] A. A. Sattar, A. H. Wafix, K. M. Ei-Shokrofy, M. M. El-Tubby; Phys. Stat. Sol(a) 171 (1999) 563.

[1.13] M. H. Mahmoud, A. A. Satter; "Mössbauer study of Cu-Zn ferrite Substituted with rare earth ions"; J. Magn. Magn. Mater. 277 (2004) 101-105.

[1.14]   T. Giannakopoulou, L. Kompotiatis, A. Kontogeorgakos, G. Kordas, "Microwave behavior of ferrites prepared via sol–gel method", J. Magn. Magn. Mater. 246 (2002) 360.

[1.15]   E. Olsen, J. Thonstad, "Nickel ferrites as inert anodes in aluminium electrodes: Part I Material fabrication and preliminary testing", J. Appl. Electrochem. 29 (1999) 293.

[1.16]   C. O. Augustin, D. Prabhakaran. L. K. Srinivasan, "Fabrication and characterization of $NiCr_2O_4$ spinel", J. Mater. Sci. Lett. 12 (1993) 383.

[1.17]   P. C. Rajath, R. S. Mannab, D. Baneree, M. R. Varma, K. G. Suresh, A. K. Nigame, J. Alloys Compd. 453 (2008) 298.

[1.18]   J. G. Lee, J. Y. Park, Y. J. Oh, C. S. Kim, J. Appl. Phys. 84 (1998) 2801.

[1.19]   R. K. Sharma, O. Suwalka, N. Lakshmi, K. Venugopalan, A. Banerjee, P. A. Joy, J. Alloys Compd.419 (2006) 155.

[1.20]   Stanley, K .J. K. J. Oxide Magnetic Materials 204pp.

[1.21]   Smart, J. Samuel, "The Neel Theory of Ferromagnetism", Amer. J. Physics, 23 (1955) 356.

[1.22]   Wolf, W. P., "Ferrimagnetism," Reports on Prog. in Phys., 24 (1961) 212.

[1.23]   Y. Yafet and C. Kittel, "Antiferromagnetic arrangements in ferrites", Phys. Rev. 87 (1952) 290.

[1.24]   K. H. J. Buchow, Handbook of Magnetic Materials, Vol. 8, Elsv. Sci, 1995, 189.

[1.25]   M. A. Gobal, S. S. Afa-Allah; "Effect of diamagnetic Substitution on the structural, electrical and magnetic propertie of $CoFe_2O_4$"; Materials Chemistry and physics 85 (2004) 104

[1.26]   J. L Dormann, M. Nogues; "Magnetic Structures of Substituted Ferrites". J. phys. Condence Mater 2 (1990) 1223.

[1.27]   A. Balayaehi, J. L. Dormann and M. Nogues, "Critical Analysis of magnetically Semidisordered system; Critical Exponents at Various trasitions"; J. Phys. Condens. Matter. 10 (1998) 1599.

[1.28]   J. L Dormann, M. Nogues; "Magnetic Structures of Substituted Ferrites". J. phys. Condence Mater 2 (1990) 1223.

124

[1.29] P. N. Vasambekar, C. B. Kokkar and A. S. Vaingankar; " Cation distribution and Susceptibility study of Cd-Co and Cr^{+3} substituted Cd-Co ferrites". J.MagnMath.Matter. 186 (1998) 333.

[1.30] O. M. Hemeda and M. M. Barakat, "Effect of hopping rate and jump length of hopping electrons on the conductivity and dielectric properties of Co-Cd ferrite" J. Magn. Magn. Mater., 223 (2001) 127.

[1.31] Saroaut Noor. " Study of additive effect on the structural, Magnetic and Transport properties of Cobalt ferrites: Ph.D. Thesis April 2011

[1.32] Rodmarcq, B. M. Piecuch, Chr. Jonta. G.Machal and Ph. Manging; 1980, phys. Rev. B21, 1911

[1.33] Chappert J. J, M. D. Coey, A. Lienard and J. P. Rebouillat; 1981, J. Phys. F11, 2727.

[1.34] Chien C. L, and K. M. Unruch. 1982, Nucl. Instrum methode 199, 193.

[1.35] Gubben P. C. M, J. H. F. Appeldom, A. M. Vander Kraan and K. H. J. Buschow; 1974, J, Phys. F4, 921

[1.36] A. M. ABDEEN, O. M Hemeda, E. E.Assem, M. M. El-sehly; " Structural. Electrical and transport phenomenon of Co-ferrite substituted by Cd" J.Magn.mater. 238(2002) 75-83.

[1.37] M. Mousa, N. SUMMAN, M. Ahmed; J. Mater. Su. 24 (1989) 2478.

[1.38] A. B. V. Groenou, J. H. N. Creyghton, J. G. M. D. Lan; J.phys. Chem. Solids .35 (1974) 1081

[1.39] T. Y Byun, S. C.Bycon, K. S. Hong; IEEE Trans. Magn. 35(5) (1999) 3445.

[1.40] M. A. Ahmed; 'Electrical Properties of Co-Zn ferrites"; Phys.stat. Sol(a) 111 (1989) 567.

[1.41] P. B. Pandya, H. H. Joshi, R. G. kulkarni; "Bulk magnetic properties of Co-Zn ferrites prepared by the Co-precipition method", J. Materials science 26 (1991) 5509.

[1.42] R. V. Upadhyay, R. B. Jotania and R. G. kulkarn;. " Magnetic ordering in a Zn Substituted Co-Ti-Fe-O ferrite system"; Physics B 190 (1993) 1183-189.

[1.43] A. K. M. Akther Hossain, H. Tabata, T. kawari; " Magnetoresistive properties of Zn_{1-x} $Co_xFe_2O_4$ ferrites"; J. Magn. Magn. Mater. 320 (2008) 1157-1162.

[1.44] Suman Kumar Nath, S. S. Sikder, M. Mahabubur Rahman, M. A. Hakim S. Manjura Hoque; "Magnetization and magnetic Behavior of $Ni_{1-x}Cd_xFe_2O_4$ ferrites" ARPN Journal of science and Technology, Vol-3. No.1 January 2013.

[1.45] A. R. Shitre, V. B. Kawade, G. K. Bichile, K. M. Jadhav, " X-ray diffraction and dielectric study of $Co_{1-x}Cd_xFe_{2-x}Cr_xO_4$ ferrite system" Materials Letters 56 (2002) 188-193.

[1.46] B. H. Liu, .Dins, Z. L. Dong, C. B. Yi; "Microstructural evolution and its influence on the magnetic properties of $CoFe_2O_4$ powders during mechanical milling"; Physical Review B74, 184427(2006).

[1.47] Z. H. Khan, M. Mahbubur Rahman, S. S. Sikder, M. A. Hakim, Shireen Akhter, H. N. Das and B. Anuman; "Thermal Hysteresis of Cu Substituted $Ni_{0.28}Cu_{0.10+x}$ $Zn_{0.62-x}$ $Fe_{1.98}O_4$ ferrites" Advanced Chemistry Letters, Vol, pp1-6,2013.

[1.48] K. O. Low and F. R Sale; J.magn.magn.mater, 30, 246(2002).

[1.49] Z .H. khan, M. Mahbubur Rahman, S. S. Sikder, M. A. Hakim, D. K. Saha, " Complex Permeability of Fe- deficient Ni-Cu-Zn ferrites"; Journal of Alloys and compounds 548 (2013) 208-215.

[1.50] Saroaut Noor, M. A hakim, S. S. Sikder, S Manjura Hoque, Kazi Hanium Marja, per Nordblad; "Magnetic behavior of Cd^{+2} Substituted Cobalt ferrites" Journal of physics and chemistry of solids, 73(2021), pp.227 -231.

[1.51] A. M. M. Farea, Shatendra Kumar, Khalid Mujasam Batoo, Ali Yousef, Alimuddin. "Influence of frequency, temperature and composition on electrical properties of polycrystalline $Co_{0.5}Cd_xFe_{2.5-x}O_4$ ferrites" physica B 403(2008)684.

[1.52] A. A. Ghani, A. A . Sattar, "Composition dependence of Magnetization in $Co_{1-x}Cd_xFe_2O_4$ ferrites" J. Magn .Magn. Mater. 97(1991) 141.

[1.53] Saroaut Noor, S. S. Sikder, M Samirullah, M. A. Hakim and Shireen Akhter; "Effects of Cd properties of Co-Cd ferrites", Journal Of Bangladesh academy of science,Vol.35No.2229-235,2011.

[1.54] Saroaut Noor, M. Mahbubur Rahman, S. S. Sikder and M. A. hakim, "Effect of Cd-substitution on Structural and Transport properties of Co-ferrites,Jahangirnagar University,Journal of science, Vol.34,no.2 pp.01-11,2011

[1.55] Chul Sung kim, Woo chul kim, Sung yong an, Senng wha lee; " structure and Mossbauer studies of Cu doped Ni-Zn ferrite", J.magn.magn.mater215-216(2000) 213-216.

[1.56] M. Arshed, M.siddique, M. Anwar-ul-islam, N. M. Butt, T. Abbas, M.almed;solid state commun.939 (1995) 599.

[1.57] M. Mohan, I. A.Shaikh, R. G. Kulkarni,"Magnetic properties of the Mixed Spinel $CoFe_{2-x}Cr_xO_4$": Physics B, 403(2008)684

[1.58] M. A Hakim, .S. S. Sikder, M. A Asgar B. K. Srivastava and A. Krishnamurthy; "The study of hyperfine field of amorphous ribbons with composition $Co_{80-x}Fe_xB_{10}Si_{10}$ By Mossbauer technique", Nuclear science and Application on Vol.13 No.12 November 2004

Chapter II

[2.1] B. Jeyadevan, C. N. Chinnasamy, K. Shinoda, K. Tohji, "Mn–Zn ferrite with higher magnetization for temperature sensitive magnetic fluid", J Appl. Phys., vol. 93(2003) pp. 8450.

[2.2] William D. Callister, The University of Utah; Materials Science and Engineering 6th ed., Wiley 2003; R. E. Rosensweig, Ferrohydrodynamics, Dover, New York. 1997; R.E. Rosensweig, Regenerative thermomagnetic power. Journal of Energy and Power. (1967) pp. 399.

[2.3] D. Hadfield, Lliffe Books, LTDT, London, John Wiley and Sons, "Permanent magnets and Magnetism", Inc., New York, 1961.

[2.4] Rollin j. parker and Robertj. Studders, john Wiley and Sons, "Permanent magnets and Their Applications", Inc., New York, 1962.

[2.5] Rollinj. Parker, John Wiley and sons, "Advances in permanent Magnetism", Inc., New York, 1990.

[2.6] Malcolm McCaig, John Wiley and Sons, "Permanent magnets in Theory and Practice", Inc., Toronto, 1977.

[2.7] D. S. Parasnis, Harper and Brothers, "Magnetism: From Lodestone to polar Wandering", New York, 1961.

[2.8] J. Smit, H. P. J.Wijn. Ferrites, John Wiley and Sons, New York, (1959).

[2.9] W. H. Bragg; " The structure of magnetic and the Spinels",95(1915),561.

[2.10] J. D. Livingston, Driving Forces. The Natural Magic of Magnets: Harvard University Press: Cambridge, (1996).

[2.11] E. H. Frei. S. Shtrikman, D. Treves. Phys. Rev., 106(1957)446.

[2.12] B. D. Cullity; "Introduction to Magnetic Materials", Addison -Wesley Publishing Com; 1972.

[2.13] Alex Goldman, "Modern Ferrite Technology" Van nosttrand Reinhold New York, 1990.

[2.14] R. W. C ahn, P. Haasen, E. J. Kramer, "Materials Science and Technology", Vol.3B, VCH publishers Inc., New York, NY (USA) and Verlagsgesellschaft mbH, Weinheim (Federal Republic of Germany), (1994).

[2.15] C. W Chen; " Magnetism and Metallurgy of Soft Magnetic Materials", New York (1977)

[2.16] D. J. Craik, 1957, Magnetic Oxide, part I, John Wiley and Sons, Ltd, Bristol England.

[2.17] E. J. W Verway and E. L Heilmann, J. Chem. Phys. 15(4), (1947), 174.

[2.18] F.C. Romeign, Philips Res. Rep. 8, NR-5 (1953), 304.

[2.19] A. Land; " Quantum Mechanics", pitman, London(1951)

[2.20] J. H. Van vleck; "Theories of Electric and magnetic susceptibility", Claredon press, Oxford(1932)

[2.21] P. Weiss; "L'hypothese du champ moleculair et la propriete ferromagnetic", J. phys. Theor. Appl.6(1907)661.

[2.22] Vowles, P. Hugh; "Early evolution of power Engineering" 17(2): (1932) 412.

[2.23] Fowler.Michael; "Historical Begimmry of Theories of Electricity and magnetism",Retrived 2008.

[2.24] R.W. Cahn, P. Haasen, E. J. Kramer, "Materials Science and Technology",spring Verlag naorosa Publishers House, New Delhi, 1990.

[2.25] J. Smit and W. J. P. Wijn, Ferrites, Philips Technical Library (Wiley, New york, (1959).

[2.26] Y. Yafet and C. Kittel, "Antiferromagnetic arrangements in ferrites", Phys. Rev. 87 (1952) 290.

[2.27] D. H. Leyons, T.A.Keplan, K.Dwight and N.menyuk: "classical theory of the ground spin state in cubic Spinels", phys Rev. 126(1962)540.

[2.28] J. T. S. Irvine, E. Amano, A Huanosta, R. Valenzula and A.R West; " solid state ionics 40/41, 220,(1990)

[2.29] E. Amans, R.vanlen Zuela, J.T.S. Irivne and A.R. west; J. Appl. Phys. 67,5589(1990).

[2.30] J. T. S.Irvine, E. Amano, R. Valenzula Matever,sc. Eng.A133, 140(1991).

[2.31] R. M. Jones; IEEE Trans . Mag. MAG-18,1559(1982).

[2.32] M. R. J. Gibbs; Proc. Conf. Metallic Glasses Science and Technology, Budapest 1980, Vol .2c. hargitai, J. Bakonyi and T. Kermeny (Kultura, Budapest) p.37.

[2.33] Alex Goldman; "Moern ferrite technology", Van Nostrand Reinhold, New York (1940)p.15

[2.34] William D. Callister, The University of Utah; Materials Science and Engineering 6th ed., Wiley 2003.

[2.35] L. W. Eagg and S. S.Hanna; Rev. Mod. phys,31,711(1959).

[2.36] S. S Hanna, J. Herberle, C. Littejohn, G. J. Perlow, R. W. Perston and D. D. Vincent; phys. Rev Letters, 4,177(1960)

[2.37] Mössbauer effect: Principle and Applications Gunther K.Werthein Academic Press,New yourk,1964.

[2.38] U. Gonser; Ed., Topics in Applied physics, Springerverlag, Berlin Heidelberg, New York(1973)

[2.39] O. C Kistner and A. W. sunyar; Phys. Rev. letters 4,229(1960)

[2.40] V. L. Goldnskii and R. H. Herber; Eds, Chemical Application Academic Press, New Yourk (1964)

[2.41] H. Koferman; Kernmoments Akad, Verlagesges; M.Franfrut(1956)

[2.42] L. May; "An Intrduction to Mössbauer spectroscopy", Plenum Pren, New yourk(1971)

[2.43] M. H. Cohen and F. REIFT: Solid state Physics, 5, 321(1957)

[2.44] R. M Sternheimer: Phys. Rev, 84, 244(1951)

[2.45] G.K.Wertheim: "Mössbauer effect:Principles and application", Academic press, New yourk (1964)

[2.46] Anjali Krisnaorthy; Mössbauer study of Electric field Gradients in Natural Mica and Synthetic spinel System", Ph.D. thesis, University of Rajsthan, Jaipur,1980.

[2.47] E. Fermi; Z.physics , 60,320(1930)

[2.48] R. A. Ferrel; Am.J.phys, 28,484(1960)

[2.49] G. T. Rado; Am. J.phys, 30,716(1962)

[2.50] K. E. Watson and A. J. Freeman; Phys.Rev.123, 2027(1961)

Chapter III

[3.1] L. B. Kong, Z. W. Li, G. Q. Lin and Y. B. Gan, "Magneto-dielectric properties of Mg-Cu-Co ferrite ceramics: II. Electrical, dielectric and magnetic properties", J. Am. Ceram. Soc. 90(7) (2007) 2104.

[3.2] S. K. Sharma, Ravi Kumar, Shalendra Kumar, M. Knobel, C. T. Meneses, V. V. Siva Kumar, V. R. Reddy , M. Singh and C. G. Lee, "Role of interparticle interactions on the magnetic behaviour of $Mg_{0.95}Mn_{0.05}Fe_2O_4$ ferrite nanoparticles", J. Phys.: Condens. Matter 20 (2008) 235214.

[3.3] Soilah Zahi, Mansor Hashim and A. R. Daud, "Synthesis, magnetic and microstructure of Ni-Zn ferrite by sol-gel technique", J. Magn. Magn. Mater. 308 (2007) 177.

[3.4] M. A. Hakim, D. K. Saha and A. K. M. Fazle Kibria, "Synthesis and temperature dependent structural study of nanocrystalline Mg-ferrite materials", Bang. J. Phys. 3 (2007) 57.

[3.5] A. Bhaskar, B. Rajini Kanth and S. R. Murthy, Electrical properties of Mn added Mg-Cu-Zn ferrites prepared by microwave sintering method", J. Magn. Magn. Mater. 283 (2004) 109.

[3.6] Zhenxing Yue, Ji Zhou, Longtu Li, and Zhilun Gui, "Effects of MnO_2 on the electromagnetic properties of Ni-Cu-Zn ferrites prepared by sol-gel auto-combustion", J. Magn. Magn. Mater. 233 (2001) 224.

[3.7] P. Reijnen, 5th Int. Symp. React. In Solids (Elsevier, Amsterdam) (1965) p-562.

[3.8] C. W. Chen, Magnetism and Metallurgy, Soft Mag. Mat., North-Holland Pub.Com.xv (1977) 288.

[3.9] C. Kittel, Introduction to Solid State Physics, 7th edition, John Wiley and sons, Inc., Singapore (1996).

[3.10] J. B. Nelson, D. P. Riley, "An experimental investigation of extrapolation methods in the derivation of accurate unit-cell dimensions of crystals", Proc. Phys. Soc. London 57 (1945) 160.

[3.11] Tahir Abbas, M.U Islam, and M.Ashraf Ch., Mod. Phy.Letts.B, 9(22), (1995), 1419.

[3.12] J. Smit and H.P.J Wijin, Ferrites, Wiely, New York, (1959)250.

[3.13] Simon Forner, "Versatile and sensitive Virating Sample Magnetometer",Rev.Sci.Instr. 30(1959),p.548

[3.14] "An Introduction of Mössbauer spectroscopy", Leopold May, Plenum press, New Yourk, 1971

[3.15] "Mössbauer Spectroscopy" N.N Gree Wood and T.C Gibb Chapman and Hall Ltd., London, 1971.

[3.16] "Mössbauer study of Electric field gradients in Natural Mica and Synthetic Spinel System"; Anjali Krishnamoorthy, Ph.D. Thesis, University of Rajasthan, Jaipur,.1980.

CHAPTER IV

[4.1] G. A Sawataky, F. Van Der Woude, A.H. Morrish; J. Appl. Phys. 39 (1968) 1204.

[4.2] A. Vasili, U. E. Cuciuureara, N. Rezlescu, E. Luca; Phys. Status solidi A 14k (1972) 105.

[4.3] S. Hudson; Marconi Rev. 37 (1968) 33.

[4.4] V. A. M Brabers; progress in spinel Ferrite Research in Hanbook of Magnetic Materials, Editted by K. H. J. Buchow, North Holland Publishing Inc. 8 (1995) 189.

[4.5] P. N. Vasambekar, C. B. Kolekar, A. S. Vaingankar, J. Mater.Chem.Phys, 601, p. 189, 1999.

[4.6] A. Goldman, Modern Ferrite Technology, Van Nostrand. Reinhold, New York, 1990.

[4.7] L. I. Rabkin, Z. I. Novikova; Ferrites (Minsk), USSR, Vol. 146, 1960.

[4.8] M. A. Gabal, S. S. Ata-Allah.Materials Chemistry and Physics 85 (2004) 104-112, 2004.

[4.9] A. A. Ghani, A. A.Sattar, J. Pierre, J magn.magn. Mater. Vol.97 (1991) p. 141.

[4.10] J. L. Dormann and M. Nogues, "Magnetic structures in substituted ferrites", J. Phys. Condens. Matter 2 (1990) 1223.

[4.11] A. Belayachi, J. L. Dormann and M. Nogues; "crystal analysis of magnetically semi-disordered systems: Critical exponents at various transitions", J . Phys.: Condens. Mater 10(1998) 1599.

[4.12] P. N. Vasambekar, C. B. Koleker, A. S. Vaingankar; "Magnetic behavior of Cd^{2+} and Cr^{2+} substituted cobalt ferrites", J. Matt. Chem. Phys. , 60 (1999) 282.

[4.13] A. M. Samy, H. M. E. L Sayed, A. A. Sattar, Ply.stat.Sol. (a). 200 (2) (2003) 401-406.

[4.14] J. B. Nelson, D. P. Riley, "An experimental investigation of extrapolation methods in the derivation of accurate unit-cell dimensions of crystals", Proc. Phys. Soc. London 57 (1945) 160.

[4.15] L.Vegard, "Die konstitution der mischkristalle und die raumfullung der atome" Z. Phys. 5(1921)17.

[4.16] O.M. Hemida, M.M. Barakat "Effect of hopping rate and jump length of hopping electrons on the conductivity and dielectric properties of Co-Cd ferrite" J. Magn. Magn. Mater. 223 (2001) 127.

[4.17] A.R. Shitre, V. B. Kawade, G. K. Bichile, K. M. Jadhav, " X-ray diffraction and dielectric study of $Co_{1-x}Cd_xFe_{2-x}Cr_xO_4$ ferrite system" Materials Letters 56(2002)188.

[4.18] A. Globus, H. Pascard and V. Cagan, "Distance between magnetic ions and fundamental properties in ferrites"

[4.19] A.M. Abdeen, O.M. Hemeda, E.E. Assem, M.M. El-SAehly, "Structural, electrical and transport phenomena of Co ferrite substituted by Cd" J. Magn. Magn. Mater. 238 (2002) 75.

[4.20] Wang Li and Li Fa- Shen "Structural and magnetic properties of $Co_{1-x}Zn_xFe_2O_4$ nanoparticles" Chinese Phys B 1674-1056/ 2008/17(05) 1858-05.

[4.21] S. A. Patil, V.C. Mahajan, A. K. Ghatage, S.D. Lotke. "Structure and Magnetic Properties of Cd and Ti/Si Substituted Cobalt ferrites", Materials Chemistry and Physics 57(1998)86.

[4.22] A. Land; "Quantum Mechanics", Pitman, London (1951).

[4.23] J. H. Van Vleck; "Theories of Electric and magnetic susceptibilities", Clearendrom Press, Oxford (1932).

[4.24] P. Weiss; "L' hypotheoses du champ molecularie et la propriete ferromagnetique", J. Phys.Theo. Appl. 6, (1907) 661.

[4.25] M. Srivastava, S. N. Shringi, R. G. Srivastava and N. G. Nandikar, "Magnetic ordering and domain-wall relaxation in zinc-ferrous ferrite", J. Mater. Sci. II (1976) 1335.

[4.26] M. Rajendran, R.C. Pullac, A.K. Bhattacharya, D. Das, S.N. Chintalapudi and C.K. Majumdar, J. Magn. Magn. Mater, 232 (2001) 71-83.

[4.27] J. Smit, H.P.J. Wijn, Ferrites, Wiley, New York, 1959, P. 157.

[4.28] Y. Mi and H. Jan; J. Zhejiang Univ. Sci. 6B (6) (2005), P. 580.

[4.29] Saiduzzaman, "The of additives on the physical and Magnetic Properties of Cu-substituted Ni-Zn ferrites"; Ph.D. Thesis; Dept. of Physics, Jahangirnagar University, Savar, Dhaka, Dec. 2012.

[4.30] J.L. Snoek; "Dispersion and Absorption in magnetic ferrites at frequencies above on M_C/s"; Physica 14 (4) (1948) 207.

[4.31] K.J overshot; "the causes of the anomalous loss in amorphous ribbon materials"; IEEE Trans. Magn.17 (1981), p.2698.

[4.32] F.G. Brockmann, P.H. Dowlins and W.G steneck; Phys. Rev.77 (1950), p.85.

[4.33] J. Smit; "Magnetic Properties of materials", Megraw Hill Book Co.(1971) p89.

[4.34] L.Neel; Aun, De phys., 3(1948)137

[4.35] Y. Yafet and C. Kittel, "Antiferromagnetic arrangements in ferrites", Phys. Rev. 87 (1952) 290.

[4.36] S. Geller, "Comments on "Molecular-Field Theory for Randomly Substituted Ferrimagnetic Garnet Systems" by I. Nowik", Phys. Rev. 181(1969)980.

[4.37] S. S. Bellad, and B. K. Chougule, "Structural and magnetic properties of some mixed Li-Cd ferrites", Mater. Chem. Phys. 52(1998)166.

[4.38] S. S. Bellad, S. C. Watawe, and B. K. Chougule, "Microstructure and permeability studies of mixed Li-Cd ferrites", J. Magn. Magn. Mater.195 (1999) 57

[4.39] S. S. Bellad, and B. K. Chougule, "Microstructure-dependent magnetic properties of Li-Cd ferrites" Mater. Res. Bull. 33(8) (1996)1165.

[4.40] C.S. Kim, S.W. Lee, S.L. Park, J. Y. Perk, Y.J. Oh; J. Apl. Phys. 79 (1996) 5428.

[4.41] M. H. Mahamud, A. M. Abdallas, H.H.Hamdeh, W.M.Hikal,S.M. Taher, J.C.HO; "Mössbauer Spectroscopic evalution of high-energy ball-milled $CdFe_2O_4$", J. Magn. Magn. Mater. 263 (2003) 269-274.

Publications

1. **M. Torikul Islam,** S. S. Sikder, M. A. Hakim, Saroaut Noor and D. K. Saha "**Study on Complex permeability of Cobalt-Cadmium Ferrites**" Journal of Engineering Science, Vol. 5, No. 1, 2014.

2. **M. Torikul Islam,** Saroaut Noor, S. S. Sikder and M. A. Hakim "**The study of Hyperfine field of Co-Cd ferrites with Composition $Co_{1-x}Cd_xFe_2O_4$ by Mössbauer technique**" National Conference on Physics for Sustainable Development, KUET, 15 February 2014.

3. **M. Torikul Islam,** Saroaut Noor, S. S. Sikder and M. A. Hakim "**Complex Permeability and Magnetic structure of Cd-substituted Co-Cd Spinel Ferrite**" ; National Conference on Physics for Sustainable Development, KUET,15 February 2014.

4. **M. T. Islam,** S. Noor, S. S. Sikder, M. A. Hakim and D. K. Saha; "**Mössbauer Spectroscopy Studies of Co-Cd Ferrites with Composition $Co_{1-x}Cd_xFe_2O_4$**"; International Conference on Physics for Energy and Environment, 06-08 March, 2014.